UNIVERSITÀ
DEGLI STUDI
FIRENZE

Università degli Studi di Firenze
Dipartimento di Ingegneria dell'Informazione (DINFO)
Corso di Dottorato in Ingegneria dell'Informazione

Curriculum: Dinamica non lineare e sistemi complessi
SSD MED/04

A system biology approach to study pancreatic ductal adenocarcinoma (PDAC) cells in *in vitro* culture

Candidate
Nirmala Kuppalu Ramappa

Supervisors
Prof. Annarosa Arcangeli

Dr. Giacomo Innocenti

PhD Coordinator
Prof. Luigi Chisci

---

ciclo XXX, 2014-2017

Università degli Studi di Firenze, Dipartimento di Ingegneria
dell'Informazione (DINFO).

To My Husband

Acknowledgments

First and foremost, I would like to thank my supervisor and guide Prof. Annarosa Arcangeli. Thank you for providing me an opportunity to work in your laboratory. I am grateful for your constant support and guidance during my entire PhD work. Your passion about scientific research and enthusiasm always encouraged to work hard. Thank you for supporting me during tough times.

I would also like to thank my another PhD supervisor and guide Prof. Giacomo Innocenti. Thank you for teaching me mathematical modelling from basics and dedicating hours of time to teach the mathematical concepts. Thank you for your insightful comments during thesis writing.

I also thank Dr. Martin Stelzle and Dr. Meike Beer for the collaboration of some parts of my research work at NMI Germany. I also thank Prof. Duccio Fanelli and Prof. Luigi Chisci for their constant guidance in academic and administration work during my PhD.

I would like to thank all my former and present lab members for all the support and fun we had. Specially I would like to thank Dr Massimo D'Amico for his constant support and guidance during three years of work. Thank you so much Massimo spending your precious time in teaching me from Italian to Flowcytometer. I am very grateful to you. I thank Dr. Olivia Crociani for teaching most of the cell culture techniques, Mab production, purification and of course my never ending dark room. Thank you so much. I thank Dr Elena Lastraioli for all my Italian translational work and administration work. Thank you for spending hours of time on filling my applications and assisting me in all the bureaucracy. I also thank Dr. Serena Pillozzi for constant support and guidance during my PhD. Claudia, Jessica and Tiziano you three are very good friend of mine without you guys it would have been very difficult. Thank you guys for all the support, fun and lunch we had together. I will definitely miss you guys. I also thank Dr Giulia Petroni for all the help during my experimental work. I also thank Laura and Matteo Stefanini for all the support.

I thank Alice (helping hand) for supporting and guiding me in all the engineering related works from Matlab to lunch. I am very grateful for all the help you did in writing my thesis in latex and printing my thesis. I miss our gossips and of course you Alice. I thank Lorenzo for all the support and cafe offers. I cherish our menza breaks, thank you for being part of that. I also thankful to Anna, Anastasia, Matteo Lulli and Marco for being

supportive during these 3 years.

I also thank Adriano for treating me as one of his family member and teaching me all the varieties of pasta and italian. I am grateful to Rossita, Jessy and Mary for being supportive at home.

I thank all my friends (I am scared to take the names since I may miss someone) for being supportive and calling me all the time just to know I am doing good. Thank you friends.

I also thank all my family members Appaji, Amma, Anna, Tamma, Prakashanna, Padma, Monal, Atte, Mava, Sahana, Sachin, Aadya and Aarna for being supportive and encouraging all the time. Without your support and advise I never been accomplished this, thank you and love you all.

At last but not least, I would like to thank my husband Sagar for being supportive and encouraging me to do PhD, without you I wouldn't have done this. I am very happy that I worked as your junior for 2 years and teaching me all the cell culture techniques. Those 2 years of togetherness at home and lab are cherishable. Thanks for being my strength during my difficulties.

And above all, I submit myself before the almighty, who has given me the strength, courage and blessings.

Abstract

Pancreatic ductal adenocarcinoma (PDAC) is the fourth leading cause of death with a five-year survival of less than 5%. The dismal survival rate and prognosis are due to its aggressiveness, high incidence of metastasis, inability to detect the disease at an early stage, lack of specific symptoms and diagnostic methods. Despite the therapeutic advancement, there are few or no effective therapies for advanced pancreatic cancer. Most of the drugs tested fail due to the usage of drug testing models that are physiologically irrelevant. In this regard we studied three human PDAC cell lines PANC1, BxPC3 and MiaPaCa2 in different cell culture systems including 2D, 3D spheroids and 3D microfluidic chip to understand its growth characteristics and more importantly drug responses. In addition, we developed the mathematical models for growth kinetics of three PDAC cell lines cultured in 2D culture.

Initially, we studied the PDAC cell lines in conventional two-dimensional (2D) culture. In 2D culture, all the three cell lines, PANC1, MiaPaCa2, and BxPC3 showed similar growth rate. As three-dimensional (3D) culture bridges the gap between 2D and *in vivo* culture, we studied the PDAC cell lines in 3D culture using U tube technique. Interestingly, in 3D culture BxPC3 showed compact spheroids of null growth compared to larger MiaPaCa2 and PANC1 spheroids where cells were of loosely assembled. Later we have cultured the same human PDAC cell lines in the novel microfluidic chip, HepaChip® coated with collagen1, the most abundant extracellular matrix in PDAC tumor microenvironment, having a combination of microfluidics and dielectrophoresis (DEP) as well as perfusion systems for the continuous supply of nutrients. In HepaChip® microfluidics, both PANC1 and BxPC3 cells greatly attached to the collagen1 whereas MiaPaCa2 cells were poorly attached, perhaps due to low expression of collagen1 binding adhesion receptors in MiaPaCa2. We have shown PDAC cells cultured into the HepaChip®

(1) are vital and grow, provided they properly attach to collagen; (2) show morphological appearance and growth characteristics closer to those of cells grown as spheroids than in conventional 2 dimensional (2D) *in vitro* cultures.

Further, for drug testing in the above *in vitro* cell culture models we used the only PANC1 because BxPC3 cells showed null growth as 3D spheroids and MiaPaCa2 cells failed to attach to the collagen1 matrix in the 3D microfluidic chip. We tested the cytotoxic effect of cisplatin, commonly used chemotherapeutic drug, on PANC1 in 2D, 3D, microfluidic chip and *in vivo*. The IC_{50}s of Cisplatin determined for PANC1 cells cultured as a 2D monolayer *in vitro* is 3.25 µM, and around 14.6 µM when PANC1 cells were cultured as 3D spheroids. However, PANC1 cells in collagen1 in 3D microfluidic chip showed more resistance to cisplatin where even 100µM of cisplatin treatment did not induce more than 30% cell death whereas for *in vivo* we used cisplatin at 10mg/kg equivalent to 250µM and observed significantly smaller tumor formation.

Finally, we studied the growth characteristics of PDAC cell lines cultured in 2D culture using mathematical modeling to understand the growing behavior of different cell lines. We built a mathematical model for cell growth of three PDAC cell lines using discrete non-linear autoregressive model of the form

$$Y(k) = \underbrace{G(Y(k-1))}_{\text{growth rate}} Y(k-1)$$

We have tested mathematical modeling for cell growth data of 42 cases for three PDAC cell lines, PANC1, MiaPaCa2, and BxPC3. Initially, we tested nine different structures for all the three cell lines and selected the most suitable three models based on a special error index, which is a measure to represent the ability of the model to describe the actual data. Then, the selection of best sampling time for these best three models followed. The top three models with their best sampling times were finally re-identified using data from all the experiments. Among them, the best model of each cell line has been chosen according to the least error index paradigm.

All the three best model identified so far showed monotonically decreasing growth rates, with some difference in the slopes. However, since each cell line had a couple of experiment definitely not reliable, we narrowed the data only to the reliable sets and repeated the identification. The new results showed an interesting convergence of all the three cell lines to third order growth

rates, which, however, differ for their peaks. For example, for MiaPaCa2 the peak is reached when the cell count is still small, while PANC1 has the biggest growth rate for an intermediate value. Moreover, BxPC3 showed slower growing behaviors with 6H sampling time compared to others having 3H sampling time.

Contents

Chapter 1

Introduction

1.1 Pancreatic ductal adenocarcinoma (PDAC) and PDAC progression

Cancer in simple terms defined as a disease that stemmed from the uncontrolled growth of the normal cell. According to the National Cancer Institute (NCI) "Cancer is the name given to a collection of related diseases". Cancer is caused by multiple factors including exposure to cancer-causing agents (carcinogens), chronic infections (such as hepatitis viruses, papilloma virus), lifestyles (eating, drinking, smoking habits, physical activities) and inherited a genetic susceptibility to environment factors (Ames and Gold, 1998).

The pancreas is a complex organ consisting of three cell lineages; Islet (endocrine), Acinar and Ductal cells (exocrine). Pancreatic cancer is classified based on the function part that is affected either in endocrine or exocrine part. Pancreatic cancer related to endocrine constitutes only 3% of pancreatic cancer whereas exocrine cancer of pancreas begins in glands or ducts of exocrine and accounts for about 95%. Most of the exocrine cancer of pancreas arises from ductal cells and it is called as pancreatic ductal adenocarcinoma (PDAC). PDAC is one of the most trivial types of pancreatic cancer and the most lethal form of cancer with a five-year survival rate of less than 5% and characterized as highly desmoplastic with significant deposition of extracellular matrix, especially collagen1. PDAC, like any other cancer, is caused by multiple factors such as; advanced age (> 65), smoking (Fuchs *et al.*, 1996), sex (male has 30% higher risk than female) and long-standing

chronic pancreatitis (Guerra *et al.*, 2007) are the major risk factors followed by dietary like high in meats and fat, obesity, diabetes and family history of PDAC patients (Hezel *et al.*, 2006, Kloppel, 2011; Swartz *et al.*, 2002).

1.2 Precursor of pancreatic ductal adenocarcinoma (PDAC) and its microenvironment

Between the normal pancreas and metastasized cancer stage PDAC progression has been classified into precursor lesions, infiltration, dissemination and metastasis [32] (Figure 1.1). There are three types of precursor lesions; pancreatic intraepithelial neoplasias (PanIN-1, 2 and 3), Intraductal Papillary Mucinous Neoplasms (IPMN) and mucinous cystic neoplasms MCN, that are indicators of future PDAC. PanIN1 lesions first observed around 40 years ago and are histologically characterized to be small and clinically difficult to detect precursor lesions to invasive ductal adenocarcinoma (Cubilla and Fitzgerald, 1976). PanIN 2 and 3 are, by comparison, have larger lesions, characterized by moderate and severe disorganized architectural atypia [51]. As depicted in figure 1.1 below the earliest precursor lesions (PanIN1) possess some of the prominent alternations in genetic landscapes like telomere shortening and K-Ras mutation followed by acquiring several more mutations that transform the normal ductal cells to malignant invasive cells. The estimated timeline from telomere shortening to invasive behavior of cells is approximately 12 years [32]. Deep global genomic analyses and copy number variations from 100 PDAC reveal that each patient contains on average 119 somatic chromosomal variants ranging from 15-558, exceeding the previously reported average of 63 mutations. Most importantly these gene mutations are implicated in twelve-core cell signaling pathways that range from 67-100% tumors. Other lesser-studied precursor lesions like IPMN arises from ducts or its branches and resembles PanIN like structure. However, large enough to detect clinically and serves as an indication of pancreatic cancer. IPMNs have also shown to harbor mutations like KRAS and GNAS that are associated with invasive PDAC (Wu *et al.*, 2011). MCNs are large mucin-producing columnar epithelial cystic lesions that typically occur in women in the body and tail of pancreas [86] and [22] Unlike the IPMNs the MCN lesions are not directly related to pancreatic duct and patients with non-invasive MCN have 5-year survival is almost of 100%, while patients with invasive MCNs have 5-year survival of up to 60% [22].

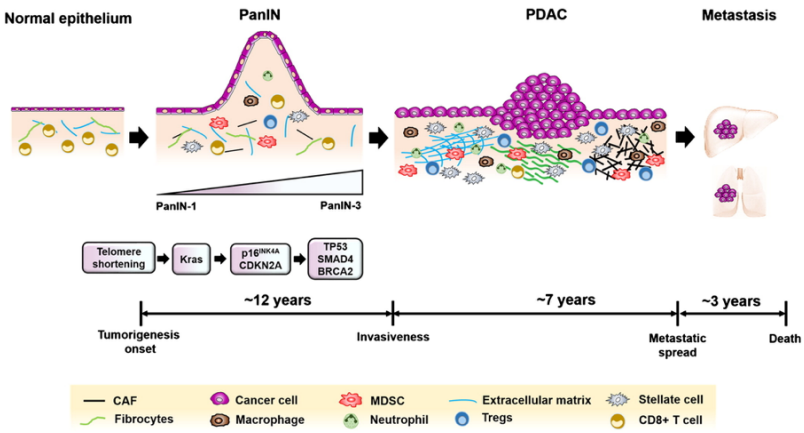

Figure 1.1: *Schematic representation of the approximate timeline for transformation of normal pancreatic ductal epithelial cells towards metastasis and the changing tumor microenvironment associated with the tumor progression (Adapted from [32])*

From genetics point-of-view, PDAC occurs due to the accumulation of somatic mutations in normal ductal epithelial cells. Firstly, a most common phenomenon in the initiation of PDAC might be the telomere shortening followed by mutations in the oncogene KRas that shows constitutively gain of function in >90% of the PDAC [22]. In addition, there are three more commonly identified mutations that occur in tumor suppressor genes (leading to loss of function); CDKN2A, TP53, and SMAD54 in subsequent stages towards PDAC [3]. During the course of progression towards PDAC, there are, on average, as many as 119 genetic mutations on average. Intriguingly, the predictive duration required between the occurrence of telomere shortening and time of PDAC diagnosis is approximately 20 years, which suggests how slow and stealthy is the evolution and clonal expansion of these cancer cells (Campbell *et al.*, 2010; Yachida *et al.*, 2010). However, the computational analysis of 200 patient samples predicts that the rate of pancreatic cancer growth increases exponentially during the time of diagnosis (Haeno *et al.*, 2012). Early stage detection provides a significant window of opportunity for effective chemotherapy or surgical interventions.

The invasive cells from a primary tumour escape the primary tumor site and disseminate through blood or lymphatic system into distant organs caus-

ing metastasis. Metastasis is the main perpetrator of cancer-related deaths. Albeit, the PDAC cancer progression is more than a decade-long process the metastasized tumor might retain most if not all of the mutations that were present in the primary tumor (Yachida *et al.*, 2010). Loss of SMAD4, a tumor suppressor gene, has been shown to be closely associated with metastasis in PDAC (Iacobuzio-Donahue *et al.*, 2009). Moreover, the tumor microenvironment plays a larger role towards tumor progression and metastasis of PDAC cells is by the tumor microenvironment. Tumor microenvironment (TME) is composed of desmoplastic stroma containing pancreatic stellate cells, cancer-associated fibroblasts, immune cells and increased deposition of extracellular matrix and secreted growth factors, cytokines etc. [108] [81]. Below is the brief description of the role of significant components in TME.

1.3 Pancreatic tumor microenvironment

1.3.1 Pancreatic stellate cells (PSCs)

PSCs form one of the key components in TME. In healthy tissues, PSCs, exist in a quiescent state as circular shaped cells that have large lipid droplets rich in vitamins. Under pathophysiological conditions such as acute or chronic pancreatitis (inflammation), a major risk factor in developing PDAC (Lowenfels *et al.*, 1993) the PSCs are activated, which exhibits elongated phenotype with loss of lipid storage and gain of alpha-smooth muscle actin (α-sma). The activated PSCs then, through secretion of various growth factors, ROS, proteases induce epigenetic changes, genomic instability and mutations in normal ductal epithelial cells and thus transforming into a malignant cell. This malignant PDAC cells then activate the quiescent PSCs and the cycle of activation of one another continues [98]. Two-dimensional tandem mass spectrometry was employed by researchers to analyze the secretome of both quiescent and activated human PSCs. The most striking difference between the quiescent and activated PSCs is the secretomes between the two states of cells with quiescent PSCs secreting up to 46 types of proteins into its microenvironments whereas activated cells secrete as many as 641 (Wehr *et al.*, 2011). Accordingly to KEGG database, ˜50% of the secretomes of activated PSCs, according to KEGG database, are associated with cellular metabolism, genetic information processing, signaling pathways, cellular processes and human diseases (Wehr *et al.*, 2011). These secretomes include

many types of growth factors, cytokines, interleukins, proteases and most importantly extracellular matrix proteins (Figure 1.2). There is an exhaustive list of experimental evidence reviewed on how PSCs promote PDAC cell proliferation, migration, invasion, and tumorigenesis and help acquire resistance to chemotherapy and radiation in both *in vitro* and *in vivo* models [43]

1.3.2 Extracellular matrix proteins

PDAC is characterized to be highly desmoplastic with large amounts of ECM proteins deposited around the tumor cells. PSCs are the chief source of ECM consisting of collagen-1 (more than 90%), fibronectin, proteoglycans, hyaluronic acid and other ECMs. The constant accumulation of these ECMs distorts the normal architecture of the pancreas tissue and induces abnormal blood and lymphatic vessels as well as brings the ECMs and PSCs closer to cancer cells (Gnoni *et al.*, 2013; Armstrong *et al.*, 2004). In addition, ECM deposition around the tumor cells protects them against any therapeutic drugs and, also confines the tumor cells within the microenvironment. However, ECM turnover (synthesis, secretion, and degradation) is critical in tissue remodeling in both normal as well as pathological processes. PSCs, when exposed to proinflammatory proteins like TGF-B, IL-6, secrete enzyme class matrix metalloproteinases (MMPs) that degrade ECM (Phillips *et al.*, 2003). Cancer cells exploit this well-coordinated ECM turnover to migrate closer to blood vessels and further induce angiogenesis for eventual dissemination to distant organs.

1.3.3 Immune cells in TME

The TME has shown to be infiltrated by various inflammatory immune cells as an act of immune surveillance. This includes cells of adaptive immunity like T lymphocytes, dendritic cells and occasionally B cells as well as cells of innate immunity like macrophages, natural killer (NK) cells etc. (Whiteside, 2008). The size of the infiltration of these cells could vary from tumor-to-tumor. Despite the recruitment of these immune cells as a defense mechanism against tumor cells, the tumor continues to grow: it could be because the adaptive immunity is weak and largely inefficient (Arcangeli, 2011). In addition, the cellular and molecular events in TME are often orchestrated and dominated by tumor cells in which tumor cells cause dysfunction and death

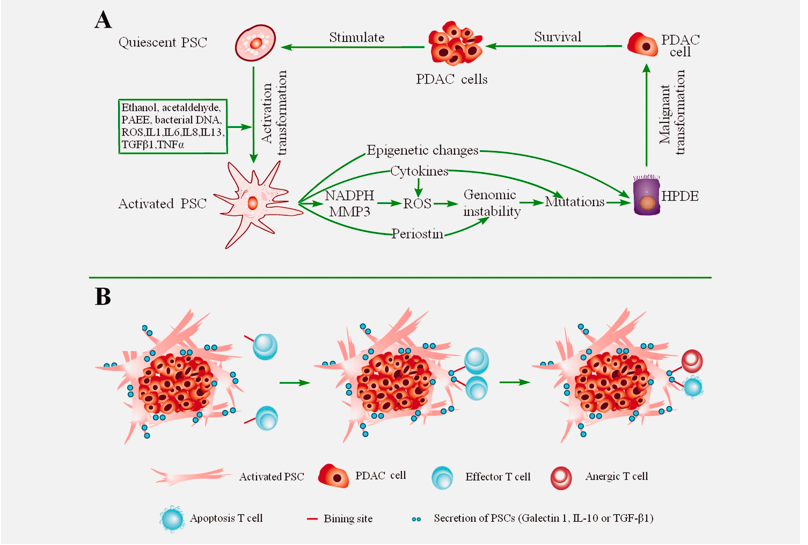

Figure 1.2: *Schematic representation of interaction between PSC, PDAC and immune cells in tumor microenvironment (TME) (adapted from [98]). (A) The role of PSCs (activated state) in transforming normal human pancreatic ductal epithelial (HPDE) in to malignant PDAC cells. Firstly, quiescent PSCs could be activated by chemical or biochemical as well as foreign agents in chronic pancreatitis. These PSCs secrete growth factors like TGF-b, PDGF, FGF-2 and other cytokines that induce epigenetic changes, genomic instability and mutations in HPDE and transform to PDAC. PDAC cells then stimulate the (remaining) quiescent PSCs further and constant stimulation of one-another continues. (B) PSCs further involved in immunosuppression mechanism. When recruited T cells in immune surveillance encounter antigens secreted by PSCs they undergo angeric state and eventually apoptosis.*

of immune cells or in worst cases immune cells are involved in promoting the growth of tumor cells (Whiteside, 2008; Arcangeli, 2011). For example, tumor-infiltrating lymphocytes (TIL) the major components of immune infiltrates in tumors obtained from tissue samples, the major component of immune infiltrates in the tumor, showed inhibited proliferation in response to antigens, compromised signaling through a T-cell receptor (TCR) and inability to induce cytotoxicity towards tumor cells. It is also shown that except for effector T cells, immunosuppressive cells like tumor-associated macrophages, myeloid-derived suppressor cells (MDSC) and T regulatory cells (Treg) are recruited to the tumor site at the early stage and persist till invasive cancer but tumor still grows. This suggests that effective immune defensive mechanism against the tumor is undermined from the start (Clark *et al.*, 2007). Recently, a comprehensive study identifies some of the key immune cells that, when recruited to TME in higher levels, are either associated with shorter or longer survival of PDAC patients (Ino *et al.*, 2013).
The treatment for cancer includes mainly surgical resection, radiation therapy, chemotherapy, immunotherapy, hormonal therapy (breast and prostate only), targeted therapy and to lesser extent stem cell transplant and precise medicine. Surgical resection remains a most desirable form of treatment followed by radiation therapy, provided cancer has not formed distant metastasis. However, most of the cancers at the time of diagnosis show multiple metastases leading to patients to opt for chemotherapy. Small molecule drugs are the chemotherapeutic agents that are designed and developed to target tumor cells at primary and distant metastasized sites. *In vitro* studies are conducted to screen for the 'promising' drug, from the library of hundreds of thousands of small molecule drugs in the pharmaceutical industries, which has the ability to arrest growth and kill the cancer cells. Even the so-called promising drug will be not able to arrest growth and kill 100% cancer cells as some cancer cells exhibit resistance. In addition, most of the drugs screening tests are conducted on two-dimensional (2D) cell culture system that by no means represents the physiological three-dimensional (3D) systems. Hence the there's an increase in the trend towards using more robust screening tests like 3D *in vitro* tests.

1.4 Three-dimensional (3D) cell culture of cancer cells

The first known isolation and maintenance of animal organ part were performed by Ludwig in 1985 and principle of tissue culture was established by Wilhelm Roux in 1885 [116]. Since then the advancements in tissue culture techniques has led to a tremendous understanding of cell responses to drug treatment. *In vitro*, cell-based assays have long been and continue to be the approach for drug discovery against many diseases. Two-dimensional (2D) cell culture technique is the best characterized, easy to expand cell line banking and easy-to-handle cell culture technique that is widely used drug-screening assays. However, 2D culture does not represent the actual physiological organization of the cells *in vivo* that has a 3D architecture and the drug responses also vary greatly between the 2D and 3D systems. Therefore, 3D culture is gaining increasing attention towards understanding the cell behavior, especially towards drug responses. In fact, the first reported (in PubMed) 3D cell culture was nearly 50 years ago [9] and there has been little application of 3D techniques culture until 2000. Recently, the 3D culture techniques have received tremendous importance due to the natural advantages in understanding drug screening, cytotoxicity assays, cell growth, gene expression, cell differentiation that are a step closer to *in vivo* conditions [88]. The advancements in (bio) material science has enabled scientists to develop novel 3D cell culture methods including simple suspension of cells as 3D droplets [60], growing cells as spheroids on low attachment plates or agarose coated flat bottom plates [33], embedding the cells in extracellular matrix as organoids [60], levitating the cells [42].

Three-dimensional (3D) cell culture techniques can be broadly classified into two main categories; scaffold-free and scaffold based culture systems.

1.4.1 Scaffold-free 3D cell culture

Scaffold-free cell culture involves that cells resuspended in single cells form loosely arranged clumps or multi-cellular aggregates, in which cells produce their own extracellular matrix proteins. This multi-cellular aggregates or spheroids can be formed by hanging-drop methods where cells are resuspended in growth media and added as droplet on the lid of cell culture dish and inverted (figure 1.3, left) or alternatively cells are seeded in low adherence wells where cells aggregate and form multi-cellular clumps (figure 1.3,

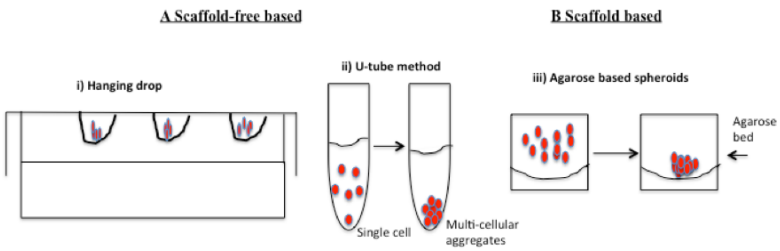

Figure 1.3: *Simple three-dimensional (3D) cell culture methods. A) Scaffold-free based 3D cell culture includes (i) hanging drop and (ii) U-tube methods where cells form aggregates at the apex of the drop or tube and are not under the influence of any external support. B) Simple scaffold-based method include (iii) agarose gel bed where cells are seeded. The agarose gel forms concave shaped bed like structure where cells collect form aggregates and grow as spheroids.*

right) at the apex of the droplet. The growth of cells in the spheroids mimics the artificial environment that resembles *in vivo* organization of the cells. This is of particular importance in studying *in vitro* stem cell differentiation where such spheroids are called as embryoid bodies (EBs) and the size of EBs is one of the key parameters that affect cell differentiation [75] [73]. From cancer studies point-of-view the growth of cells in spheroids lead to a heterogeneous population of cells where cells at the periphery of the spheroids are highly proliferative in contrast to quiescent cells at the core of the spheroids. This could be due to the gradient in terms of nutrient availability, and diffusion of gas creating the hypoxic core and normoxic periphery, a phenomenon observed in cancer tissues [68].

1.4.2 Scaffold-based 3D cell culture

Use of scaffold-based 3D culture presents with additional advantages as scaffold materials increase the complexity of the 3D organization of the cells. Scaffolds include natural materials like collagen, fibronectin, laminin, fibrin, agarose, hyaluronic acid etc. and synthetic materials like polymers, ceramic-based bioactive glasses, self-assembled peptides [60]. Synthetic scaffolds, due to defined chemical or biochemical compositions, provide reproducibility in terms of experimental studies whereas the natural scaffolds consist of sites

that enable near physiological interaction with cells [60]. Scaffold-based 3D culture methods are further classified into hydrogels based and solid scaffolds based 3D culture. Agarose hydrogels are an example of simple scaffolds that are used to form 3D cell spheroids and require minimal optimization of concentrations of agarose depending on cell type. ECM proteins are another set of hydrogel-based scaffolds that are widely used that mimic the *in vivo* cell microenvironment. ECM scaffold usage for 3D culture includes either mixture of ECMs like matrigel that consists of laminin, collagen 1, entactin etc. or single ECM like collagen1, fibronectin etc. ECM based 3D culture is created by either sandwiching the cells between two layers of coated ECM proteins [64] [6] or cells are mixed with ECMs, added as droplets [105] where ECMs solidify at the growth temperature. Despite providing the cell-tissue matrix interactions *in vitro* the ECM based 3D systems also has its intrinsic limitations in creating highly complex and well-controlled microenvironment.

1.5 Microfluidic technique

The development of microfluidics in the 1990s provides an opportunity to create highly complex, reproducible and well controllable microenvironment for 3D cell culture. Microfluidics deals with small volumes of fluid flow that are precisely controlled and manipulated in the constrained geometry. Further advancements in the integration of microfluidics and cell biology have reached a significant milestone with the development of "organs-on-chips", smart technological platforms that, once applied to the study of human diseases, such as cancer, might ultimately contribute to design personalized treatments and hence improve health outcomes [1] [114]. There are several advantages over conventional methods as simple demonstrations of biological cells being transported and manipulated in microchannels for basic short-term analysis, has now advanced to the point where we can engineer living cellular microsystems with controllable microenvironments that behave and function – with organ-level complexity – like their counterparts *in vivo* [7] [53]. Organ-like features include continuous perfusion and physiological cell–matrix and cell-cell interactions. Development of these techniques as "cell-on-chips", "tissue-on-chips" and "organs-on-chips" resulted in a major contribution to drug testing and toxicological studies.

There are several types of the microfluidic chamber that work on different principles and used for different application. A lot of review articles

can be found in their applications. Wlodkowi and Cooper reviewed on the usage of a microfluidic chip in the field of cell imaging techniques and micro sorting technology. Huh, *et al.* described the possibilities and challenges of microfluidic technology for next generation of cell culture. Young reviewed on verities of design consideration of microfluidic devices used in culturing tumor microenvironment for both solid and liquid tumors. Navid Kashminjad has categorized the chip based on a tumor and described chip design, fabrication, and characterization of tumor microenvironment [57].

Different types of microfluidic systems have been established to support cancer cell detection, sorting, and drug testing. These microfluidic chips are fabricated on different platforms. Mainly there are 3 types of fabrication have been used in microfluidic chip [40].
1) Glass \Silicon Based Systems: These enhance the optical properties and are useful in high-resolution microscopy. These can also be used for longer-term studies with reproducibility. These are impermeable to oxygen and helpful for only hypoxic studies. Silicon systems are not much popular because of their high cost and complicated fabrication procedure.
2) Polymer Based System: These are dominated because of its permeability to oxygen and cost-effectiveness. Various polymers such as PDMS, Polycarbonate, Polyester, Polymethyl methacrylate can be used for fabrication. All these devices are optimized for the flow of medium and perfusion of oxygen. Typically, these have 2 ports one for inlet of medium and other for remaining medium ejection.
3) Paper Based System: These are very simple and cost-effective approach compared to glass and polymer system. Multiple papers are stacked over each other to mimic the 3D architecture.

Microfluidic chips or devices are engraved with channels for liquid flows that are typically in sub microliters rage. Microfluidic devices for cell culture also use scaffolds such as polydimethylsiloxane (PDMS), agarose, collagen, fibronectin etc. [66] As we know that extracellular matrix (ECM) plays an important role in cancer growth, differentiation and cell-to-cell signaling, the ECM can be utilized to support the 3D culture as a scaffold. This scaffold dependent microfluidic chips are called gel-supported system and without scaffold are called gel free system [40]. In-gel supported system scaffolds are made up of hydrogels and this supports the development of complex and clinically relevant 3D cellular architecture. As these hydrogels limit the transport of nutrients and oxygen through thick scaffolds, efforts have made to get rid

of these gels. There are many microfluidic chips that support the 3D culture by different techniques such as hanging drop, polyethyleneimine-hydrazide an intracellular polymer linker and dielectrophoresis (DEP) technique.

Cells grown in microfluidics are sorted by various methods, namely cell affinity chromatography, magnetic activated cell sorting and differences in cellular biophysics such as cell size, adhesion, deformability, dielectrophoresis, and impedance [13].
1) Cell affinity micro chromatography sorters: In this method cancer cells selectively bind to substrate immobilized high-affinity ligands by separating healthy cells from a heterogeneous mixture (Du *et al.*).
2) Magnetic activated cell sorters: In this cell, sorting happens on the interaction between cell surface antigens and antibodies conjugated to suspended magnetic particles. This technique readily permits the manipulation of captured cancer cells using a magnetic field.
3) Size based sorters: In this system separation happens based on the size of the cell. Mohamed *et al.* reported the 1st size based sorter microfluidic chip with four decreasing channel width.
4) Dielectrophoresis (DEP) based sorters: DEP uses the polarization of cells in the non-uniform electrical field to exert forces on cells.

Collagen-based microfluidics is one of the commonly used 3D cell culture systems to study cancer cell behaviors like cell migration, response to drug candidates [65] [4]. Scientists have also attempted to recapitulate some parts of the TME by co-culturing cancer-stromal cells. Drifka CR *et al.* studied the interaction between PDAC and PSC cells and paclitaxel drug response in tri-layered ECM coating in microfluidic chip [23].

Cells were grown as a 2D monolayer on plastic or glass surface typically show spread morphology and experience uniform access to nutrients whereas cells in 3D grow as multilayer aggregates, experience gradient nutrient accessibility that is usually observed *in vivo.* Interestingly certain cells like colorectal cancer cells, HEK293, mammary epithelial cells when grown in 2D show higher proliferating rates than grown as 3D whereas some breast cancer cells grow faster in 3D than in 2D. This could be because cells show differential gene expression patterns, between 2D and 3D culture, that are associated with cell proliferation, migration, invasion, angiogenesis, and chemosensitivity [23]. Comparison studies in gene expression show ˜30% of the genes are differentially expressed between cancer cell lines like breast, colon, lung etc. and their tissue origins [23]. Intriguingly, cells when removed from *in vivo*

and cultured in 2D loose native characteristics but, when the same cells are placed back either *in vivo* or in basement membrane based 3D they retain their characteristic features [23], [59], This indicates the importance of using 3D based cell culture systems that recapitulate the *in vivo* like phenotype and genotype. In fact, the 3D cell culture system is increasingly recognized as an attractive alternative to most commonly used 2D cell culture systems to study cancer cell behavior particularly screening for anti-cancer drugs.

1.6 Differential drug responses between 2D and 3D cell culture models

Various research groups have studied drug responses by cancer cells in 2D and 3D culture models. Cancer cells especially were grown in 3D respond to drugs differently depending on both cell type and the scaffold used in culture. For ex-human breast cancer line, SKBR3 cells grown on polyHEMA showed more sensitivity to trastuzumab than even cells grown in 2D [84]. Whereas SKBR3 and other cells were grown in matrigel exhibited increased resistance to trastuzumab in contrast to cells in 2D monolayer [106]. However, another drug screening study against breast cancer cell line JIMT2 reveals that cells in 3D matrigel are more sensitive than cells in 3D polyHEMA [49]. Similar higher drug resistance was observed in ovarian cancer cells treated with paclitaxel when they were grown in 3D hydrogel matrix that consists of integrin binding motifs (RGD peptides) in contrast to cells in the 2D model [69], breast cancer cells in 3D biodegradable polymer and bladder carcinoma in 3D spheroids treated with doxorubicin. The reasons for higher chemoresistance in 3D models could be due to the inefficient drug penetration, cell-matrix interaction mediated increased cell survival signaling [50] [29].

For PDAC treatment fluorouracil-based chemotherapy was the mainstay of since the 1950s which showed a mean survival duration of ˜3 months [78]. Since then there have been many drugs that are developed and used either solely or in combination with other drugs against PDAC that improved the survival duration ranging between 4 to 9 months [99]. For example, patients receiving gemcitabine was the first drug to increase the overall survival of patients more than Fluorouracil by 2.7 months [11]. Gemcitabine, in combination with other drugs like cisplatin, oxaliplatin, erlotinib etc., is currently most widely used the drug in the treatment of PDAC with the marginal increase in overall survival by up to 3-6 months [99] [82]. The mechanism

of action of gemcitabine on pancreatic cancer cells and the mechanism of resistance shown by pancreatic cancer is outlined somewhere else [37].

In our work, we employed a single chemotherapeutic agent, cisplatin to study the differential responses of cells grown in different culture systems. Cisplatin, [Pt(NH3)2Cl2], was first synthesized in 1844 by M Peyrone and its chemical structure was resolved by Alfred Werner in 1893. However, cisplatin gained the importance in medical investigations only since 1965, when Rosenberg *et al.*, at Michigan State University showed for the first time that cisplatin treatment inhibited the cell division of E. coli but not cell growth. This discovery prompted attention to use cisplatin as a potential drug against cancer. Cisplatin has indeed showed anticancer activity in many solid cancers such as cancers of ovaries, testes, head, and neck. Eventually, cisplatin became the first platinum-based drug that was approved by Food and drug administration (FDA) authority for cancer treatment in 1978 [58]. The mechanism by which cisplatin inhibits cell growth and exhibit cytotoxicity is not fully understood but believed to induce DNA damage in the cells.

In our studies, we employed three of the most commonly used PDAC cells, BxPC3, MiaPaCa2 and PANC1 for comparative studies in terms of growth kinetics and cisplatin drug responses in 2D, agarose-based 3D spheroids, 3D collagen-based microfluidics systems and *in vivo.* Scientists have isolated various PDAC cell lines from the patients, either from the primary site or metastasized organs, and characterized the genotypic as well as phenotypic behaviors *in vitro* and *in vivo.* Table 1.1 is the compilation of characteristic features of three of the most commonly used PDAC cell lines; PANC1, MiaPaCa2 and BxPC3 cells that we employed in our studies.

Table 1.1: Characteristic features of three PDAC cell lines; PANC1, MiaPaCa2 and BxPC3

Description	**PANC1**	**MIAPACA2**	**BXPC3**
Source	56y old male Caucasian. Isolated from the head of pancreas. Metastasis was observed in peripancreatic lymph node [67]	65y old male. Tumor involved both tail and body of pancreas and metastasized in to periaortic area [113]	61y old female. Tumor development on the body of pancreas. No evidence of metastases observed [97]
Key Gene Mutations	KRAS: G12D,	KRAS: G12C	KRAS: WT
	TP53: R273H	TP53: R248W	TP53: Y220C
	CDKN2A: HD	CDKN2A: HD	CDKN2A: WT/HD
	SMAD4: WT	SMAD4: WT.	SMAD4: HD
	[18]		
Anchorage independent growth [63]	>800 colonies (seeding cell number 3000)	∼700 colonies (seeding cell number 3000)	∼200 colonies (seeding cell number 5000)
Cell adhesion	Collagen1 PANC1 and BxPC3 show almost similar affinity to collagen1 substrate that is higher than MiaPaCa2.		
	Collagen IV: Between the three cell lines, Panc1 shows highest affinity followed by MiaPaCa2 as moderate and BxPC3 has lowest affinity for Col-IV.		
	Fibronectin: Studies show that the degree of affinity of these three cell lines for fibronectin is inconsistent and inconclusive as summarized by Deer L *et al.,* 2010		
	Laminin: In summary all three-cell lines show similar affinity towards laminin binding [39] [79] [5]		
Pro-angiogenic factors	Cox-2: BxPC3 has more than 30X levels of cox-2 than PANC1 and MiaPaCa2 [18]		
	VEGF: BxPC3 has more than 1.7X fold VEGF than PANC1 and 5.3X fold than MiaPaCa2 [72]		

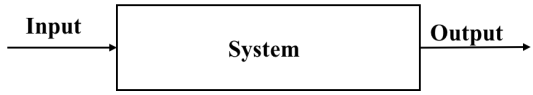

Figure 1.4: *Pictorial representation of mathematical modelling key features*

Table 1.1: Characteristic features of three PDAC cell lines; PANC1, MiaPaCa2 and BxPC3

Description	**PANC1**	**MIAPACA2**	**BXPC3**
Invasive abilities	Matrigel: Various studies have consistently shown that all three cells are equally invasive in matrigel [39], [96], [35], [80]. Invasion comparison of all three cells on other ECMs has not been performed.		

1.7 Mathematical Modelling

Oxford English dictionary states, a model is "a simplified or idealized description, representation or conception of a particular system, situation, or process, often in mathematical terms, that is put forward as a basis for theoretical or empirical understanding, or for calculations, predictions, etc." Mathematical Models can be simple as possible, yet as complex as necessary to describe the given question of interest.

George Box states that 'All models are wrong, but some of them are useful'.

In other words, mathematical modeling represents the existing system in a usable form. So the models are in a simplified form not the replicates of reality. This simplification allows presenting the essential features leaving the burden or unnecessary details [94]. While building a mathematical modelling we should consider key features such as 1) List of quantities, which can be measured or observed called as 'output' 2) List of quantities, which can be controlled or acted upon called as 'input' and 3) System, where the process takes place (Figure 1.4).

Mathematical models typically consist of 1) Variables: These are either dependent or independent. 2) Parameters: These can be varied during the experimental conditions and 3) Constants: Fixed values.

Based on the above concept, there is a great variety of mathematical modeling. The following are the some of the main categories [94] [110]. Firstly, categorized based on type of outcome they predict such as 1) Deterministic Model: These model always predict the same output from the starting point by ignoring the random variation 2) Stochastic Model: In this model, the outcome is more statistical and has all the possible outcomes. Secondly, categorized based on the level of understanding of the data. In this again there are two types 1) Mechanistic Model: In this type of modeling they take an account of the mechanism through which the change occurs. 2) Empirical Model: These type of modeling they don't consider any mechanisms. Indeed, it is a change occurred. Thirdly, categorized based on the relationship between the parameters used in mathematical modeling. 1)Linear Model: In this input and output parameters are linearly related 2)Nonlinear Model: In this input and output parameters are not linearly related

1.8 Mathematical Modelling in Biology

These mathematical models are used in biology process for a long time to simulate the data. This has many advantages as [110]

1. It helps in summing up of large volume of experimental data
2. In exploring the concepts and testing the hypothesis
3. Predicting the behaviour of the systems under non-tested conditions
4. Identifying the conditions for optimal performance of a process

In addition to understanding, mathematical models also simulate the complex system in a relatively fast time without the enormous cost of lab expenditure and biological variation. These mathematical models have the power to reveal the previously unknown or counterintuitive physical principles that might have been overlooked or missed by a qualitative approach to biology. These models can be adapted to complement or even replace *in vivo* or *in vitro* experiments for the interpretation of biological phenomena. Mathematical models have proved in understanding the mechanism and processes in cancer and have been *in a silicon* trial that predicts different treatment modalities [8]. These mathematical models systematically evaluate assumption, investigate alternative mechanism and make predictions. These predictions can be validated.

With the recent advances in medical and computational methods, mathematical biology has grown extensively. Mathematical biology has covered a submicron length of DNA polymers to the kilometer length scale of migration patterns of animal herds. It has been applied in a broad spectrum of life science. The main contribution of mathematical modeling in the areas of biology and medicine are epidemiology, cell physiology, cancer modeling, genetics, cellular biology, and biochemistry.

1.9 Mathematical Modelling in Cancer

As we stated earlier cancer is a complex disease, multiple factors involved in the carcinogenesis of this disease such as DNA replication, errors in cells, interactions between cells and the tissue microenvironment and environmental factors such as radiation and diet. Therefore, an understanding of this disease is required from the point of the cell to its environment. Mathematical models have proved in understanding this disease from the mechanism and processes involved in this [2].
The use of mathematical models to study cancer dates back to many decades. The evolvement of mathematical models in cancer is represented in figure 1.5. The first mathematical modeling to study cancer was in 1950, during those days' models were simple in terms of maths. The advancement in the mathematical filed in 50 years has enormously increased the knowledge of modeling [2]. There are many mathematical models to describe cancer at various stages of cancer.

Cancer initiation and hierarchy can be explained by the mathematical model using 'Branching process' and its commonly used model in cancer evolution. It helps in understanding dynamics of mutation accumulation. Passenger mutation and driver mutation of the tumor growth have been analyzed using branching process. Branching process is a stochastic process model of cell division, mutation events and cell death that leads to increase or decrease in total population size. The model starts with single cell harboring a specific driver mutation then accumulates the further mutation during the subsequent cell division. As the mutation accumulates in a cell population, each new cell type has a new set of rates. These models depend only on the current state of the population and not the past. Later in the improvement of these models, epistatic interactions are added to this

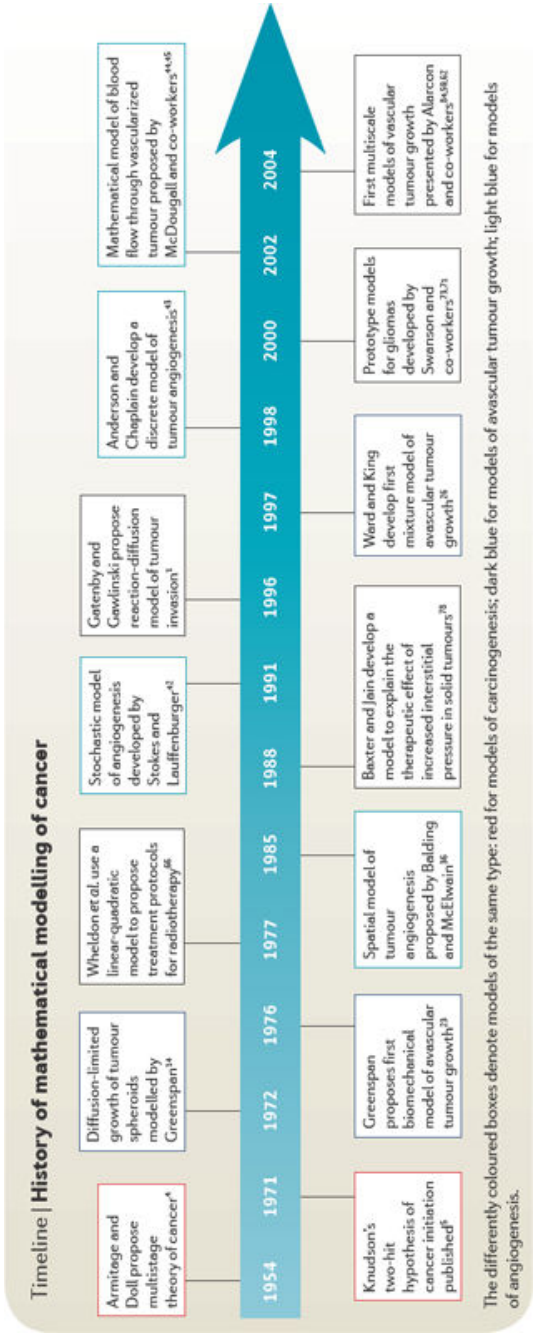

Figure 1.5: *History of mathematical modelling of cancer (Adapted from [12])*

branching process. These epistatic interactions help in understanding the alterations depend on the genetic background of the cell. Still, these branching process rarely describe the interactions between the cells and microenvironment. The dynamics of mutation accumulation can also be studied using other stochastic models such as Wright-Fisher process.
Modelling the tumour microenvironment need complex mathematical models. Usually, partial differential equations are used for describing uniform spherical spheroidal growth. They also use the discrete model to describe individual cell and continuum deterministic model for the cell population. These models also include dynamic of nutrients, chemical factors, and extracellular matrix. Markov process of discrete stochastic models describes cell growth, migration, and interaction.
Mathematical modelling of metastases has long been recognized. Earlier mathematical models explain the competition between cancerous and healthy tissues. Now a day many mathematical models describe development and predictors of metastases by modeling dormancy and cell kinetics.
Treatment response and resistance acquired are modeled using stochastic processes. Linear and quadratic models have been used in radiotherapy.

1.10 Mathematical models of tumour growth

There are several growth models to explain the tumor growth kinetics in heterogeneous tumors and its interaction with subclonal population, differential response to therapy and differential metastatic characteristics. Here we explain only about the growth of cancer cells, which has unbounded growth rate theoretically exponential having constant doubling time. Practically exponential growth is true for small tumors, but it decelerates as the time progress. To address this deceleration of growth there are many growth models [87]. Here we explain few models, which are widely used in cancer studies to address the growth and deceleration rate of cancer cells. The classical growth models are logistic, Gompertz and von Berta-lanffy models [77].
Logistic Model: The Logistic model is the most commonly used model for estimation of tumor growth. It was first formulated by Pierre Fran coins Verhulst in 1838 [36]. This model is used to explain the dynamics of a population using growth rate, whose population is limited by a carrying capacity. Carrying capacity is at which cells reach maximum growth. According to this model, there is a linear decay in the volume of the relative growth.

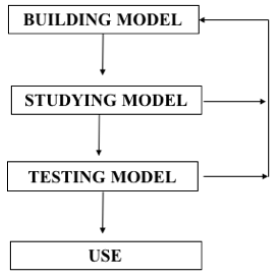

Figure 1.6: *Steps involved in building mathematical modelling*

Gompertz model: It is widely used model to show the growth of a variety of tumors of mouse, rat, and rabbit. Gompertz means the equal proportion of the 'power to oppose destruction'. According to this model, the growth is considered as exponential process limited by an exponential retardation. In this, the growth of a tumour is interpreted based on the exponential proliferation of tumor cells according to the exponential equation [62].
Von Berta-lanffy Model: According to Van Bertanlaffy, both the rate of production and destruction follow the law of allometry. The law of allometry states that they scale with a power of the total size. The van Bertanlaffy equation was developed by Beverton and Holt in 1957. It is used mostly in fishery biology to study the fish population dynamics. When the destruction term is neglected, the von Bertalanffy model reduces to a power law for applications to tumor growth [62]. These growth models are based on balance equations of metabolic processes.

1.11 Stages of Modelling

There are mainly four stages involved in modeling any data. The schematic representation stages involved in building model is represented in figure 1.6

1. Building Model

    - ***Objective:*** Getting started we need to be clear about our objective so that we know the purpose and usage of the model. After setting up the objective, divide the system (data) into 2, one which can be modeled another one has the surrounding system, which can't be modeled.

- **System Analysis:** In this assumption of the data has to be done. Later we need to give the basic framework for the model, which explains how the model works.
- ***Choose the mathematical equation:*** Once we know our system structure, we should select the mathematical equation that describes the system. This can be done from the literature since some areas of science are intensively studied so it's appropriate and safe to choose them. We can also choose the equations by fitting the data got from our experiments.
- ***Solving equations:*** Then these mathematical equations can be solved to get the numerical solutions.

2. Studying Model
   Once we build the model, we need to understand the qualitative and quantitative behavior of the model. Qualitative helps in understanding 'how' the model is fitted, however, quantitative helps in knowing 'how much'. Later we need to identify the sensitivity of the model, which identifies the weak point of the model.

3. Testing the Model
   After identifying all the factors, we need to test our built model against different observations, this is also called as validation. This helps in the verification of the predictions and how much the model is faithful.

4. Using Model
   Model is ready to use with all the information. It can be used to test a new set of data.

We followed these stages to build the mathematical model for pancreatic ductal adenocarcinoma cells (PDAC) growth.

1.12 Objectives

Pancreatic cancer is the fourth leading cause of death in western society presenting a 5-year survival rate of 3% and a median survival of fewer than 6 months. This is due to its aggressiveness, high incidence of metastasis, inability to detect the disease at an early stage, lack of specific symptoms and diagnostic methods strongly limit the treatment options for patients affected

by pancreatic cancer. In spite of recent advances in medicine there are few or no effective therapies for advanced pancreatic cancer, clearly, there is a thorough understanding of this disease is strongly needed to design effective interventions. Hence we aimed to study pancreatic ductal adenocarcinoma (PDAC) human cell lines in different models.

1. Characterisation of Pancreatic ductal adenocarcinoma (PDAC) cells in different culture models
    - Studying PDAC cells in Two-dimensional culture (2D) system
    - Studying PDAC cells in Three-dimensional culture (3D) system
    - Studying PDAC cels in novel microfluidic chip
    - Comparison of drug Cisplatin resistance within *in vitro* system and *in vivo*
2. Developing mathematical model for pancreatic ductal adenocarcinoma (PDAC) cells

Chapter 2

Characterisation of Pancreatic ductal adenocarcinoma (PDAC) cells in different culture systems

2.1 Introduction

The understanding of a tumor biomolecular features and growth dynamics and the identification of novel targeted therapeutic strategies is being one of the major challenges in oncological research. Various cell culture platforms have been developed and employed both *in vitro* and *in vivo* models for pre-clinical studies [74], [31]. Two-dimensional (2D) cell culture has been the cornerstone of many studies including drug testing ever since the success in growing the mammalian cells *in vitro*. However, 2D cell culture is a simple system that fails to mimic the complexity of biological systems, especially diseases like cancers. In particular 2D culture is a monolayer of cells whereas cells situated *in vivo* are organized as 3D architecture which is surrounded by other cell types, extracellular matrix proteins and other factors. Due to these fundamental differences cancer cells grown as 2D monolayers do not experience the ECM-cancer cell interactions, intra-tumoral gradients in terms of pH, oxygen and nutrients availabilities that are typical characteristics of the cancer microenvironment. Hence many drugs, that pass pre-clinical *in vitro* testing, fail in the patients [16], [26], [10], [101]. *In vivo* studies, on the other hand, typically use mouse models for ex-subcutaneous or orthotopic xenografts of human tumour cells in immuno-compromised mice that

poorly recapitulate the proper tumour behavior and undermine the impact of the tumour microenvironment, in particular of acquired immunity. Moreover, animal models are expensive, time-consuming and under some aspects "non-ethical" [26], [10].

In order to bridge the gap between simple 2D and *in vivo* animal models for cancer studies scientists have been using an alternative 3D cell culture model. 3D cell culture can be broadly classified as scaffold-free and scaffold-based. Scaffold-based 3D includes growing the cells on a simpler hydrogels likes agarose or complex ECM like collagen or matrigels. Cells grown on agarose forms 3D spheroids likes structures that mimic physiological conditions over 2D monolayers, as 3D resembles more accurately the architecture and biomechanical properties of the tumour tissue.

Further, 3D spheroid cultures lead to reproducing several parameters of the tumour microenvironment, including oxygen and nutrient gradients as well as the development of a dormant tumour region [46], [89]. Overall, 3D cultures allow to monitor cell growth dynamics and response to treatments more appropriately, and could hence fill the gap between *in vitro* and *in vivo* systems for preclinical oncological research. As a result, there has been increasing focus in developing 3D techniques, and many different platforms have been proposed, with different grades of complexity and expression of a tumour microenvironmental conditions [10], [28].

To further increase the complexity of the 3D culture, cells can be grown under the influence of ECM like collagen1 that are particularly abundant in pancreatic ductal adenocarcinoma (PDAC). However, the possibilities to manipulate the cells under 3D are also desirable feature of the cell culture systems. Advancement in microfluidic technologies where cells are transported and manipulated in micro-channels and we can engineer living cellular microsystems with controllable microenvironments that behave and function – with organ-level complexity like their counterparts *in vivo* [7], [52], [103], [30], [53]. Further microfluidics enable the possibilities to control few parameters like fluid flow, perfusion systems for the continuous supply of nutrients and drugs and collection of cell-spent media for analysis. Recently microfluidics reached a significant milestone with the development of "organ-on-chip" technologies Organ-like features include continuous perfusion and physiological cell–matrix and cell-cell interactions. More recently, the "organ on chip" technology has been transferred to study human disease models, including cancer [1], [21], [92], [104], [112], [114]. As a further step,

the combination of microfluidics and dielectrophoresis (DEP) to assemble primary human cells, has enabled the automated *in vitro* construction of micro-organs, which mimic proper *in vivo* structures. As a unique feature of organ-on-chip technology, the use of DEP selectively assembles only viable cells [91], [47]. For the HepaChip® organ-specific 3D cell culture chambers are designed and validated by multiphysics simulations and realised by injection moulding of the cyclic olefin polymer (COP) [91], [41], [48]. Proprietary surface functionalization enables selective deposition of ECM proteins in a simple perfusion process [90]. High resolution optical imaging of micro-organs along with the complete set of staining technologies is possible due to the exceptional optical properties of COP. We applied these concepts to create a novel platform for studying pancreatic ductal adenocarcinoma (PDAC), one of the human cancers with worst prognosis, for which the design of novel therapeutic options is urgently needed. For these reasons, various model systems are being developed, from *in vitro* 2D and 3D cell cultures, to whole animal models [54].

In this chapter, we explain about culturing human PDAC cells in all the three different culture systems and studied the differences in morphological appearance, growth characteristics and response to chemotherapeutic drugs.

[1]

2.2 Materials and Methods

2.2.1 Cell lines

Three human pancreatic ductal adenocarcinoma (PDAC) cell lines; PANC1, BxPC3 and MiaPaCa2 were used for our experimental work. The PANC1 and MiaPaCa2 cells harbor a mutation in KRAS and TP53, homozygous deletion (HD) in CDKN2A/p16 and wild type (WT) SMAD4, while BxPC3 cells harbor mutation in TP53, HD in SMAD4 and WT KRAS [18].

[1] This chapter has been published as "A novel microfluidic 3D platform for culturing pancreatic ductal adenocarcinoma cells: comparison with *in vitro* cultures and *in vivo* xenografts" in *Scientific Reports* 7, *Article number:* 1325 (2017)

2.2.2 Two dimensional (2D) cell culture

Cell culture

PANC1 and MiaPaCa2 cells were cultured using Dulbecco's Modified Eagle Medium (DMEM) supplemented with 10% defined fetal bovine serum and 4mM glutamine. BxPC3 was cultured using RPM1-1640 medium supplemented with 10% defined fetal bovine serum and 2mM glutamine. Cells were cultured in a humidified 5% CO_2 at 37°C.

Growth Profile

For studying growth profile of PANC1, BxPC3 and MiaPaCa2, ten thousand cells were initially seeded into each well of 96 well plate containing 200 μL of respective media. Cells were maintained in a humidified 5% CO_2 at 37°C. Cell growth was estimated every day by trypsinizing the cells and manual counting using trypan blue method.

Live/Dead cell imaging

Cell viability was done by Calcein-acetoxymethyl(AM) and Propidium Iodide (PI) staining. Calcein-AM is a membrane permeable live-cell labeling dye. After acetoxymethyl (AM) ester group enters the live cells, cleaves the intracellular esterases, yielding the membrane-impermeable Calcein fluorescent dye, which gives a green color to the live cells. Calcein is excited at 495 nm and has a peak emission of 515 nm (Green color). Propidium Iodide is a membrane impermeable. PI binds to DNA of dead cells by intercalating between the base pairs and gives red color. PI is excited at 488 nm and has a peak emission at 617nm (Red color). We used this technique to observe the cells. After 48H of culturing, cells were incubated with Calcein-AM (2 μg/mL) propidium iodide (10 μg/mL) for 20 minutes in the fresh culture medium. Then washed with PBS and Images were taken using Nikon fluorescence microscope.

Effect of cisplatin

Cisplatin is a platinum-based drug used in the treatment of most of the cancers. We used this drug to identify the IC_{50} (which is the concentration to kill 50% of the cells) value for PANC1.

Drug treatment:To find out the IC_{50} value, ten thousand cells were seeded per well in 96 well plate. After 24H of culturing, cells were treated with different concentration of cisplatin such as 1, 2.5, 5, 10, 25, 50 and 100μM. Meanwhile cells were maintained without cisplatin also for control conditions.

Analysis of drug efficacy: After 24H of drug treatment, cells were detached using trypsin and counted manually using trypan blue.

Estimation of IC_{50}: IC_{50} values were calculated using origin, by fitting sigmoid dose-response curve for the cell density calculated at different concentration of cisplatin-treated cells.

Cytoskeleton Staining

Cytoskeleton structure was studied by staining on actin filaments. To stain the actin filaments firstly thin glass-cover slips were ethanol and flame sterilized. Then cells were seeded on the glass coverslips for 24H. The unattached cells were washed away with PBS and cells were fixed with 4% methanol-free para-formaldehyde (PFA) for 20 minutes at RT. Cells were permeabilized with 0.01% Triton-X for 5 minutes at room temperature, washed with PBS. Nonspecific sites were blocked using 10% BSA for 1H. Then cells were stained using Rhodamine-conjugated phalloidin at room temperature for 1 hour at dark, followed by nucleus staining using DAPI (Invitrogen). Then these coverslips were mounted using ProLong antifade mounting solution (Invitrogen). Images were captured using a C1 confocal microscope (Nikon).

2.2.3 Three dimensional (3D) cell culture

Cell Culture

Three-dimensional spheroids were generated using liquid overlay technique. Cells were trypsin treated and counted using trypan blue. Subsequently cells were seeded onto agarose-coated (1.5% agarose 50μL/well) 96 well plate in 100 μL of medium [14]. Figure 2.1 shows the spheroid formation on agarose-coated well. After 72H, 100 μL medium was added and afterward for every 48H, 50% of the supernatant was replaced with fresh medium. Spheroids were cultured in a humidified 5% CO_2 at 37°C.

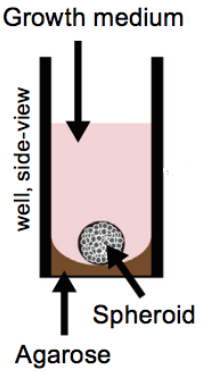

Figure 2.1: *Schematic representation of agarose coated well with cells forming spheroids [107]*

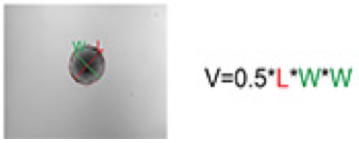

Figure 2.2: *Volume estimation by SpheroidSizer program. The volume was calculated using major and minor axis. L - major axis: the line segment connecting a single pair of farthest points on the contour (referred to length); W - minor axis: the longest line perpendicular to the major axis (referred to width) (taken from [14])*

Growth Curve

For growth curve experiments, five hundred cells were seeded on to agarose coated 96 well plate and maintained for 10 days as mentioned above. Every day spheroids were imaged using bright field microscopy (Nikon) to estimate cell growth with a 10x objective. Volume was calculated using the major and minor axis of the spheroid as shown in the figure 2.2. Image resolution at this objective was 0.757 μm/pix. Spheroid volume was calculated using MATLAB SpheroidSizer program as reported by Chen W. *et al.* ([14]). Figure 2.3 shows the screenshot of volume estimating using MATLAB.

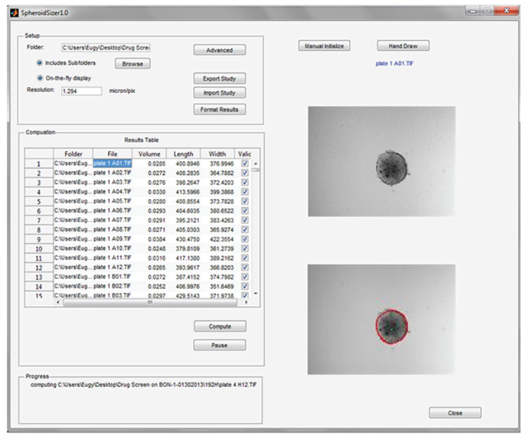

Figure 2.3: *Screenshot of SpheroidSizer, in which the volume is displayed based on the volume measurement (taken from [14])*

Live/Dead cell imaging

After 72H of culturing, cells were incubated with Calcein-AM (2 μg/mL) propidium iodide (10 μg/mL) for 20 minutes in the fresh culture medium. Then washed with PBS and Images were taken using Nikon fluorescence microscope.

Effect of cisplatin

To determine the IC_{50} of cisplatin, the cisplatin concentration to kill 50% of the cells, we treated PANC1 3D spheroids with different concentrations of cisplatin.

Drug Treatment: Initially, 1000 cells were seeded per well (96well plate). Once the spheroids attained specific volume i.e. after 72H, spheroids were treated with 0, 5,10, 20, 50 and 100μM of cisplatin diluted in 200μL of the medium. Untreated spheroids were also cultured in parallel as control. Spheroids were maintained without changing medium for the whole experiment.

Analysis of drug efficacy: After 72H of drug treatment, 20 to 30 spheroids were collected, washed with PBS. Spheroids were dissociated using 5mM Ethylenediaminetetraacetic acid (EDTA) and incubated with propid-

ium iodide (PI) (0.05μg/mL) for 5 min. Stained cells were analyzed using flow cytometer.

Estimation of IC_{50}: IC_{50} values were calculated using origin, by fitting sigmoid dose-response curve for the cell density calculated at different concentration of cisplatin-treated cells.

Cytoskeleton staining

Cytoskeleton structure was studied by staining actin filaments. To stain the actin filaments, we started culturing 1000 cells per well (agarose coated 96well plate). Once the spheroids attained specific volume i.e. after 72 h of culturing, spheroids were fixed with 4% formaldehyde, then permeabilized using 0.01% Triton-X for 5 minutes at room temperature, and washed with PBS. Cells were then blocked using 10% BSA for 1 h at room temperature and then stained using rhodamine- conjugated phalloidin at room temperature for 1 hour under dark condition. The nucleus was stained using DAPI (Invitrogen). Images were captured using a confocal microscope (Nikon Eclipse TE2000-U).

2.2.4 Microfluidic device cell culture

Microfluidic Chip design

Microfluidic chips were made of cyclic olefin copolymer (COC) Topas 5013 by microfluidic ChipShop, Jena, by microinjection molding [91], [41], [48]. The COC chip was cleaned with isopropanol and dried under nitrogen flow. Subsequently, the COC surface was irradiated through a mask using a low-pressure mercury lamp (Heraeus Noblelight, Hanau, Germany, NIQ lamp, l $\frac{1}{4}$185 nm, quartz tube, 5 W) to achieve site-specific formation of reactive carbonic acid groups (Figure 2.4). These activated groups were blocked by Collagen from a 20 μM solution for 90 min and nonactivated groups were blocked with Pluronic F127 [90]. Then chip was sealed with an adhesive foil (polyolefin cover foil, HJ-Bioanalytik Moenchengladbach).[2]

The device comprises eight identical cell chambers, containing three cell culture regions each, sized 1 mm x 60 μm, i.e. 24 cell culture regions per chip. On the sidewalls of each cell chamber electrodes are integrated which are used to generate an inhomogeneous high-frequency electrical field. This gives rise

[2]Microfluidic work was done in collaboration with NMI Germany

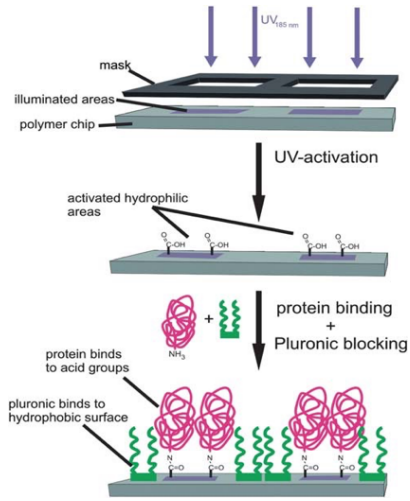

Figure 2.4: *Process scheme applied for patterned surface biofunctionalization in microfluidic devices by UV-irradiation and subsequent binding of collagen and Pluronic F-127 (Taken from [90])*

to dielectrophoretic forces by which cells entering the cell chamber are drawn into the assembly areas. Only viable cells will be selectively assembled as only they exhibit intact cell membranes with their intracellular permittivity differing from that of the extracellular medium they are suspended in.

The microfluidic device was mounted in a fixture providing for fluidic, electrical, and thermal contact and control of the chip by an external periphery unit containing Polytetrafluoroethylene (PTFE) tubes and syringe pumps as well as a function generator, amplifier and electronic heat control as shown in figure 2.5.

Cell assembly and culture in HepaChip

Cells were suspended in a DEP medium exhibiting an especially low conductance of 80 to 200 μS/cm. It comprised 95 g/L sucrose, 1 g/L glucose, 57.9 mg/L sodium pyruvate, 28.4 mg/L calcium chloride and 24.6 mg/L MgSO4 (aq). From this suspension, cells were assembled by dielectrophoresis at a flow rate of 100 μl/min, a peak to peak voltage between 140 and 150 V and a frequency of 350 kHz, for durations of 3 to 5 min. After cell assem-

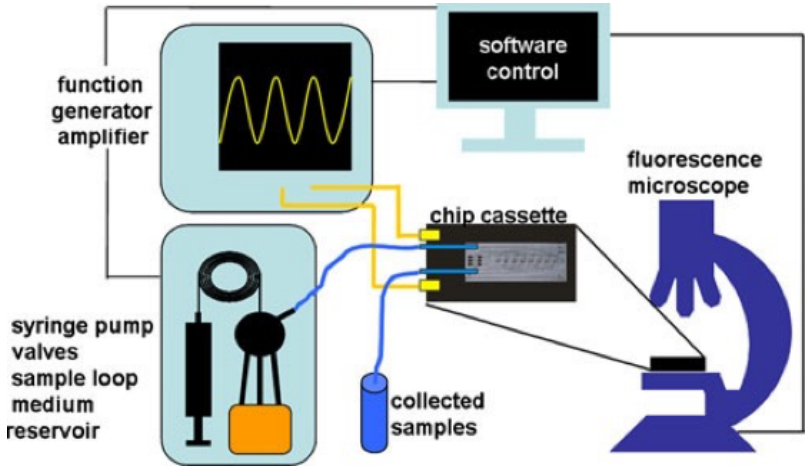

Figure 2.5: *Experimental setup: the chip is inserted into a chip fixture, which is mounted onto a fluorescence microscope (adapted by [91])*

bly, the culture medium was perfused through the chip for 3 to 9 days at a perfusion rate of 3.125 μl/min. During culture the chips were maintained at temperatures between 35°C and 37°C while the medium reservoirs were heated to between 37°C and 39°C. To make sure that no gas or air bubbles enter the microfluidic chips, a bubble trap was inserted in the inlet tubing of each chip. In this trap, the medium flows underneath a gas permeable PTFE membrane where bubbles can exit but the medium is kept inside the system.

Viability assay in HepaChip

Each day the cells in the microfluidic chip were stained with green fluorescent Calcein AM (2 μg/mL) and red fluorescent propidium iodide (10 μg/mL) in order to visualize viable cells in green and nuclei of dead or dying cells in red. After incubating with the staining solution for 20 min at 7μL/min the chip was washed with culture medium before the perfused culture restarted. Images were captured with Nikon DS 2MBWc microscope camera using Nikon Eclipse Ti.

Phalloidin staining in HepaChip

The chip was flushed with 4% paraformaldehyde for 20 min at 15 μL/min to fix the cells. Next the cells were permeabilized by pumping phosphate buffered saline (PBS) with 1% Triton X through the chip for 10 min at a flow rate of 50μL/min. Then cells were stained with green fluorescent Phalloidin and DAPI in PBS for 20 min at 15 μL/min and finally washed with PBS at 50 μL/min. The cells in the chips were then imaged as those stained in the viability assay.

Effect of cisplatin in HepaChip

After 24H of culturing PANC1 and BxPC3 on microfluidic culture, 0μM, 25μM, and 100μM cisplatin were continuously perfused for 72 hours at a rate of 3μL/min. Then viability was checked as stated in viability assay.

2.2.5 *In vivo* experiments on nu/nu mice

In vivo experiments were performed at Dival Toscana Srl, inside the Animal Facility of the University of Florence. All experiments on live vertebrates were performed in accordance with relevant guidelines and regulations. We confirm that the Ethical Committee of the University of Firenze approved all the experiments described. Female, 9 weeks aged, athymic nude nu/nu mice (Envigo-Harlan Italy; Udine) were subcutaneously (s.c.) injected with 3x10^6 PANC1 cells per mouse.

Effect of cisplatin *in vivo*

Mice were treated daily intraperitoneal (i.p.) with cisplatin (10 mg/kg) (n=4 masses) or with saline (n=4 masses) for one week, starting the day the masses reached the measure of (0,2 x 0,2 cm). Tumor growth was monitored daily by measuring two perpendicular diameters, the volume of the tumor masses was calculated using the ellipsoid equation. At the end of the treatment, all mice were sacrificed, and tumor masses were collected measured and weighted.

2.2.6 Statistical Analysis

Data are generally given as mean values $\pm$ standard error of the mean (SEM), with n indicating the number of independent experiments. When the mean $\pm$ standavd deviation (SD) was calculated, it is indicated in the figure legend.

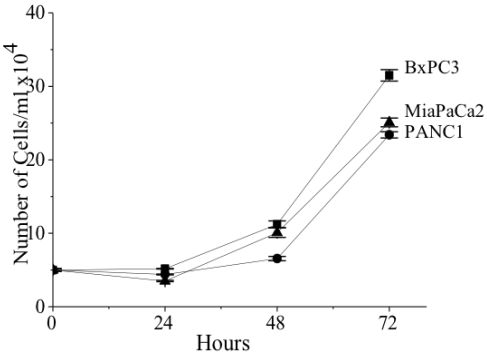

Figure 2.6: *Growth rate comparison of three PDAC cell lines in terms of increase in a number of cells per day (n = 3). Data represented are means ± SEM of three separate experiments each carried out in triplicate. At the 0.05 level, the PANC1, MiaPaCa2, and BxPC3 are not significantly different in growth rate. (Taken from B in which I am a first co-author).*

Statistical comparisons between two groups of data were performed with the Mann-Whitney test.

2.3 Results

2.3.1 Two dimensional Culture (2D Culture)

Growth Profile

Three human PDAC cell lines (PANC1, BxPC3, and MiaPaCa2) were cultured to study the growth characteristics. Thorough characterization of these cell lines, along with other PDAC cells, with respect to genotypic and phenotypic properties, are reviewed by Deer EL *et al.*, 2010 [18]. To compare the growth rate, ten thousand cells were seeded per well in a 96 well plate containing 200μL of media. Every day cell density was estimated by trypan blue method. All the three cell lines grew at the same rate with a maximum cell count of 3×10^5 cells/ml after 72 hours of incubation (Figure2.6).

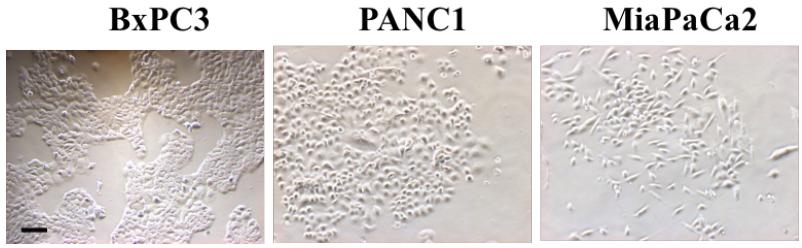

Figure 2.7: *Microscopic images of PDAC cell lines after 48 h of culturing. The difference in morphology was observed among the cell lines. Scale bars represent 100 µm. (Taken from B in which I am a first co-author).*

Morphology

Pancreatic ductal adenocarcinoma (PDAC) cell lines morphology was studied using phase contrast image of 48H of the cultured cell shown in figure 2.7. PANC1 displayed heterogeneity in phenotype with not fully epithelial, more mesenchymal structure, but more adherent to the substrate. MiaPaCa2 has two types of structure (1) adherent cells with a mesenchymal morphology, with round body and more or less long and substrate adherent cytoplasmic extensions and (2) round, fewer adherent cells. Similar observations were made by Rui *et al* [38]. in immunohistochemistry analysis. BxPC3 cells showed flattened morphology unlike PANC1 and MiaPaCa2 cells and also with the tendency to grow as small "islands". These cells are more adherent to substrate compared to PANC1 and MiaPaCa2 cells.

Live/Dead cell imaging

Cell viability was also studied by fluorescence microscopy in which cells were incubated with calcein and propidium iodide (PI) as mentioned in material and methods. In live cells esterase will convert non-fluorescent calcein into green fluorescent whereas only dead cells take up PI, red fluorescent. Roughly all the PDAC cells in 2D cultures are vital after 48 hours of incubation, as witnessed by the Figure 2.8.

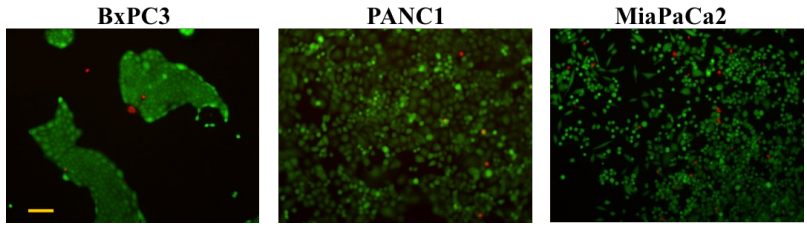

Figure 2.8: *Live and dead cells staining, showing live cells by green (Calcein) and dead cells by red (PI) after 24 h of culturing. Scale bars represent 100 µm. (Taken from B in which I am a first co-author).*

Cytoskeleton structure

One of the functional characteristics of cancer is their propensity to migrate, an essential step for metastatization. During cell migration cells undergo morphological changes in cytoskeleton organization, particularly actin structures. Hence invasive cancer cells are characterized by a particular organization of their actin cytoskeleton which can underlie the formation of lamellipodia [111] We then chose to determine the organization of actin cytoskeleton, determined by the phalloidin staining in different PDAC cell lines as a functional indication of their pro-migratory propensity, and hence "invasive" behavior.

All PDAC cells have a cancer-type organization of their cytoskeleton, with dendritic arrays of actin filaments (Figure 2.9). PANC1 on 2D culture shows elongated actin filaments and distributed across the cytoplasm. BxPC3 actin structures are short and present outside the cells, whereas MiaPaCa2 has short and localized near the membrane level, giving a clear structure to the cells.

2.3.2 Three dimensional Culture (3D Culture)

Growth Profile

In this study, all the three PDAC cells, PANC1, MiaPaCa2 and BxPC3 were seeded as individual suspension cells on agarose-coated 96 well plate with a starting cell density of 500 cells per well and maintained for 10 days. Solidified agarose forms concave shaped curvature where cells aggregate to form spheroid like structure. PANC1 and MiaPaCa2 cells collected to form

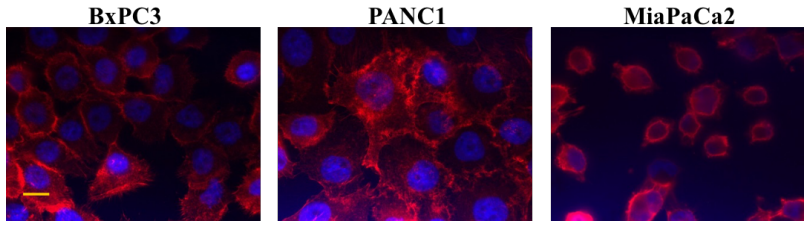

Figure 2.9: *Actin filaments of all the three cell lines were stained with rhodamine-conjugated Phalloidin (Red) and nucleus was stained with DAPI (Blue). Scale bars represent 10 µm. (Taken from B in which I am a first co-author).*

spheroids and size of the spheroids increased with time as cell grew. PANC1 and MiaPaCa2 cells had comparable growth rate over the 10 days' culture period. On the other hand, BxPC3 showed very low or null growth rate shown in figure2.10. Interestingly, the compactness of the spheroids formed by all the three PDAC cells varied.

Morphology

Morphological appearance of PDAC was studied using the microscope images shown in figure 2.11 at different stages of growth. Interestingly, the compactness of the spheroids formed by all the three PDAC cells varied. Morphology of the PANC1 spheroids showed cells at the core of the spheroid showed tight compact cell-cell attachment whereas cells at the periphery of the spheroid were loosely attached with some cells indeed migrating away from the spheroid, perhaps suggesting the invasiveness phenotype. Moreover, they showed a clear distinction between tightly formed round central dormant and loosely ruffled peripheral cells. MiaPaCa2 cells grown as spheroids were uniformly shaped with a compact core and loosely attached periphery similar to PANC1 spheroids. On the contrary, BxPC3 formed very small and highly compact spheroids, with only a few scattered cells outgrowing from the original mass, with no distinction between central and peripheral region.

Live/Dead cell imaging

Calcein/PI staining was done after 72 h of culture. Live/dead cell staining showed after 72 h of incubation majority of cells in the spheroid were viable.

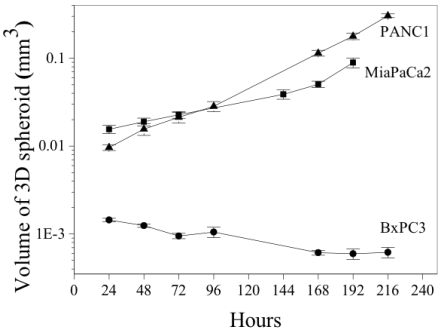

Figure 2.10: *Comparison of 3D cultured PDAC cell lines growth rate ($n = 3$). Data are means $\pm$ SEM of three separate experiments each carried out in triplicate. PANC1 and MiaPaCa2 are not significantly different at 0.05 level, whereas MiaPaCa2 are significantly different from BxPC3 ($p = 0.003$) and PANC1 are significantly different from BxPC3 ($p = 0.002$). (Taken from B in which I am a first co-author).*

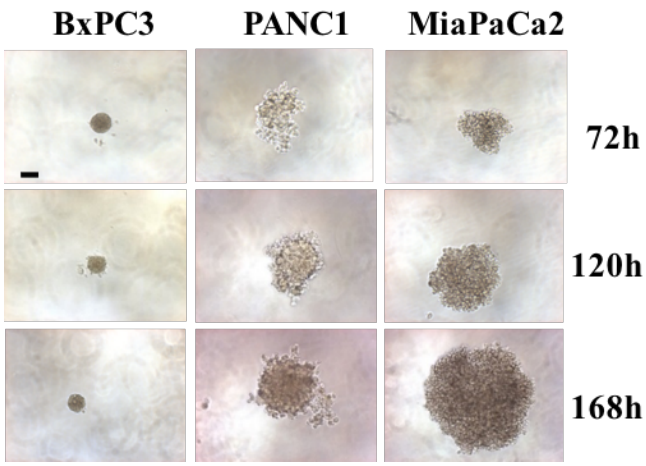

Figure 2.11: *Microscopic images of three PDAC cells at 72 h (top layer), 120 h (middle layer) and 168 h (bottom layer). Scale bars represent 100 µm. (Taken from B in which I am a first co-author).*

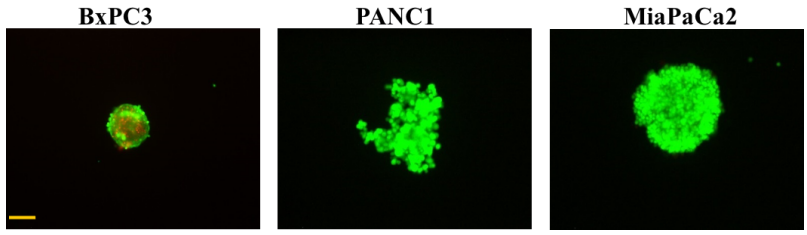

Figure 2.12: *Live and dead cell staining after 72 hours of culturing showing live green cells (Calcein) and read dead cells (PI). Scale bars represent 100 μm. (Taken from B in which I am a first co-author).*

(Figure 2.12).

Cytoskeleton structure

We had seen the differences in morphology of 3D PDAC cells compared to 2D culture and, as cytoskeleton assembly supports cell morphology, we studied the cytoskeleton assembly by staining filament actin (F-actin) of 3D spheroids. The PDAC cells in the spheroids showed actin cytoskeleton arranged with short actin filament distributed around the periphery of cells, especially at the cell-cell interaction and aggregation took place in all the 3 cell lines (figure 2.13), whereas in 2D culture actin filaments were elongated as cells showed spread morphology. A similar arrangement of f-actin was observed by Ying *et al* in mesenchymal studies of actin filaments in 3D culture; they also observed small and loose aggregates, and show that this is associated with a decline in the level of F-actin stress fiber and cell size (35).

2.3.3 Cell culture on Microfluidic device

Cell growth in HepaChip

The same PDAC cell lines were cultured in a novel type of microfluidic cell culture chamber, the HepaChip®. Figure 2.14 A shows the HepaChip®, The device comprises eight identical cell chambers, containing three cell culture regions each, sized 1 mm x 60 μm, i.e. 24 cell culture regions per chip with fluid inlet and outlet, microchannels addressing eight cell chamber, electrodes contacting the lateral faces of each cell chamber (Figure 2.14 B). On the

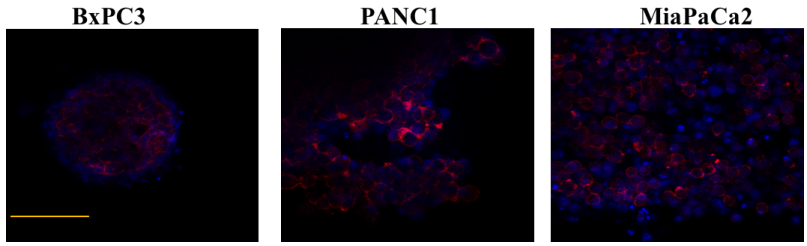

Figure 2.13: *Actin filaments of 3D spheroids were stained with rhodamine-conjugated Phalloidin (Red) and nucleus was stained with DAPI (Blue). Red filaments are short and found around the cell periphery and cell-cell interactions. Scale bars represent 100 µm. (Taken from B in which I am a first co-author).*

sidewalls of each cell chamber electrodes are integrated which are used to generate an inhomogeneous high-frequency electrical field. This gives rise to dielectrophoretic forces by which cells entering the cell chamber are drawn into the assembly areas. Only viable cells will be selectively assembled as only they exhibit intact cell membranes with their intracellular permittivity differing from that of the extracellular medium they are suspended in. Figure 2.14 C shows a multiphysics simulation of hydrodynamic and electrical forces acting on cells. The trajectory of a cell is calculated using multiphysics simulation of hydrodynamic and electrical forces acting on cells. [53] [15].[3]

Figure 2.15 A and B show PANC1 cells on assembly ridges after assembly and after 146 h of culture under continuous perfusion, respectively.

All the three PDAC cells were assembled inside the HepaChip® using DEP. All the cell lines showed initial adherence to the chip surface. PANC1 (Figure 2.16) cells PANC1 cells showed less adhesion to collagen-coated areas but tended to slide over the surface before adhering. They were incubated for 10 to 15 min in DEP medium and left to sink onto the microstructured surface before the DEP medium was exchanged for culture medium. After that, PANC1 adhered everywhere in the chip, on collagen coating as well as on pluronic coated ramps of the ridges (2.16 Day-0), on channel walls and on gold electrodes. They spread on any of these surfaces and grew one on top of others (2.16 Day-1 to Day-6). In order to demonstrate the cell growth inside the 3D microstructure, 2.16 Day-6 was taken in two focal planes: that

[3]Microfluidic work was done in collaboration with NMI Germany

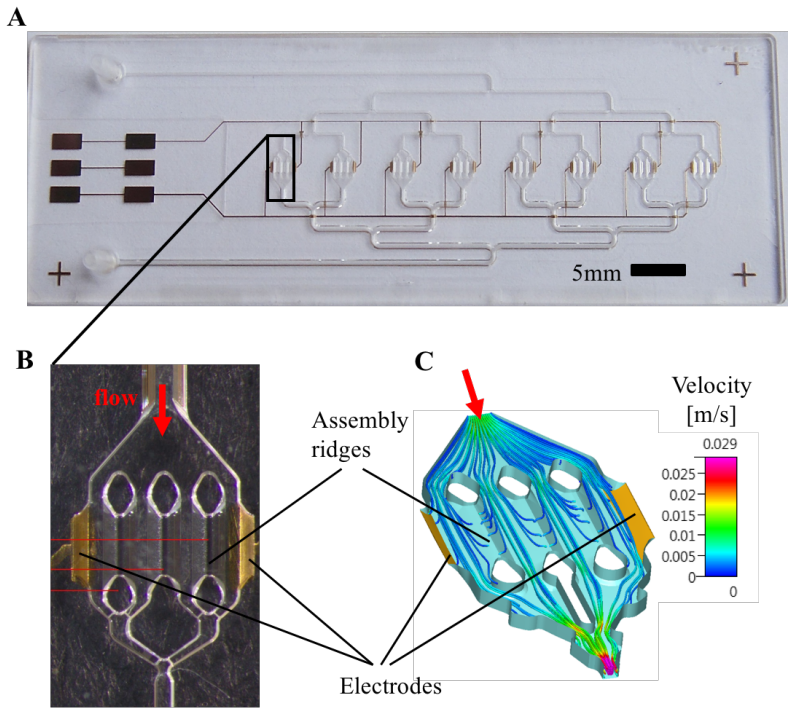

Figure 2.14: *HepaChip: (A)HepaChip having 8 cell culture chambers, fluidic inlet and outlet and gold electrodes. (B)the chamber containing 2 electrodes and 3 assembly ridges coated with collagen. (C) Simulation of flow velocity and trajectories of cells during DEP assembly inside a culture chamber. (Taken from B in which I am a first co-author).*

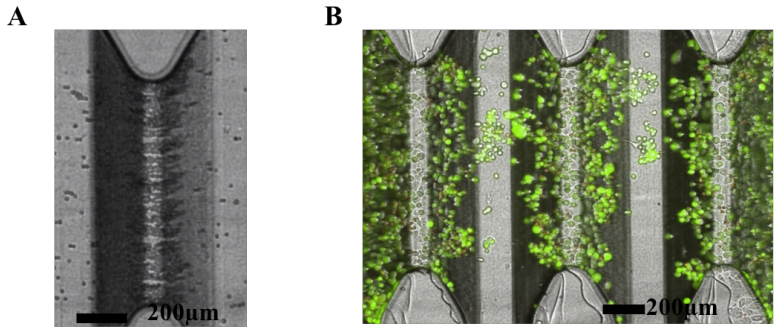

Figure 2.15: *PANC1 on HepaChip: (A) PANC1 cells assembled on one assembly ridge right after assembly. (B) Live/Dead staining of PANC1 cells after 146 hours of perfused culture inside the HepaChip® chamber. (Taken from B in which I am a first co-author).*

of the channel (left) as well as that of the collagen-coated ridge (right). It shows that PANC1 also formed small aggregates on any of these surfaces after 6 days of cell culture. Overall, PANC1 cells behave inside the chip as a spheroid forming type.

BxPC3 cells adhered and spread on the collagen coated ridges until they formed a dense layer. During perfused culture for several days, they slowly extended up the ramp and formed a thick rim. This rim grew thicker with culture time rather than further extending into the channel region (Figure 2.17 Day-0). After 24 and 48 h, we observed mainly adherent, flattened cells, which continuously changed their shape. Furthermore, we observed small spheroids growing on top of the adherent cells as shown in Figure 2.17 Day-1 to Day-3.

Cells grew inside the HepaChip® under perfusion with culture medium shown the increase in cell number and density. We observed mitosis of both BxPC3 and PANC1 cells, as a clear index of their functionality. Figure 2.18 shows a representative example thereof obtained with BxPC3 cells.

MiaPaCa2 cells showed very weak adhesion to the collagen-coated surfaces. This fact could be related to the differential expression, of integrin adhesion receptors on plasma membrane with lower affinity for collagen (Manoli S., personal communication). While some of them spread on the surface during the first 24 hours, others remained in a spherical shape and aggregated

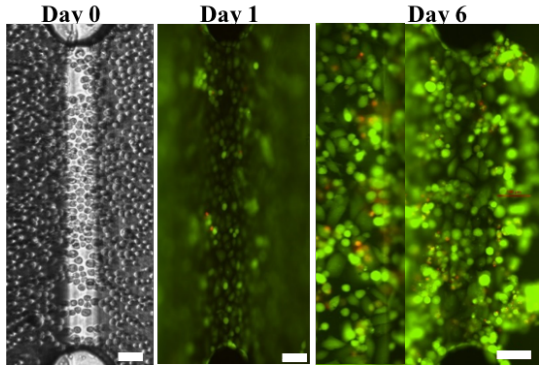

Figure 2.16: *Microscopic images of PANC1 cells in the microfluidic chip after increasing culture time starting from the first change from DEP medium to the culture medium to 6 days (Live/Dead cell staining). PANC1 cells spread as well on channel walls and bottom, so the pictures after 6 days were taken in two focal planes at the bottom and on the ridge. Scale bars: 100µm. (Taken from B in which I am a first co-author)*

.

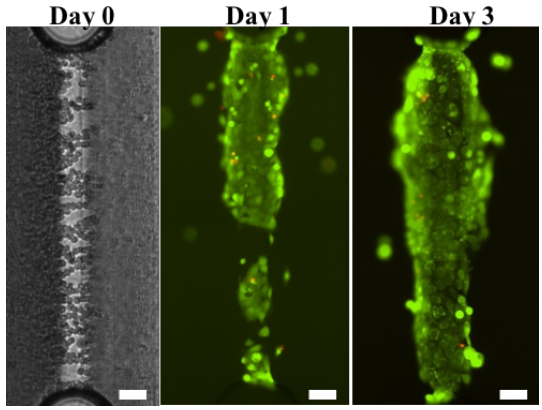

Figure 2.17: *Microscopic images of BxPC3 in the microfluidic chip after increasing culture time starting from the first change from DEP medium to the culture medium for 3 days. BxPC3 grow selectively on the ridge. Scale bars: 100µm. (Taken from B in which I am a first co-author).*

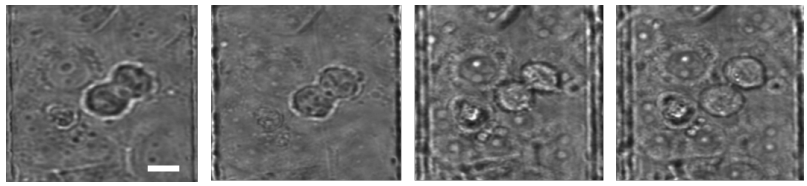

Figure 2.18: *Mitosis of BxPC3: Mitosis was observed inside the chip on the collagen-coated area after 16 h culture. From left to right pictures taken after 0 min – 1 min – 4 min – 16 min using an inverted microscope. Scale bars: 10µm. (Taken from B in which I am a first co-author).*

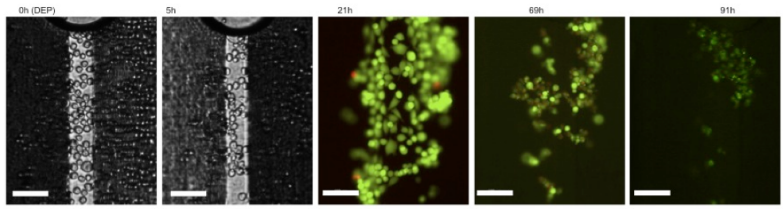

Figure 2.19: *Microscopic images of MiaPaCa2 in the microfluidic chip after assembly using DEP. MiaPaCa2 cells viability decreased after 24H of culturing. Less viable cells are seen at 69H and 91H. Scale bars: 100µm. (Taken from B in which I am a first co-author).*

at columns and edges inside the chip. During the following three days of perfused culture, the majority of MiaPaCa2 cells was transported out of the chip while vitality of the remaining cells decreased as shown in (Figure 2.19).

Cytoskeleton assembly in HepaChip

Actin stained with Phalloidin extended over the entire cytoplasm of both BxPC3 (Figure 2.20) and PANC1 (Figure 2.21) cells cultivated in the chip. As expected, actin filaments appeared denser along the cell membrane. PANC1 showed additional short actin filaments that extend from the membrane both into the cell and outside, a sign of the maintenance of their pro-migratory, cancerous features, even when cultured on the chip.

Morphological and functional features of PDAC cells cultured in 2D, 3D and inside the microfluidics HepaChip device is shown in figure 2.22.

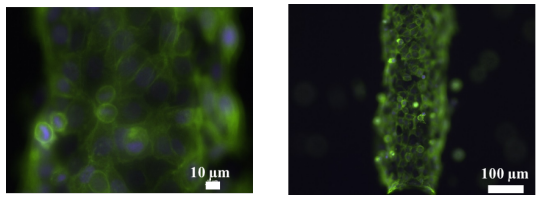

Figure 2.20: *Cytoskeleton assembly of BxPC3 staining with phalloidin and DAPI (taken from B in which I am a first co-author).*

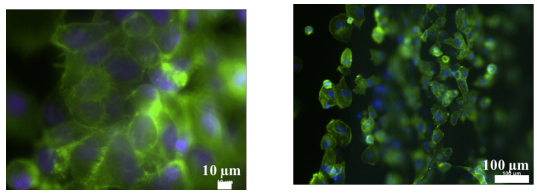

Figure 2.21: *Cytoskeleton assembly of PANC1 staining with phalloidin and DAPI(taken from B in which I am a first co-author).*

2.4 Effect of Cisplatin on PANC1

Finally, we tested chemotherapeutic drugs in the different system. In particular, we tested the effects of Cisplatin, a widely used drug for many cancer types including PDAC, on PANC1 cells. We chose to test Cisplatin as a model drug, since Platinum-based drugs are used in both the neo-adjuvant and the adjuvant settings for PDAC treatment. Cisplatin acts as an antitumor agent by inhibiting the synthesis of DNA and RNA transcription, cell cycle arrest and induction of apoptotic pathways [56]. It is also shown that cisplatin induces the apoptosis by deactivation of proapoptotic factors such as Bad and Caspase-3 in pancreatic cells [56].

2.4.1 Effect of cisplatin in 2D culture

After 24H of culturing PANC1 cells were treated with different concentrations of cisplatin. Post 24H of cisplatin treatment, cell viability was determined using trypan blue exclusion method as mentioned above in materials and methods. The concentration of cisplatin drug to kill 50% of the viable cells called, as 'IC_{50} ' value was determined for PANC1was 3.25 ± 0.2 µM

Culture type	Cell type	Adhesion	Spreading	Morphology	3D aggregate formation + aggregate size	Cytoskeleton
2D	BxPC3	Strong	Forms tight cell-cell clusters or islands of clusters with spread morphology	Epithelial	Forms large uniform clusters or islands of clusters.	Actin: Long and distributed across the cytoplasm
	PANC1	Moderate to strong	Spread morphology with few round shaped cells on top of spread cells	Epithelial	Forms moderate cell-cell aggregates	Actin: Long and distributed across the cytoplasm
	MiaPaCa2	Loose	Both round and spread shaped cells with few elongated feet like structures	Epithelial	Mostly separate cells with few cell-cell aggregates	Actin: Long and localized near the membrane level

Culture type	Cell type	Adhesion	Spreading	Morphology	3D aggregate formation + aggregate size	Cytoskeleton
3D	BxPC3	No adhesion to agarose		Smoothly tight small spheroid with no visible distinction between central and peripheral regions		Actin: Short and distributed around the periphery of the cell
	PANC1	No adhesion to agarose		Loosely assembled spheroid with clear distinction between tightly formed round central dormant and loosely ruffled (and proliferating) peripheral regions		Actin: Short and distributed around the periphery of the cell
	MiaPaCa2	No adhesion to agarose		Moderately tight spheroids with visible central dormant and peripheral proliferating regions		Actin: Short and distributed around the periphery of the cell

Culture type	Cell type	Adhesion	Spreading	Morphology	3D aggregate formation + aggregate size	Cytoskeleton
HepaChip	BxPC3	Selective on collagen	On collagen and cells	Mostly flat cells 20-30 µm diameter, few round 10 µm cells on top	At the edges of the coated microstructure w=20-80 µm *	Actin: Long and distributed across the cytoplasm
	MiaPaCa2	Poor adhesion on collagen	Few cells spread on collagen, most stay spherical	Mostly spherical, 5-50 µm, after 24h few flat cells with "feet"	Small aggregates at the edges of ridges and at pillars w=80-90µm*	
	PANC1	On microtopography independent of coating	On any surface and on top of other cells	Many flat cell with "feet", various shapes, spherical ones on top, 10 – 50 µm	On the ramps w=50-120 µm*	Actin: Long and distributed across the cytoplasm

Figure 2.22: *Morphological and functional features of PDAC cells cultured in 2D, 3D and inside the microfluidics HepaChip device. *Maximum aggregate thickness in the HepaChip® culture chamber was in the range of the measured width of the aggregates on the ramps. It is limited by the 3D geometry of the chamber between 40 µm on the assembly ridges and 190 µm inside the channels if assuming that at maximum aggregates can fill the height between the lid of the chamber and this ramp at the channel bottom. (Taken from B in which I am a first co-author).*

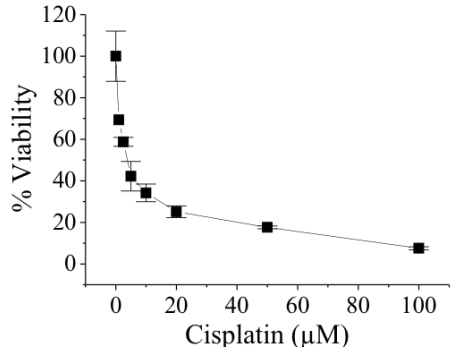

Figure 2.23: *Dose-response curve of Cisplatin on PANC1 cells in 2D culture conditions after 24H of treatment. The calculated IC_{50} was 3.25 ± 0.2 μM. Data are means ± SD of two separate experiments, each carried out in triplicate. (Taken from B in which I am a first co-author).*

(n = 2) (Figure 2.23).

2.4.2 Effect of cisplatin in 3D culture

Cisplatin exerted cytotoxic activity on 3D PANC1 cells, with IC_{50} values of 14.6 ± 1.6 μM (n = 2) after 72H of treatment. This is more than 4 fold higher than 2D culture and also in 2D culture IC_{50} value was determined just after 24H of cisplatin treatment. The dose-response curve is shown in figure 2.24 (Left panel). In 3D cultures 100 μM Cisplatin caused a decrease in cell viability (roughly 80%) after 72 h of incubation, and caused the spheroids to disaggregate after 72 h of treatment (Figure 2.24 right panel).

Effect of cisplatin in *in vivo*

We also tested the effects of Cisplatin *in vivo*, in immunocompromised mice subcutaneously injected with PANC1 cells, at 10 mg/kg [34]. As expected, this Cisplatin dose fully blocked tumor growth after 10 days as shown in the figure 2.25.

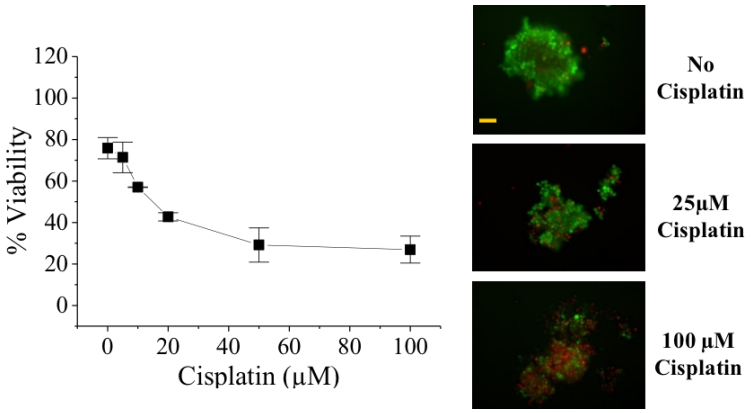

Figure 2.24: *Dose-response curve of Cisplatin on PANC1 cells in 3D culture conditions after 72H of drug treatment. The calculated IC_{50} was $14.6 \pm 1.6\,\mu M$. Data are means $\pm$ SD of two separate experiments, each carried out in triplicate. Panels on the right show the live/dead cell staining of the spheroids in control (panel on the top), $25\,\mu M$ (panel in the middle), and $100\,\mu M$ (panel at the bottom). (Taken from B in which I am a first co-author).*

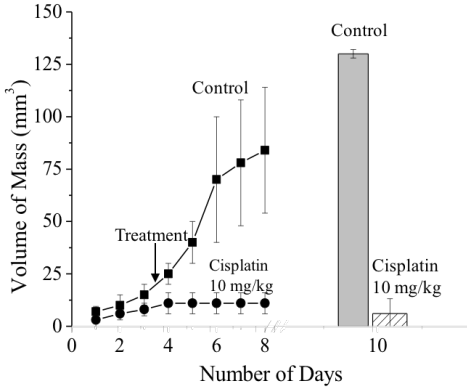

Figure 2.25: *Effect of cisplatin on PANC1 cells subcutaneously injected into mice (in vivo). The trend line shows the volume of the masses during the duration of experiment, histogram on the right shows the tumour masses of explant from the animals. (Taken from B in which I am a first co-author).*

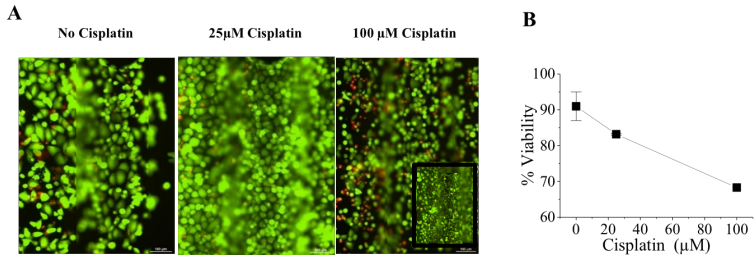

Figure 2.26: *Cisplatin effect in the microfluidic chip: (A) PANC1 cells inside the HepaChip® under continuous perfusion of 3 µL/min of cisplatin. Live/Dead cell staining after 72 h incubation with 0 µM, 25 µM, and 100 µM cisplatin; inset: black-framed area of the chip cell culture before incubation with 100 µM Cisplatin. Scale bars 100 µm. (B) Different cisplatin concentration was tested on PANC1 cells cultured inside the HepaChip. (Taken from B in which I am a first co-author).*

Effect of cisplatin in microfluidic chip

Cisplatin effect on PANC1 cells cultured in the microfluidic chamber was analyzed (Figure 2.26). After 72 h of perfusion with 25 µM Cisplatin in the culture medium, a certain reduction of viability from 95 to 83% was seen in both chips and a slight decrease in cell density was observed. The highest concentration of 100 µM Cisplatin perfused through the cell culture chip started to reduce viability from 92 to 85% after 24 h incubation, reaching 68% after 3 days. At this time an overall reduction of the cell density in the chip was observed as shown in the black framed area of Figure 2.26 A on the right compared to the inset below that shows the same area of this chip before incubation with Cisplatin. Viabilities in the control chips without Cisplatin remained between 90 and 78% over a culture time of 5 days in total. Overall a trend in concentration dependence of Cisplatin effects is evident in the graph in Figure 2.26 B.

Overall our study suggests that PANC1 cells, when cultured on collagen matrix coated in microfluidic chip under continuous perfusion systems, showed higher resistance to Cisplatin even at higher doses compared to classical *in vitro* cultures. Our data showing no adsorption of the drug to polymer surfaces, lead to excluding drug adsorption as the cause of this chemoresistance. We tested the recovery of a number of compounds covering a wide

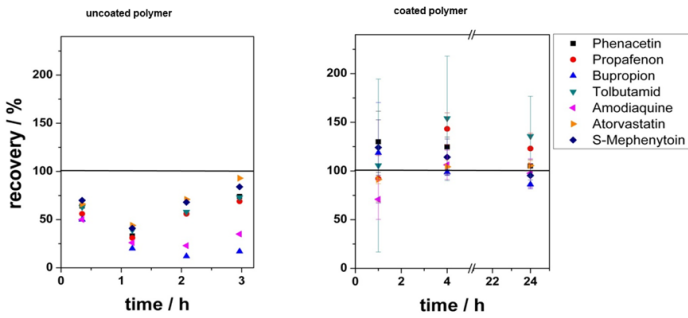

Figure 2.27: *Recovery of different compounds from uncoated and coated polymer. (Taken from B in which I am a first co-author).*

range with respect to hydrophobicity. Uncoated chips showed a considerable degree of adsorption, so that that the most hydrophobic compounds tested (Bupropion, Amodiaquine) were recovered at below 50% even after 3 hours of perfusion. On the contrary, coated chips identical to those used in this study, exhibited almost complete recovery after only 1 hour of perfusion (Figure 2.27). So cisplatin adsorption to polymer surface can be ruled out. The proper culture in the chip needs cell adhesion to collagen, that can re-establish the cell-cell and cell-ECM interactions that, at least in part, mimic the physiological microenvironment.

2.5 Discussion

In this chapter we explain about three different cell culture systems for studying biomolecular characteristics of PDAC cells. We chose to study PDAC cells since PDAC is one of the human cancers with poor prognosis, with a 5-year survival rate less than 5%. Due to its aggressiveness, high rate of metastasis and inability to detect at an early stage, strongly limit the treatment options for patients. Overall new strategies are needed for effective interventions. Many cancer models have been developed in this regard [54] from *in vitro* 2D and 3D cell cultures to whole animal models to study the

PDAC.

Cells grown in the static dish are monolayers of 2D culture and cells assuming spread morphology display epithelial like characteristics. All the PDAC cell lines grown in 2D culture proliferated to the same extent with similar growth rate. However, in terms of phenotypic appearance, BxPC3 showed to form uniform tight colonies and grow as cobblestone, while MiaPaCa2 cells consist of a pool of round and elongated (mesenchymal-like) structures and Panc1 cells intermediate morphology between mesenchymal and epithelial. This is coherent with the results of Rui Gradiz *et al.* showing the polymorphism of MiaPaCa2 and pleomorphic expression of PANC1 cells.

In three-dimensional (3D) culture, cells, when seeded on concave shaped agarose, aggregate to form 3D spheroids and leads to cell-cell attachment and interaction partially mimicking the *in vivo* environment. We used U tube technique to culture PDAC cells that do not include extracellular matrix components (ECM). In contrast to the similar growth rate in 2D, we observed significant differences in the growth rate when these three cell lines were grown in 3D systems. Interestingly, the aggregation and formation of 3D spheroids also varied drastically between the three cell lines. BxPC3 cells formed small smoothly arranged tight spheroids (non invasive phenotype), whereas MiaPaCa2 and PANC1 cells were loosely arranged and formed significantly larger spheroids that have ruffled periphery with some cells leaving the spheroids, perhaps an indication of invasive property. Actin filaments in cells grown in 3D culture were considerably smaller and localized around the periphery of the cell. A similar arrangement of f-actin was observed by Ying *et al.* in mesenchymal studies of actin filaments in 3D culture; they also observed small and loose aggregates that is associated with a decline in the level of F-actin stress fibre and cell size [115].

In addition to 3D spheroid culture, scientists have developed more sophisticated cell culture systems that enable to regulate and manipulate the cells as required. Cells grown in the microfluidic chip has gained considerable attention for its versatility in allowing manipulation of cells, enabling to build complex cell culture systems that are physiologically more relevant. For ex-incorporation of the multicellular system, chemical stimuli gradient for chemotaxis study, the extracellular matrix for drug testing etc. We cultured the PDAC cells onto a novel microfluidic chamber, the HepaChip®. In HepaChip cells maintained the cell vitality, morphological appearance and growth characteristics that are more similar to 3D cultures. Cells cul-

tured on the microfluidic chip also showed a functional marker of proper pro-migratory, neoplastic phenotype actin organization. There are many microfluidic structures to culture the PDAC cells, in which the cells are entrapped inside the hydrogel scaffold containing ECM proteins [54] [70]. These microfluidic chips are allowing microscopic images [70] [54] but do not mimic the flow of nutrients as *in vivo* [45] [93]. In this chapter, we have shown novel microfluidic chip (HepaChip) with continuous perfusion of cell culture without entrapping the cells inside. Cells retain the vitality by forming aggregates. These cell aggregates formed especially in reduced flow between the pillars. These aggregates are still in direct contact with the medium flow at a perfusion rate of 3.125 μl/min. Oxygen was supplied at a rate of 1.2 nmol/min to the chip*in vivo* [61].

Later we tested the cisplatin in all the three systems, as cisplatin is considered as a prospective drug for the combined chemotherapy of early and advanced or metastatic PDAC. Pancreatic cancer cells are expected to sensitive to cisplatin [76] [17]. A major hindrance to testing the chemotherapeutic drug *in vivo* is lack of response applying drug concentrations derived from *in vitro* data, obtained in standard 2D cultures [20] [44] [55]. Our results have supported this data showing IC_{50}s of cisplatin in PANC1 cells cultured in 2D culture is around 3 µM and slightly higher, 15 µM, in 3D spheroids. On the contrary, the dose used to obtain complete growth inhibition (10 mg/kg) *in vivo* is much higher, corresponding to an estimated plasma concentration of 240 µM [102]. In the microfluidic chip, around 70% of PANC1 cells were viable even after 72 hours of incubation of high doses (100 µM) of cisplatin. This is much higher than 2D and 3D cultures IC_{50}s. Even though these are singular experiments and dose response assay was not performed, our results supported the earlier reports stating the necessity of higher doses of a chemotherapeutic drug to decrease the cell viability [70] [23]. Although we can't compare the results with *in vivo*, our data suggest that the effects of cisplatin perfused in the chip are similar to *in vivo*. This result is consistent with the data reported in [100] showing IC_{50}s of five model drugs tested in microfluidic chip correlate with the IC_{50}s determined *in vivo*.

Overall PDAC cells cultured in microfluidic chip under continuous perfusion withstand higher concentration of cisplatin compared to classical *in vitro* culture. The proper culture in the micro chip requires cell adhesion to collagen, that re-establish the cell-to-cell and cell-to-ECM interactions that mimic *in vivo* [83]. Hence we can argue that cells cultured in the chip be-

have differently than 2D and could form a thin layer of ECM around the cells, which acts as a shield from perfused compounds. It is known that the ECM acts as chemoresistance [85], through triggering different molecular mechanisms [109]. Therefore 3D cell culture in presence of ECM represents physiologically more relevant system for stringent drug screening platform and acts as a potential bridge between conventional 2D and expensive and time-consuming *in vivo* animal models towards improved treatment.

Chapter 3

Developing Mathematical model for growth curves of pancreatic ductal adenocarcinoma (PDAC) cells

3.1 Introduction

In this chapter, we explain about the mathematical models, which we designed for two dimensional (2D) pancreatic ductal adenocarcinoma cells (PDAC) growth. As we mentioned in chapter 1, mathematical models are used extensively in biology because of their many advantages. Mathematical models for cell growth and tumor growth are date back to 1972 [71]. There are numerous mathematical models for tumour cell growth to describe how the size and structure of three-dimensional multicellular spheroids change when cultured in different culture conditions [12]. Most of these models are based on tumor size but we are interested in terms of numerosity of cell growth. So we chose to build a mathematical model for PDAC cell lines growth. Hereafter, we consider the 2D culture set up as starting scenario for our analysis.

We used three different cell lines of PDAC such as PANC1, MiaPaCa2, and BxPC3 for modeling the growth. All these three lines show different characteristics as mentioned in detail in chapter 1. Understanding these cell

lines growth in terms of their initial changes, rates of change, periods of acceleration and deceleration levels in a system is very much essential for tumorigenesis. We were interested in understanding the growth of these cell lines so we started with the simple discrete nonlinear autoregressive logistic-like model. Logistic models are extensively used in modeling of growth, as they are able to capture the continuous growth. Autoregressive models are able to predict the present based on the past, so using this concept in our studies we tested different models and selected the best model to predict the growth of all the three cell lines.

3.2 Data Processing

3.2.1 Data Acquisition

As we were interested in modeling the cell growth of PDAC cell lines, we monitored the growth for 10 days maintaining in the same conditions for all 3 cell lines except the change in medium composition for BxPC3 cells. We started with a cell count of 25000 cell per ml at day 0 (inoculation) in a well of 96 well plate containing 200µl of media for all the 3 cell lines. We cultured PANC1 and MiaPaCa2 cells in Dulbecco's Modified Eagle Medium (DMEM) supplemented with 10% defined fetal bovine serum and 4mM glutamine. BxPC3 cells were cultured using RPM1-1640 medium supplemented with 10% defined fetal bovine serum and 2mM glutamine. Cells were maintained in a humidified 5% CO_2 at 37°C for 10 days. Cell growth was estimated every day, by trypsinizing the cells and manual counting using trypan blue method.

All the cell lines, grew continuously for 10 days with increase in cell numbers. To make data more reliable each experiments was done in triplicate (in the same manner and at the same time). To generate more data, similar experiments were done 7 times with triplicates for all the 3 cell lines. Since then, experiments were done at the different time but with same conditions, we assume that cells were all in the same state of growth while modeling. But in the actual data there are few discrepancy as they started with 1 or 2 different passages of cells (number of times that a cell population has been removed from the culture vessel and undergone a subculture). Although this discrepancy is acceptable from the point of biology, the error introduced in the modeling procedure may have a detrimental effect on the results. These 7

set of experiments, cell counting (sampling) time for each day was not exactly the same and also the ending cell count sampling time was not exact. As already mentioned, the time window to get samples from the experiments is always ten day, so to have uniform data. However, the experiment showed slightly different speeds in their evolutions, and so there is a little loss of synchronization among them. Nonetheless, the ten days time span covers in almost all the cases the increasing and stationary stage of the cell evolution. Detailed data of all the 3 cell lines of 7 set of experiments with triplicates is mentioned in the appendix. Few examples of this data are shown in figure 3.1 and 3.2 of all the 3 cell lines.

3.2.2 Data Resampling

Since cell counts were aperiodic (Figure 3.1), auto-regressive models can't be used on raw data, since their standard formulation uses periodic sampling. So to overcome this problem, we interpolated and extrapolated the data to generate uniformly distributed fixed time samples. This interpolation and extrapolation of data were done using MATLAB command INTERP1 with 'pchip' algorithm. 'PCHIP' is Piecewise Cubic Hermite Interpolating Polynomial and it returns the interpolated vector containing a new set of data at an equally distributed time. We resampled the data with different time steps such as 3H, 6H, 12H, 18H, 24H and 30H for each cell line and for each experiment.

3.2.3 Data Normalization

Ideally, since each experiment has been performed under the same assumptions, they should exhibit the same behaviors. Nevertheless, during a ten days experiments there are many factors which may change, ranging from media to metabolites, and so data show a number of discrepancies. However, since such differences depend on factors we are not interested in taking into account for our modeling, we try to remove their influence by normalizing data from each experiment in order to fit a similar scenario. To this aim and by assuming that each experiment covers the increasing phase up, at most, to the stationary one, each time series is scaled down to have ending point at value 1. Three-hour resampling and normalized data are shown in figure 3.1 and 6H sampling with another set of data is shown in figure 3.2

3.2.4 Data Reliability

As stated earlier all the experiments were done in triplicates to verify and give the importance (weightage) to the data. As we counted the cells in triplicates at each data point, an average of these data was considered for modeling the growth of each experiment. The standard deviation calculated from triplicates was used for estimating the reliability of the data. Higher standard deviation has higher variability in the data, which is less reliable and lower standard deviation data is higher reliable. By normalizing the standard deviation a reliability index has been designed. It ranges from 0.1 (most reliable) to 1.0 (least reliable), and it will be used to weight, by its inverse, data during the modeling phase. The idea is that the least reliable sample weights one tenth (i.e. 1) of the most reliable ones (i.e. 10).The formula used to calculate the reliability index is as follows

$$\text{reliability of the } k\text{-th element} = 0.9\frac{\text{sdt}^{-1}(k) - \min(\text{sdt}^{-1}(k))}{\max(\text{sdt}^{-1}(k)) - \min(\text{sdt}^{-1}(k))} + 0.1$$

3.3 Model Structure

3.3.1 Model Equation

All the cell lines showed an increase in trend of growth for 10 days with different slopes of the growth curve. In general, all the cell lines had increased cell count with maximum (stable) cell count at the end at the end of the experiment. This increasing mode of cell growth can be described by a logistic model, which is the most commonly used model for cell growth. So we selected the general model, which belongs to the logistic family having autoregressive characteristics with discrete time. Generalised model equation is represented in equation 3.1.

$$Y(k) = \underbrace{G(Y(k-1))}_{\text{growth rate}} Y(k-1) \tag{3.1}$$

According to this equation, the previous cell count is multiplied by growth rate. Along with this structure, the increasing mode is related to always having a bigger than one growth rate, while the stationary phase is reached as the growth rate approaches 1. It is worth noticing that according to

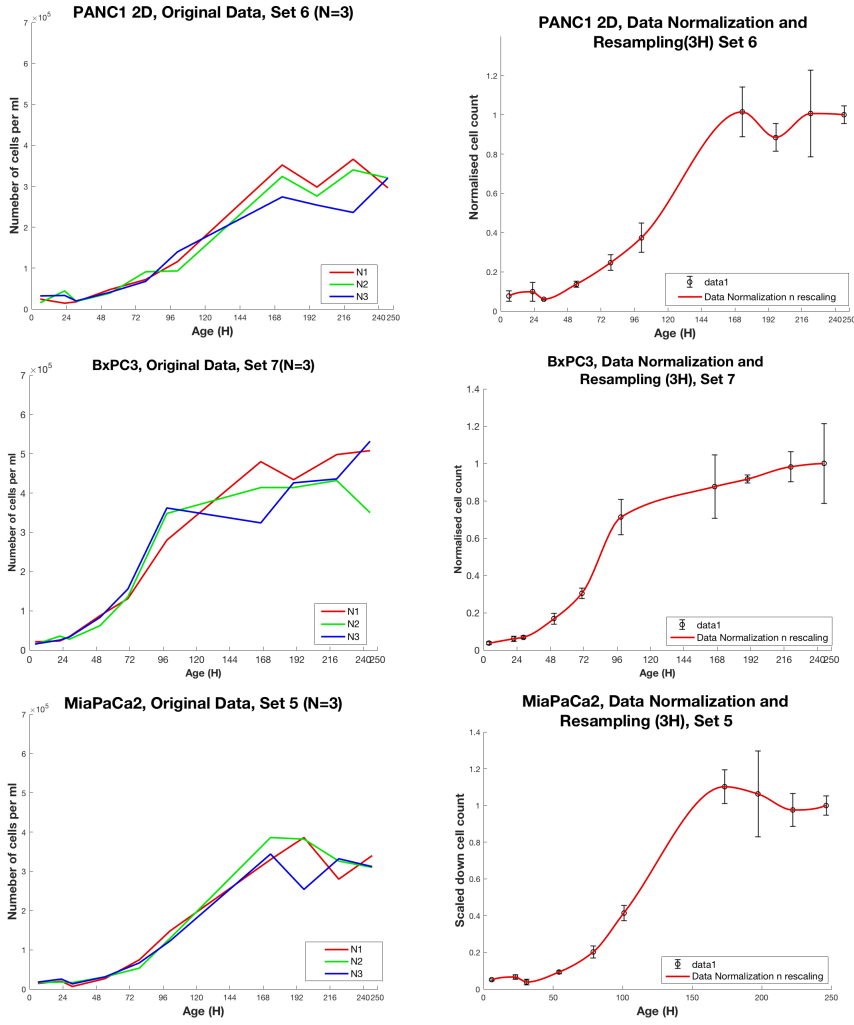

Figure 3.1: *One set of experiment for all the 3 PDAC cell lines showing original data and data normalized with resampling (3H) data*

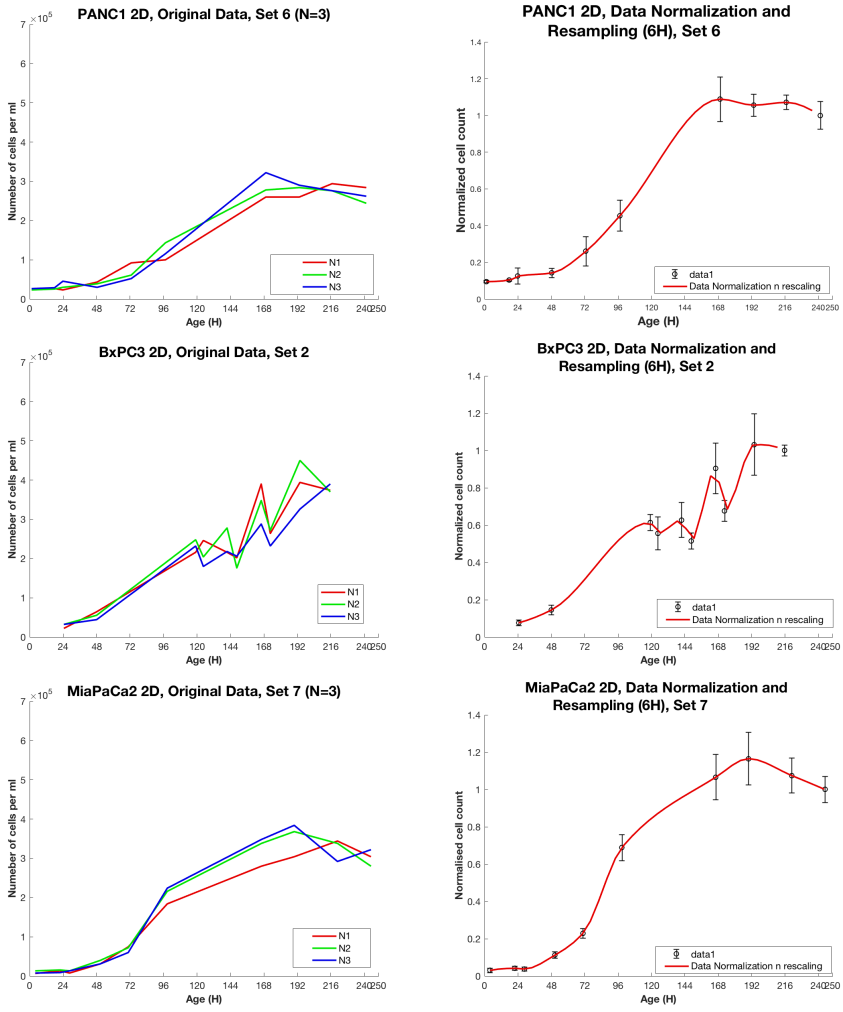

Figure 3.2: *Another set of experiment for all the 3 PDAC cell lines showing original data and data normalized with resampling (6H) data*

the general structure 3.1 the growth rate is affected by the numerosity of the cells. This reflects the idea that a cell shows it maximum reproducing capability when alone, i.e. when all the nutrients are available for itself. As the number of neighbours' increase, instead, the growth rate varies. Since, as before mentioned, almost all of our experiments feature an increasing and a stationary phase, the growth rate is expected to tend to 1 as the maximum numerosity is approached.

Constraints

According to our general model equation, the growth rate has the control over the change in cell count so we defined this growth rate with some specifications, which help us in obtaining a fitting model. The following desired features have been enforced onto the growth rate, in order to get models fitting the observations.

- Growth rate should always be positive so that it is able to capture the increasing , or at most almost stationary, nature of the data
- Growth rate should start strictly positive
- Growth rate should tend to 1 as the maximum value of the cell count is approached.

This can be written as follows,

$$G\big(Y(1)\big) > 1$$
$$G\big(Y(\text{end})\big) \geq 1$$

These constraints should be satisfied by the models to depict the data.

3.3.2 Growth Rate

Since growth rate is crucial in our modeling, in order to have more control in the model design, we rewrite the growth rate as the combination of two terms. One is ideally related to the maximum growth potential of the cell line, while the second stands for all the factors which may negatively affect the increase in cell number. This growth rate $G(Y(k))$ can be rewritten as

$$G(Y(k)) = \underbrace{G_a(Y(k))}_{\text{Increasing factor}} - \underbrace{G_b(Y(k))}_{\text{Decreasing factor}} \tag{3.2}$$

Table 3.1: *Different forms growth rate with varying decreasing factor*

Model	**Growth rate**
Logistic Model	$G(Y(k-1)) = a_1 - b_1 Y(k-1)$
Cubic Model	$G(Y(k-1)) = a_1 - b_1 Y^2(k-1)$
Squareroot Model	$G(Y(k-1)) = a_1 - \frac{b_1}{\sqrt{Y(k-1}}$
Parabola Model	$G(Y(k-1)) = a_1 - b_1 Y(k-1)^2 - b_2 Yk-1)$
Tetra Model	$G(Y(k-1)) = a_1 - b_1 Y^3(k-1) - b_2 Y^2(k-1) - b_3 Y(k-1)$
Gompertz Model	$G(Y(k-1)) = a_1 - b_1 \frac{log(Y(k-1))}{Y(k-1)}$
Bertalanffy Model	$G(Y(k-1)) = a_1 Y^{-1/3}(k-1) - b_1$

According to above equation growth rate has two factors, one is increasing factor and another one is decreasing factor. The above mentioned desired features boil down to,

$$G_a(Y(k)) - G_b(Y(k)) > 1$$

in the range (0, Y_M). Function $G_a(Y(k))$ increasing factor define the "standard" rate of growth of $Y(k)$ i.e. $Y(k)$ is supposed to grow that way indefinitely if permitted by the environment. Function $G_b(Y(k))$ decreasing factor, instead is a corrective term meant to bring the complete rate to 1 that is to the fixed point Y(end) as,

$$\begin{aligned} Y(f) &= (G_a(Y(end)) - G_b(Y(end))Y(end) \\ 1 &= G_a(Y(end)) - G_b(Y(end)) \end{aligned}$$

When Y reach a certain value, 'Decreasing factor' avoids divergence and put an end to the growth. We varied this decreasing factor in many ways to capture the best cell growth behavior. We studied 7 different forms of growth rate, to capture our data. These were designed based on literature and from our preliminary studies and same is reported in table 3.1,

Effects of the constraints on the growth rate are hereafter explained in details for logistic and cubic models. Logistic model has a linear decreasing growth rate

$$G\big(Y(k-1)\big) = a - bY(k-1)$$

Then the model constraints can be designed as follows, first we see the increasing condition is

$$a_1 - b_1 Y(k-1) > 1$$

that is

$$(a_1 - 1) - b_1 Y(k-1) > 0$$

Since $Y \forall (0, Y_M)$, one has $a_1 - 1 > 0$, i.e. $a_1 > 1$. The worst case is for $b_1 > 0$ when the above condition is satisfied over the whole interval

$$(a_1 - 1) - b_1 Y_M > 0$$

A better way to put this constraint is

$$-a_1 + Y_M b_1 < -1$$

$$-b_1 < 0$$

Cubic model has quadratic decreasing growth rate

$$G\big(Y(k-1)\big) = a_1 - b_1 Y^2(k-1)$$

Growth constraints can be designed as follows,

$$a_1 - b_1 Y^2(k-1) > 1$$

that is

$$(a_1 - 1) - b_1 Y^2(k-1) > 0$$

Since $Y \forall (0, Y_M)$, one has $a_1 - 1 > 0$, i.e. $a_1 > 1$. The worst case is for $b_1 > 0$ when the above condition is satisfied over the whole interval. The growth rate has its maximum value at Y=0, i.e. when the cells are at the beginning of their increasing phase. when the above condition is satisfied over the whole interval

$$(a_1 - 1) - b_1 Y_M^2 > 0$$

A better way to put this constraints are

$$-a_1 + Y_M^2 b_1 < -1$$

$$-b_1 < 0$$

and so on.

We can also add other constraints to $G_a(Y)$ and $G_b(Y)$ to grant the whole growth rate is bigger than 1 on a different range of interest.

3.3.3 Delayed Models

Autoregressive models use the previous data to predict the present but this previous could be in any rage. Cell growth depends on many factors like metabolism, doubling time etc and these vary with time. As we were studying cell growth at different sampling time, we wanted to check how these factors affect the cell growth so we considered a delay in our identification. In our model equation we just used one step previous data to predict, we didn't know how much single step was able to capture the data so we included 2 steps. So that we could able to cover the bigger range of data to predict.

The simplest way to extend the previous model structure to a single-step delay case is the following

$$Y(k) = \underbrace{G_1(Y(k-1)}_{\text{Primary growth rate}}\ Y(k-1) + \underbrace{G_2(Y(k-2))}_{\text{Secondary growth rate}}\ Y(k-2) \tag{3.3}$$

Primary growth rate acts on one step previous data while the secondary growth rate on two-step previous data that is, the secondary growth rate shows a single-step delay with respect to the primary growth rate. So that we could predict the present depending on the two previous values.

Constraints

To formulate the constraints for the above-delayed model was more difficult as two growth rates should be more than 1. As our cell growth was increasing with time it should be,

$$Y(k-2) < Y(k-1)$$

Then we restricted the model to hold the relation, based on the assumption for a certain $0 < \varepsilon < 1$

$$Y(k-2) > \varepsilon Y(k-1)$$

This was just an assumption so we must be careful in choosing ε since it shouldn't negatively affect the final result. Under the previous conditions one had

$$Y(k) > \left(G_1(Y(k-1)) + \varepsilon G_2(Y(k-2))\right) Y(k-1)$$

that is

$$G_1(Y(k-1)) + \varepsilon G_2 Y(k-2) > 1$$

Again, these two steps can be written individually with increasing and decreasing factors and restricting them to satisfy the model

$$G_{1a}(Y) - G_{1b}(Y) > \mu$$

$$\varepsilon\left(G_{2a}(Y) - G_{2b}(Y)\right) > 1 - \mu$$

For a certain μ (small, and even negative) at every Y in the interval $(0, Y_M)$, we have assured the initial constraint. Hence, we can arbitrarily chose a number of $Y1$, $Y2$, . . . $\in (0, Y_M)$, and impose

$$\begin{aligned} G_{1a}(Y_1) - G_{1b}(Y_1) &> \mu \\ G_{2a}(Y_1) - G_{2a}(Y_1) &> \frac{1-\mu}{\varepsilon} \\ G_{1a}(Y_2) - G_{1b}(Y_2) &> \mu \\ G_{2a}(Y_2) - G_{2b}(Y_2) &> \frac{1-\mu}{\varepsilon} \end{aligned}$$

Alternatively, we enforced a less strict constraint by imposing the fixed point of the model to be set above Y maximum (Y_M). This can be obtained by considering the final data point, whose solutions Y are the values at which the model does not change since $Y(k)$ is the same as $Y(k-1)$. Then the equation becomes,

$$Y = (G_{1a}(Y) - G_{1b}(Y))Y + (G_{2a}(Y) - G_{2b}(Y))Y$$

According to that, Y=0 was always a fixed point, while the others are given by

$$G_{1a}(Y) - G_{1b}(Y) + G_{2a}(Y) - G_{2b}(Y) = 1$$

Usually the above equation gives a certain number of solution.
Let equilibrium of Y (Y_E) be the smaller one. Then, we ask the model to satisfy

$$0 < Y_M < Y_E$$

Table 3.2: Different forms of model equation with higher order

Model	Structure
Logistic Model	$Y(k) = a_1Y(k-1) - b_1Y^2(k-1)$
Delayed Model	$Y(k) = a_1Y(k-1) + a_2Y(k-2) - b_2Y^2(k-2)$
Cubic Model	$Y(k) = a_1Y(k-1) - b_1Y^3(k-1)$
Delayed Cubic Model	$Y(k) = a_1Y(k-1) + a_2Y(k-2) - b_2Y^3(k-2)$
Squareroot Model	$Y(k) = a_1Y(k-1) - b_1\sqrt{Y(k-1)}$
Parabola Model	$Y(k) = a_1Y(k-1) - b_1Y(k-1)^3 - b_2Y^2(k-1)$
Tetra Model	$Y(k) = a_1Y(k-1) - b_1Y(k-1)^4 - b_2Y^3(k-1) - b_3Y^2(k-1)$
Gompertz Model	$Y(k) = a_1Y(k-1) - b_1log(Y(k-1))$
Bertalanffy Model	$Y(k) = a_1Y^{2/3}(k-1) - b_1Y(k-1)$

So that the time series is expected to start close to 0 and move towards Y_E, stopping at such a value. This latter constraint can be enforced onto the model differently depending on the form of the functions, and thus it must be taken into account separately for each case.

3.3.4 Different forms of Model Equation

We wanted to capture different slope of growth of all the cell lines, as simple linear models couldn't able to capture this variability we increased the order of linearity and making the model much more complex with nonlinearity. These equations were designed on the basis of preliminary outcomes and literature. All these equations were different forms of the model equation and mentioned in table 3.2.

These equations are explained briefly based on the above constraints. As these equations allow the actual rate of growth i.e. $G(Y) = G_a(Y) - G_b(Y)$, to be positive and meaningful behavior in the interval $Y\epsilon(0, Y_M)$. Above models growth rate with constraints behave as follows,

Logistic Model The general equation of this model looks like

$$Y(k) = a_1Y(k-1) - b_1Y^2(k-1)$$

According to this equation, growth rate with the above constraints becomes

$$-a_1 + b_1Y_M^1 < -1$$

$$-b_1 < 0$$

As we were solving these equations in MATLAB, it allows only lesser than constraints of the equation. We formulated all the equations in that way.

Delayed Logistic Model For the above model we added 1 more step previous and equation becomes,

$$Y(k) = a_1 Y(k-1) + a_2 Y(k-2) - b_2 Y^2(k-2)$$

Growth rate of the above equation having the constraints then

$$\begin{gathered} -a_1 - a_2 + b_2 Y_M^2 < -1 \\ -b_2 < 0 \end{gathered}$$

Cubic Model We increased the power of logistic equation to 3, so that it could be able to capture the nonlinearity of the data. Then the equation is,

$$Y(k) = a_1 Y(k-1) - b_1 Y^3(k-1)$$

The growth rate of the above model in order to binding to constraints,

$$\begin{gathered} -a_1 + b_1 Y_M^2 < -1 \\ -b_1 < 0 \end{gathered}$$

Delayed Cubic Model For the above cubic model, we added one step delay and the model equation becomes,

$$Y(k) = a_1 Y(k-1) + a_2 Y(k-2) - b_2 Y^3(k-2)$$

The growth rate bounding to constraints are,

$$\begin{gathered} -a_1 - a_2 + b_2 Y_M^2 < -1 \\ -b_2 < 0 \end{gathered}$$

Square root Model We also tested our model equation using square root form since some our data showed lagged growth and this can be explained by this model and the equation is,

$$Y(k) = a_1 Y(k-1) - b_1 \sqrt{Y(k-1)}$$

Growth rate behaves with the constraint as follows,

$$-a_1 + \frac{1}{\sqrt{Y_M}} b_2 < -1$$

Near to the maximum growth Y_M, the growth has to slow down and possibly stop, $G(Y_M) \approx 0$ is quite a desired property. We could think of a $G(Y)$ that starts and ends small, as a more complicated variant of the standard logistic map. The very simplest models of this form are the following

Parabola Model In this model we tried to capture the variability in the data between starting and ending point by enforcing two different constraints, the equation is

$$Y(k) = a_1 Y(k-1) - b_1 Y^3(k-1) - b_2 Y^2(k-1)$$

Growth rate with the two different constraints are

$$\begin{gathered} -a_1 + Y_M^2 b_1 + Y_M b_2 < -1 \\ -a_1 + (\frac{4}{5} Y_M)^2 b_1 + (\frac{4}{5} Y_M) b_2 < -1 \\ -a_1 < -1 \end{gathered}$$

The constraint at $\frac{4}{5} Y_M$ is a soft way to enforce the growth rate would be greater than one even at the 80% of the maximum value in the range, i.e. close to when the growth is expected to slow down and stop.

Tetra Model As this model able to capture the variability in very effective as the order is high, we used the following form of equation,

$$Y(k) = a_1 Y(k-1) - b_1 Y^4(k-1) - b_2 Y^3(k-1) - b_3 Y^2(k-1)$$

The growth rate with 2 different constraints to capture the change in cell growth is,

$$\begin{gathered} -a_1 + Y_M^4 b_1 + Y_M^2 b_2 + Y_M b_3 < -1 \\ -a_1 + (\frac{4}{5} Y_M)^4 b_1 + (\frac{4}{5} Y_M)^2 b_2 + (\frac{4}{5} Y_M) b_3 < -1 \\ -a_1 < -1 \end{gathered}$$

We also used widely applied growth models of Gompertz and Bertalanffy in our model equations with the constraints to examine their behavior with our data.

Gompertz Model equation is

$$Y(k) = a_1 Y(k-1) - b_1 log(Y(k-1))$$

Growth rate constraints are

$$\begin{gathered} -a_1 + b_1 \frac{1}{\log y_M} < -1 \\ -b_1 < 0 \end{gathered}$$

Bertalanffy Model our model equation,

$$Y(k) = a_1 Y^{2/3}(k-1) - b_1 Y(k-1)$$

Growth rate with the constraint is

$$\begin{gathered} -a_1 (Y_M^{-1/3}) + b_1 < -1 \\ -b_1 < 0 \end{gathered}$$

All the above growth rate equations with constraints are written in a way, which can be solved using MATLAB.

3.4 Parametric Identification of Coefficients

3.4.1 Generalised model equation

The equations of all the above models can be written in one general equation using different functions of $Y(k-1)$. These functions vary depending on the model we used. So the very general equation is,

$$\begin{aligned} Y(k) = a_1 Y(k-1) f_{a1}(Y(k-1)) + a_2 Y(k-1) f_{a2}(Y(k-1)) \\ - b_1 Y(k-1) f_{b1}(Y(k-1)) - b_2 Y(k-1) f_{b2}(Y(k-1)) \end{aligned}$$

In this a_1 and a_2 are the parameters of increasing factor and b_1 and b_2 are the parameters of decreasing factor. As we are intended to identify these parameters, we could much simplify the equation by denoting

$$F a_1 Y(k) = Y(k) f_{a1}(Y(k))$$

So our simplified generalized model equation is

$$Y(k) = a_1 F_{a_1}(Y(k-1)) + a_2 F_{a_2}(Y(k-1)) - b_1 F_{b_1}(Y(k-1)) - b_2 F_{b_2}(Y(k-1))$$

As we are interested in the identification of parameters, which can be done using MATLAB, and it works on basis of Matrix. We transformed these equations into matrix form.

3.4.2 Matrix Form

The above generalised model equation is written in the form of Matrix as follows,

$$\begin{bmatrix} Y(1) \\ Y(2) \\ . \\ . \\ . \\ Y(n) \end{bmatrix} = \begin{bmatrix} Fa_1Y(0) & Fa_2Y(0) & -Fb_1Y(0) & -Fb_2Y(0) \\ Fa_1Y(1) & Fa_2Y(1) & -Fb_1Y(1) & -Fb_2Y(1) \\ . & & & \\ . & & & \\ . & & & \\ Fa_1Y(n-1) & Fa_2Y(n-1) & Fb_1Y(n-1) & Fb_2Y(n-1) \end{bmatrix} \begin{bmatrix} a_1 \\ a_2 \\ b_1 \\ b_2 \end{bmatrix}$$

And these matrices can be represented in single letters in very compact form as follows,

$$P = MV$$

Vector V contains the coefficients (parameters), which need to be estimated.

3.4.3 Linear approach to estimate the coefficients V

Standard way of estimation

As we were using MATLAB for identification, the standard way of estimating vector V in MATLAB has two ways,

$$V = mldivide(M, P)$$
$$\text{and } V = lsqlin(M, P, [], [])$$

Both the methods implement the Least Squares Method to find the optimal set of parameters, but they differ in terms of constrained problems. In first method i.e. 'mldivide', we cant restrict the constraint but the constraint is very important in our identification so we chose 'lsqlin' method. The lsqlin method is able to estimate vector V by minimizing the quantity $||P = MV||^2$, which is a value that measures how much P is close to MV. This minimizes the average absolute error that one would have if a one-step-ahead prediction would be done on the basis of the actual value at that instant. Moreover, the function can perform such an optimization under linear constraints.

Weighted least square method

Weighted least square methods often used to maximize the efficiency of parametric estimation. Usually in the least square method, during the estimation of the parameter, all the data are equally treated so that less precisely measured point also have more influence on the estimation and highly precise points are too little influence on the estimation. Instead of weighted least square method gives the weight, which is the information of how precise the data. This weight contributes the final parameter estimation [95]. We used this concept in our estimation of parameters, by adding reliability index as weights.

Reliability index was considered as ρ, as that $\rho > 0$ is a parameter such that the reliability of sample Y is somewhat proportional to $\frac{1}{\rho}$. Then, we can modify the least Square Method in order to take into account the differences in the reliability of the samples. Such a method is also referred to as *Weighted Least Square Method*. Since the reliability indexes are related to the actual sampling time, while after resampling the data is related to a new and uniformly distributed set of instants, we tie to each sample the reliability index of the real data closest to it. This can be done as follows.

1. For each $Y(k)$, we consider the related time instant $t = k^* < time_step >$ and we find the actual sampling time t^* closest to it.
2. We find out Y^* corresponding to the sampling time t^*
3. Given the corresponding ρ^*, we define the weight $w(k) = \frac{1}{\rho^*}$
4. We build a diagonal matrix W where the elements onto the diagonal are the previous weights $w(k)$.
5. Instead of using the couple M, P we use (WM, WP)

Then our identification of V becomes,

$$V = lsqlin(M * W, P * W, [], [])$$

3.4.4 Identified Model Equation

Above identified coefficients were used to generate new time series called 'Z'. This new 'Z' time series can be called as 'identified model equation' and

written as follows

$$Z(k) = a_1 Fa_1(Z(k-1)) + a_2 Fa_2(Z(k-2)) - b_1 Fb_1(Z(k-1)) - b_2 Fb_2(Z(k-2))$$

Where a_1, a_2, b_1 and b_2 are the identified coefficients of vector V,

$$a_1 = V(1) \text{..... First element of vector V}$$
$$a_2 = V(2) \text{..... Second element of vector V}$$
$$b_1 = V(3) \text{..... Third element of vector V}$$
$$b_2 = V(4) \text{..... Fourth element of vector V}$$

Using this identified model equation, we can compute model errors. These model errors are the difference between actual data and model simulations to test the identified coefficients are good enough. Lesser the error better the identified model.

3.4.5 Error Index

We used the error between actual data and simulation to select the better model for the data. As error plays an important role in the identification, we considered 3 different types of error such as absolute error, percentage error and weighted (reliable) error for the identified model using the following formulas,

Absolute error

$$ABE = Y(k) - Z(k)$$

This error is then scaled down in the range of 1 to 10, 1 having the least error and 10 with maximum error and called as ABE index.

Percentage error

$$PRE = \frac{Y(k) - Z(k)}{Y(k)}$$

Again this error is normalized in the range of 1 to 10, with minimum having 1 and maximum with 10 and named this scaled down as PRE index.

Weighted error

$$RE = RlyY(k)((Y(k) - Z(k))$$

This error is then scaled down in the range of 1 to 10, 1 having the least error and 10 with maximum error and called as RE index

Since the single Absolute error index, Percentage error index and Weighted error index turned out unable to express the actual goodness of model, an error index has been designed properly by combining all. As all these errors are merely a numbers in the range of 1 to 10 we summed up all these 3 errors to obtain a single error index. This error index was used in our model identification, each model was given the ranking based on this overall error index.

$$ErrorIndex = ABEIndex + PREIndex + REIndex$$

3.5 Steps followed for identification of Best Model

We used the above-mentioned concepts in the identification of the best model for cell growth of each cell line. We followed the steps below to identify the best model for each cell line

1. A number of cases were obtained from a combination of 6 different samplings (3H, 6H, 12h, 18H, 24H and 30H) and 7 set of experiments, so we had in total 42 cases for each cell line containing cell growth data.

2. We estimated the best model of each structure (9 types table 3.4) in each case

3. By comparing the actual data and simulation for these cases, we created error index for each case

4. Within a case (tested with 9 structures), a model ranking was given with respect to each other (least error index is the 1st Best and 2nd least error index is the 2nd Best)

5. 1st best and 2nd best, each gets a score of one in each case and at the end all these scores were counted for all the cases and the model is selected based on the highest score.

Table 3.3: Ranking of different model structures (equations) for PANC1. 1st best is number of times least error has appeared and 2nd best is the number of times 2nd least error has appeared in 42 cases

MODELS	1st Best	2nd Best	Total
LOGISTIC	2	3	**5**
DELAYED LOGISTIC	2	3	**5**
GOMPERTZ	1	4	**5**
CUBIC	9	13	**22**
DELAYED CUBIC	6	9	**15**
PARABOLA	3	5	**8**
SQUARE ROOT	0	0	**0**
TETRA	19	5	**24**
BERTANLAFFY	0	0	**0**

3.6 Identification of best mathematical models for 2D PANC1 growth data

PANC1 normalized and resampled growth data of 7 different experiments with triplicates were used to identify the best model to explain about the growth behavior of this cell lines in two-dimensional culture. We followed the above steps and obtained the results as follows,

3.6.1 Identification of best 3 models for PANC1 growth

As we had 9 models, we wanted to identify the best 3 models and study them in detail so in that regard we followed the following steps

Selection of best models

To select the best model, we followed the section 3.5 steps, tested all the 42 cases with 9 different model equations (table 3.2) and given the ranking. A table is created containing the number of times the least error index appeared for that particular model equation and this table called as 'Ranking table'. This has 2 columns, 1st best contains the number of times least error has appeared and 2nd best is the number of times 2nd least error has appeared in 42 cases. The ranking table for PANC1 is represented in table 3.3

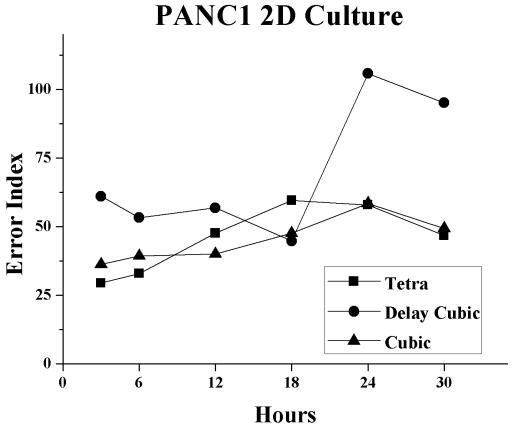

Figure 3.3: *The best 3 models of PANC1 to predict the cell growth showing different error index at different sampling time*

From the ranking table 3.3, we selected the best 3 models to identify the growth. For PANC1, Tetra, Cubic and Delayed Cubic models work better for modeling the PANC1 growth. So we selected these 3 models for further studies.

Selection of best fixed time

After selecting the best model, we selected the best sampling time for the above-selected models again based on the least error index. We checked the error index at 3H, 6H, 12H, 18H, 24H, and 30H for these 3 models (tetra, cubic and delayed cubic) and Figure 3.3 shows error index at the different sampling time. From the figure 3.3 its can be seen that for tetra and cubic model, every 3H sampling time is best and for delayed cubic 18H is the best fixed time interval for modeling.

Identification of coefficients for best 3 models

For these three identified models, Tetra, Cubic and delayed cubic models with respective best sampling time, we redid the identification. While re-identifying, the coefficients were estimated in two ways,
1) Average of the 7 models identified for each set of experiment and called

Table 3.4: Identified Tetra(3H) Model for PANC1 Growth showing both Average and Cumulative identified coefficients

Tetra Coefficients	SET 1	SET 2	SET 3	SET 4	SET 5	SET 6	SET 7	Average	Cumulative
a1	1.0000	1.0789	1.0000	1.0000	1.0000	1.0000	1.1013	**1.0257**	**1.0045**
b1	-0.2738	-0.1431	-1.1347	-0.2486	-0.1961	-0.1961	-0.1221	**-0.3306**	**-0.3698**
b2	0.6340	0.2719	1.9497	0.6468	0.5290	0.5290	0.2229	**0.6833**	**0.8250**
b3	-0.3625	-0.0518	-0.8382	-0.4154	-0.3436	-0.3436	-0.0089	**-0.3377**	**-0.4464**

Table 3.5: Identified Cubic (3H) Model for PANC1 Growth showing both Average and Cumulative identified coefficients

Cubic Coefficients	SET 1	SET 2	SET 3	SET 4	SET 5	SET 6	SET 7	Average	Cumulative
a1	1.0493	1.0275	1.0588	1.0177	1.0475	1.0389	1.0853	**1.0464**	**1.0219**
b1	0.0298	0.0107	0.0588	0.0085	0.0400	0.0365	0.0628	**0.0353**	**0.0085**

this coefficients as **'Average'**. Individually identified model for each set and then averaging

2) Single identification was done using all the 7 sets at once by defining all the 7 set of experiments in single P and M matrix as follows

$$P = \begin{bmatrix} P_1 \\ P_2 \\ P_3 \\ P_4 \\ P_5 \\ P_6 \\ P_7 \end{bmatrix} \quad M = \begin{bmatrix} M_1 \\ M_2 \\ M_3 \\ M_4 \\ M_5 \\ M_6 \\ M_7 \end{bmatrix}$$

Which can e be rewritten in compact form as earlier

$$P = MV$$

This identified coefficients called as **'Cumulative'.**

Table 3.4 shows identified coefficients for tetra model, table 3.5 for the cubic model and table 3.6 for the delayed cubic model. All these tables have both identified coefficietn in terms of 'Average' and 'Cumulative' identification

Behavior of Growth rate

After identifying the coefficients, we have studied the behavior of growth rate for Cubic and Tetra model with 3H fixed time for both 'Average' and

Table 3.6: Identified Delayed cubic (18H) Model for PANC1 Growth showing both Average and Cumulative identified coefficients

Delayed Cubic Coefficients	SET 1	SET 2	SET 3	SET 4	SET 5	SET 6	SET 7	Average	Cumulative
a1	1.5945	1.9585	2.0963	1.2285	1.4393	0.5950	1.3205	**1.4618**	**-0.9874**
a2	-0.4466	-0.8474	-0.9514	0.2131	-0.1732	1.1743	0.1964	**-0.1193**	**1.9874**
b2	0.0894	0.0433	0.1449	0.2115	0.2245	0.7468	0.3806	**0.2630**	**-1.38E-17**

'Cumulative' cases. The delayed cubic growth rate is not considered here because it can not be directly compared with those of the other two models. By this growth rate, we can understand the growth behavior of the cell. Same is represented in figure 3.4 and time series stops after growth rate reaching 1. It is worth stressing that as the cell number reaches 1 the growth stops. Figure 3.4 shows that Tetra model has a peak of the growth rate at 1.057. This means that the ability of the cell to reproduce is not maximum when it is isolated. However, since the model does not explicitly take into account the time necessary to the cell to settle in the new environment, such a behavior could be the result of this hidden factor. Cubic growth rates (both averaged and cumulative) show a more intuitive behavior, since they are at a maximum when the cell is isolated and decrease quadratically as the cell count grows. Following are the growth rate equations,

Tetra Model

Average: $G(Y(k-1)) = 1.0257 + 0.3306Y(k-1)^3 - 0.683Y(k-1)^2 + 0.3377Y(k-1)$

Cumulative: $G(Y(k-1)) = 1.0045 + 0.3698Y(k-1)^3 - 0.825Y(k-1)^2 + 0.446Y(k-1)$

Cubic Model

Average: $G(Y(k-1)) = 1.0464 - 0.0353Y(k-1)^2$

Cumulative: $G(Y(k-1)) = 1.0219 - 0.0085Y(k-1)^2$

Equations of best 3 identified models of PANC1

All the 3 identified models tetra, cubic and delayed cubic models equations with the identified coefficients are represented below,

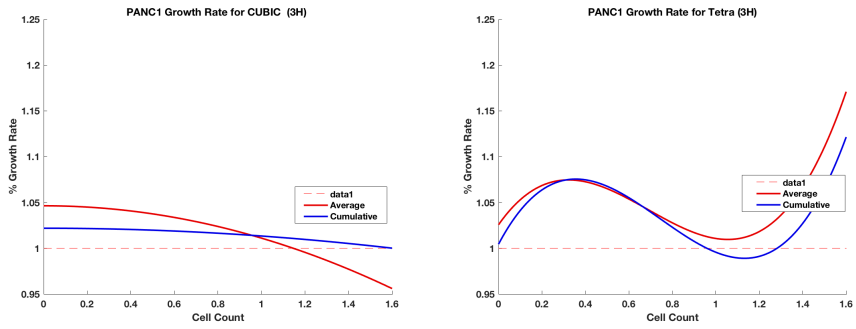

Figure 3.4: *Cubic (3H) and Tetra model (3H) showing growht rate behavior for PANC1 cells culture in 2D with 2 different nature*

Identified Tetra Model: Tetra model (3H) identified structure with coefficient (equation) is shown below

Average

$Y(k) = +0.3306Y(k-1)^4 - 0.683Y(k-1)^3 + 0.3377Y(k-1)^2 + 1.025Y(k-1)$

Cumulative

$Y(k) = +0.3698Y(k-1)^4 - 0.825Y(k-1)^3 + 0.446Y(k-1)^2 + 1.0045Y(k-1)$

Identified Cubic Model: Cubic model identified equation with the identified coefficients are shown below

Average

$Y(k) = -0.0353Y(k-1)^3 + 1.0464Y(k-1)$

Cumulative

$Y(k) = -0.0085Y(k-1)^3 + 1.0219Y(k-1)$

Identified Delayed Cubic Model: Delayed Cubic model identified equation with the identified coefficients are shown below

Average

$Y(k) = -0.263Y(k-2)^3 + 1.4618Y(k-1) - 0.1192Y(k-2)$

Cumulative

$Y(k) = +1.38exp - 17Y(k-2)^3 - 0.9874Y(k-1) + 1.9874Y(k-2)$

Table 3.7: Error Index estimated from best 3 models for each set of experiment of PANC1 growth

Best Models	1 SET	2 SET	3 SET	4 SET	5 SET	6 SET	7 SET	Sum of 7 sets error index
Tetra model (3H)	6.5840	13.0448	5.0955	16.9905	5.2378	19.3165	24.2904	90.5595
Delay cubic (18H)	4.8365	10.6270	5.4345	15.6578	14.4887	14.2767	26.4754	91.7966
Cubic (3H)	7.5446	16.1305	7.5742	22.0762	11.6657	8.9332	13.3211	87.2454

Errors of identified models of PANC1

We have re-estimated all the three errors for the identified model with respect to each data point and also absolute error for each set. Figure 3.6 shows the error of identified cubic model with respect to each experimental data point and absolute errors for both cumulative and average identification, figure 3.7 shows the error of identified delayed cubic model and figure 3.5 shows the error of identified tetra model with respect to experimental data.

3.6.2 Selection of best-identified model out of 3 identified models for PANC1

As we narrowed down our identification to 3, we wanted to select the best one model out of them. During our identification we observed cumulative and average coefficients were behaving the same way. Nevertheless, since the averaging procedure can not guarantee that the constraints are always satisfied, cumulative models turn out more reliable, and we suggest their use over the average versions. As we wanted to select one best model, again we estimated the error index using these identified cumulative models, Cubic (3H), Delayed cubic (18H) and tetra model (3H) and compared among them. Table 3.7 shows the error index for each of set of experiment estimated using cumulative identified models. According to the table 21, cubic 3H is the best model to predict the cell growth of PANC1 cells cultured in 2D culture.

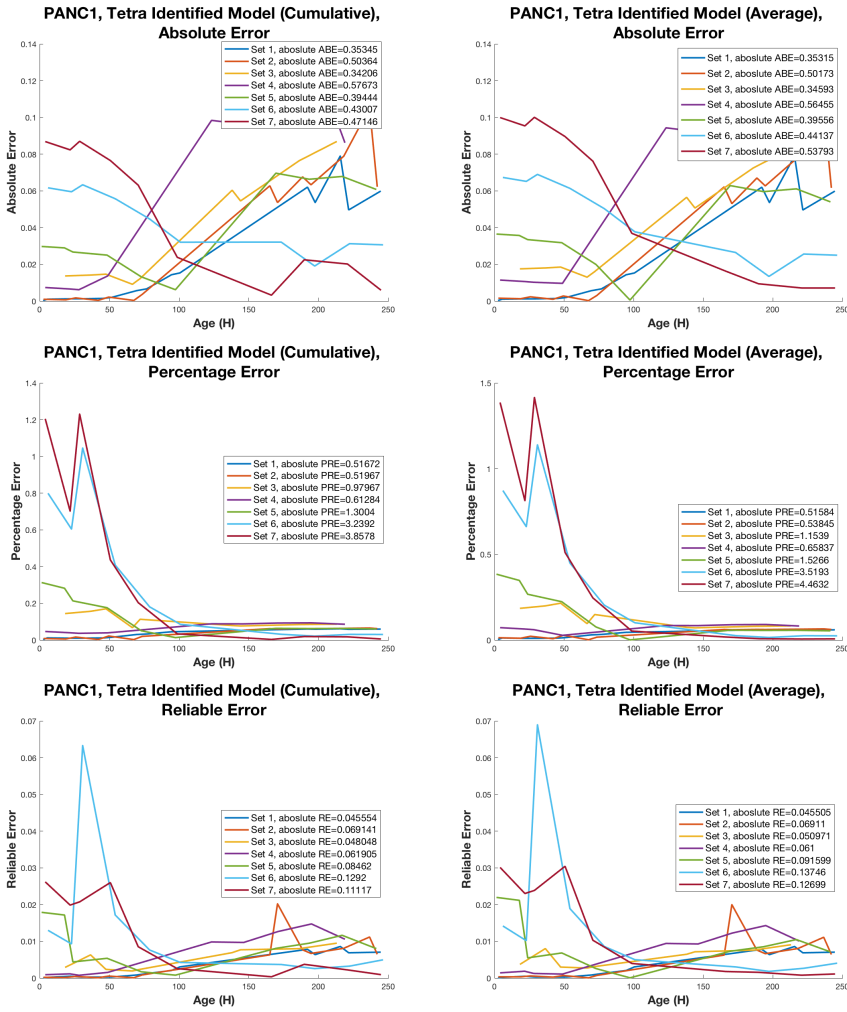

Figure 3.5: *Tetra (3H) identified model of both Cumulative and Average identification showing absolute error with respect to experimental data of all 7 sets of PANC1*

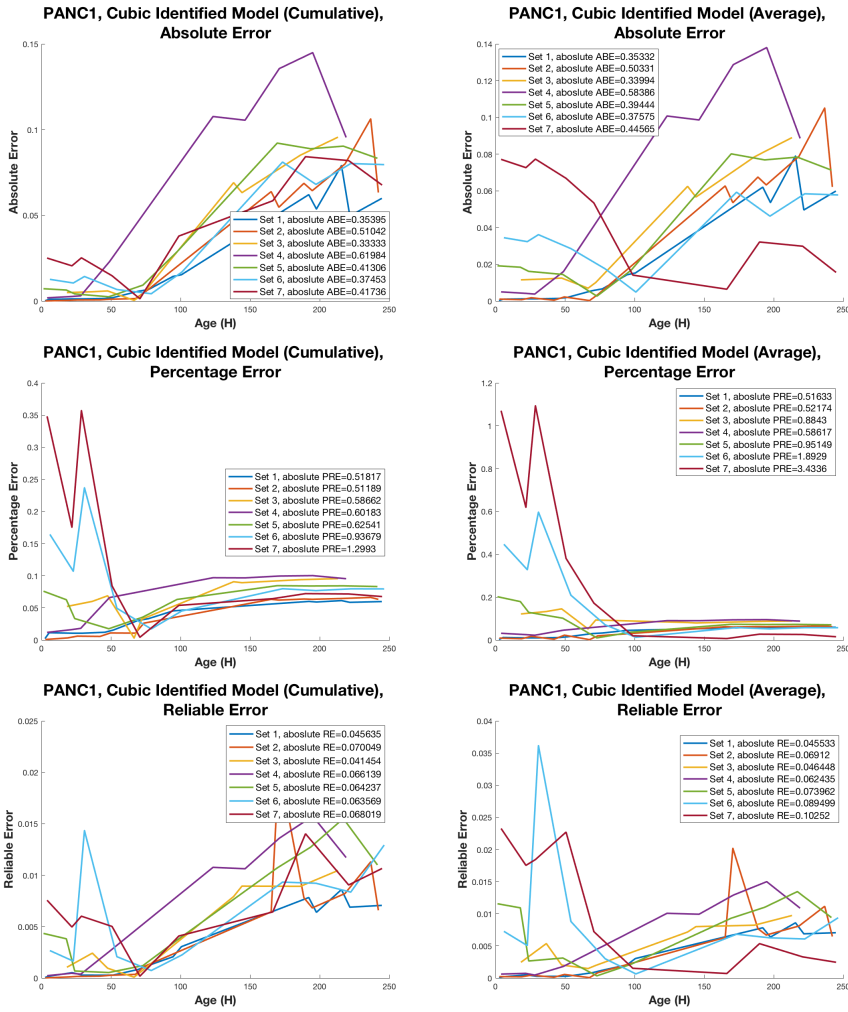

Figure 3.6: *Cubic (3H) identified model of both Cumulative and Average identification showing absolute error with respect to experimental data of all 7 sets of PANC1*

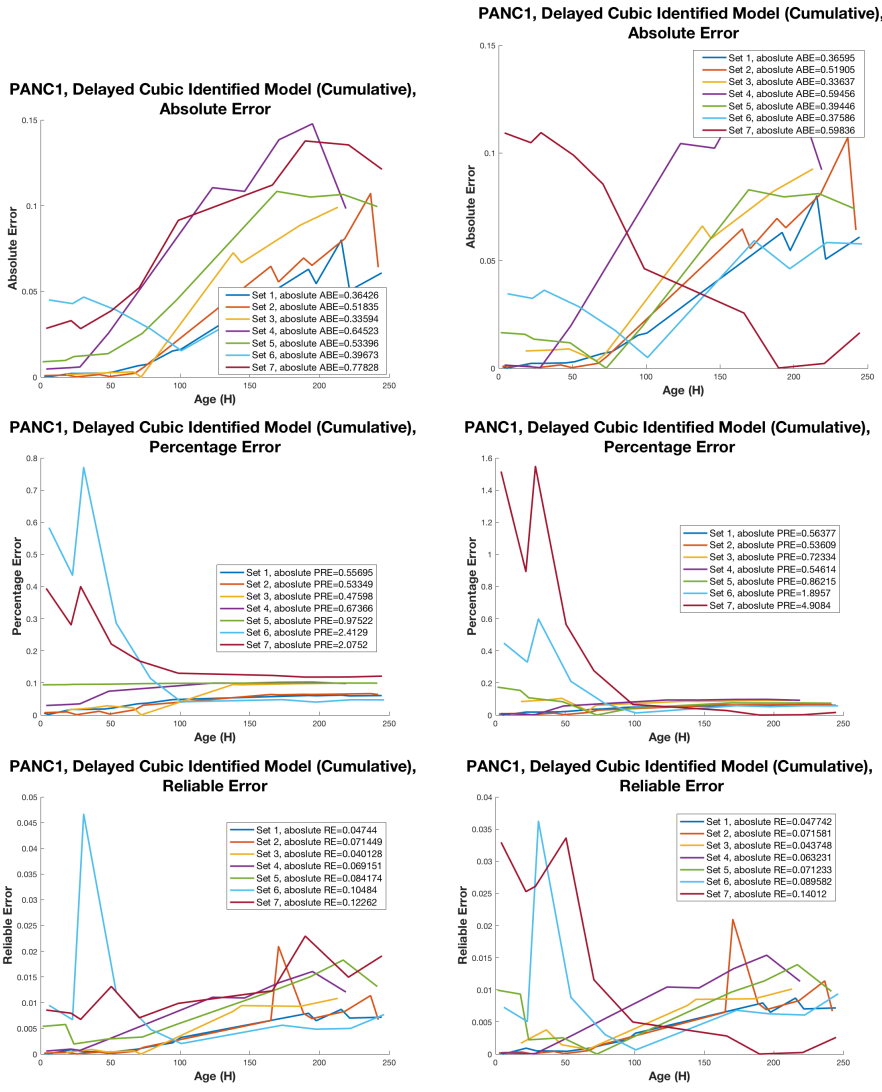

Figure 3.7: *Delayed cubic (18H) identified model of both Cumulative and Average identification showing absolute error with respect to experimental data of all 7 sets of PANC1*

Table 3.8: Ranking table of different models for BxPC3 growth. 1st best is number of times least error has appeared and 2nd best is the number of times 2nd least error has appeared out of 42 cases containing BxPC3 2D growth

MODELS	1st Best	2nd Best	Total
LOGISTIC	8	12	**20**
DELAYED LOGISTIC	2	2	**4**
GOMPERTZ	2	2	**4**
CUBIC	15	7	**22**
DELAYED CUBIC	2	2	**4**
PARABOLA	6	7	**13**
SQUARE ROOT	0	0	**0**
TETRA	6	9	**15**
BERTANLAFFY	1	1	**2**

3.7 Identification of best mathematical models for 2D BxPC3 growth data

For BxPC3 also we used normalized and resampled growth data from 7 different experiments with triplicates to identify the best model to explain about the growth behavior of this cell lines in two-dimensional culture.

3.7.1 Identification of best 3 models for BxPC3 growth

To begin with, we identified best 3 models out of 9 model equations as follows

Selection of best models

We followed the same protocol mentioned in section 3.5 for all the 42 cases containing the data of BxPC3 cell growth. Then we selected the best three models as above based on the ranking table for each model equation. Following table 3.8 is the ranking table for different models of BxPC3 growth showing a number of times the least error index has appeared.

From the ranking table 3.8, we know that Logistic, Cubic and Tetra models work better for BxPC3 growth identification. So we selected these 3 models for further studies.

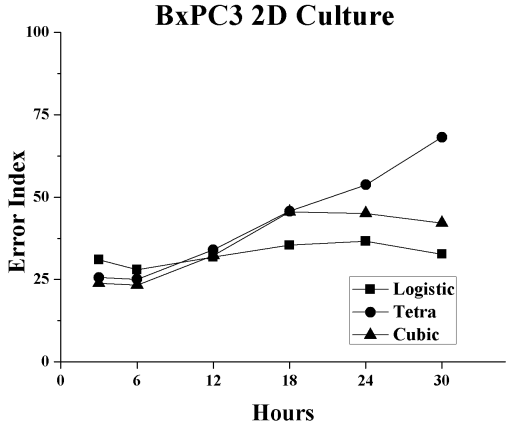

Figure 3.8: *The best 3 models of BxPC3 to predict the cell growth showing different error index at the different sampling time.*

Selection of best fixed time

We selected the best fixed time for the above-selected models of logistic, cubic and tetra models. We tested error index at a different fixed time interval such as 3, 6,12,18, 24 and 30H. Figure 3.8 shows the error index of these 3 selected models at a different time interval. From the figure 3.8, it can be seen that all the 3 models were good at 6H fixed time as they have least error index.

Identification of coefficients

For these three identified models we redid the identification with the best sampling time of 6H as mentioned earlier in section 3.6.1 and found out the average and cumulative coefficients for 7 sets of the experiment. Table 3.9 shows identified coefficients for logistic model, table 3.10 for the cubic model and table 3.11 for tetra model. All the tables contain identified coefficients for both average and cumulative at fixed sampling time 6H.

Behavior of Growth rate

Then we tried to understand the growth of BxPC3 using these identified models, logistic, cubic and tetra with a fixed time of 6H. We have studied

Table 3.9: Identified Logistic (6H) Model for BxPC3 Growth showing both Average and Cumulative identified coefficients

Logistic coefficients	SET 1	SET 2	SET 3	SET 4	SET 5	SET 6	SET 7	Average	Cumulative
a1	1.1840	1.1788	1.1364	1.2086	1.1987	1.2427	1.2511	1.2001	1.1528
b1	0.1608	0.1733	0.1364	0.1642	0.1987	0.2338	0.2511	0.1883	0.1386

Table 3.10: Identified Cubic (6H) Model for BxPC3 Growth showing both Average and Cumulative identified coefficients

Cubic coefficients	SET 1	SET 2	SET 3	SET 4	SET 5	SET 6	SET 7	Average	Cumulative
a1	1.1470	1.1193	1.0964	1.1782	1.1451	1.1677	1.1689	1.1461	1.1019
b1	0.1353	0.1121	0.0964	0.1467	0.1451	0.1556	0.1689	0.1372	0.0839

the growth rate for the identified model for both 'Average' and 'Cumulative' cases and its shown in figure 3.9 and as the cell number reaches 1 the growth stops. All the models are at a maximum when the cell is isolated at the beginning even in Average and Cumulative cases. The logistic model shows that cell count decreases linearly as the cell count grows indicating cells are very sensitive to the surrounding system. Cubic shows a quadratic decrease in cell count. Tetra also shows a gradual decrease in cell count as the cell grows. Following are the growth rates for the identified models,

Logistic Model

Average: $G(Y(k-1)) = 1.1495 - 0.1356Y(k-1)$
Cumulative: $G(Y(k-1)) = 1.1527 - 0.1386Y(k-1)$

Cubic Model

Average: $G(Y(k-1)) = 1.146 - 0.1372Y(k-1)^2$
Cumulative: $G(Y(k-1)) = 1.1018 - 0.0838Y(k-1)^2$

Table 3.11: Identified Tetra(6H) Model for BxPC3 Growth showing both Average and Cumulative identified coefficients

Tetra Coefficients	SET 1	SET 2	SET 3	SET 4	SET 5	SET 6	SET 7	Average	Cumulative
a1	1.1860	1.2333	1.0932	1.2365	1.1943	1.1295	1.1176	1.1701	1.2045
b1	0.1946	-0.5153	-0.8060	0.5910	-0.0565	-0.5967	-1.6690	-0.4083	-0.3071
b2	-0.2576	0.6830	1.2633	-0.9596	0.0936	1.2224	2.9249	0.7100	0.4131
b3	0.2389	0.0700	-0.3783	0.5544	0.1572	-0.5038	-1.1608	-0.1461	0.1033

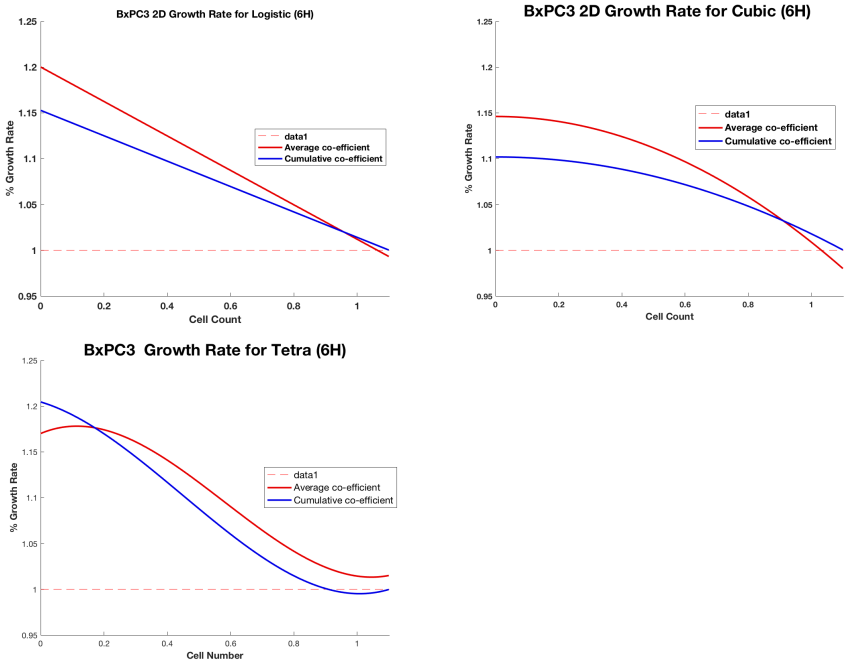

Figure 3.9: *Logistic, Cubic and Tetra model showing growth rate behavior for BxPC3 cells culture in 2D at 6H sampling time*

Tetra Model

Average: $G(Y(k-1)) = 1.17+0.4082Y(k-1)^3-0.71Y(k-1)^2+0.1461Y(k-1)$
Cumulative: $G(Y(k-1)) = 1.2045 + 0.307Y(k-1)^3 - 0.413Y(k-1)^2 - 0.1033Y(k-1))$

Equations of best 3 identified models of BxPC3

All the best 3 identified models logistic, cubic and tetra model equations at 6H sampling time are presented with their identified coefficients of both 'Average' and 'Cumulative' are as follows,

Identified Logistic Model equation with the both 'Average' and 'Cumulative' identified coefficients are as follows

Average
$Y(k) = 1.2Y(k-1) - 0.1883Y(k-1)^2$
Cumulative
$Y(k) = 1.1527Y(k-1) - 0.1386Y(k-1)^2$

Identified Cubic Model equation is shown below with its both 'Average' and 'Cumulative' identified coefficients
Average
$Y(k) = -0.1371Y(k-1)^3 + 1.1461Y(k-1)$
Cumulative
$Y(k) = -0.0838Y(k-1)^3 + 1.1018Y(k-1)$

Identified Tetra Model equation is shown below with its coefficients
Average
$Y(k) = 0.4082Y(k-1)^4 - 0.71Y(k-1)^3 - 0.146Y(k-1)^2 + 1.17Y(k-1)$
Cumulative
$Y(k) = 0.3070Y(k-1)^4 - 0.4131Y(k-1)^3 - 0.1033Y(k-1)^2 + 1.2045Y(k-1)$

Error of identified models

We have found all three different identified models errors with respect to each experimental data for both Average and Cumulative identification. Figure 3.10 shows identified logistic model errors with respect to experimental data, Figure 3.11 shows identified cubic model error with respect to experimental data and Figure 3.12 shows identified tetra model errors with respect to experimental data.

3.7.2 Selection of best-identified model out of 3 identified models for BxPC3

To select a single best model out of best three identified models, we estimated the error index again using these identified models Logistic (6H), Cubic (6H) and Tetra (6H) for all the 7 set of experiments and same is shown in table 3.12. According to the table, logistic model with 6H sampling time is the best-identified model for predicting the growth of BxPC3. We considered

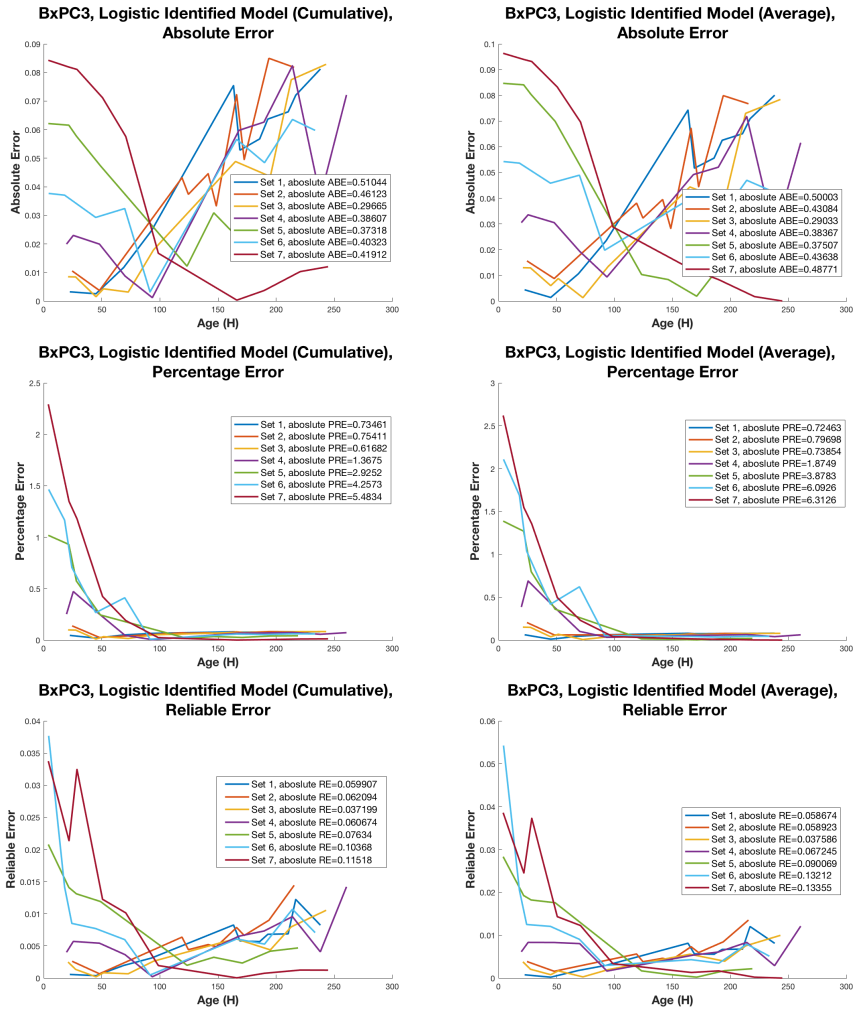

Figure 3.10: *Logistic (6H) identified model of both Cumulative and Average identification showing absolute error with respect to experimental data of all 7 sets of BxPC3*

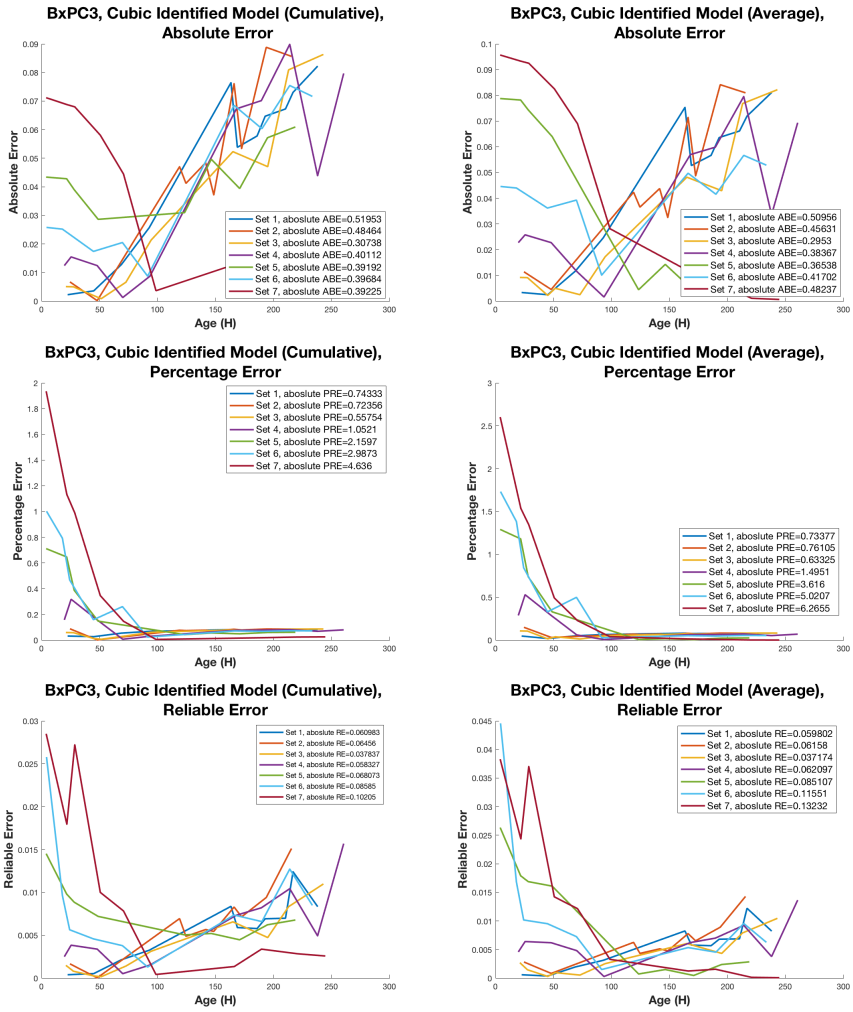

Figure 3.11: *Cubic (6H) identified model of both Cumulative and Average identification showing absolute error with respect to experimental data of all 7 sets of BxPC3*

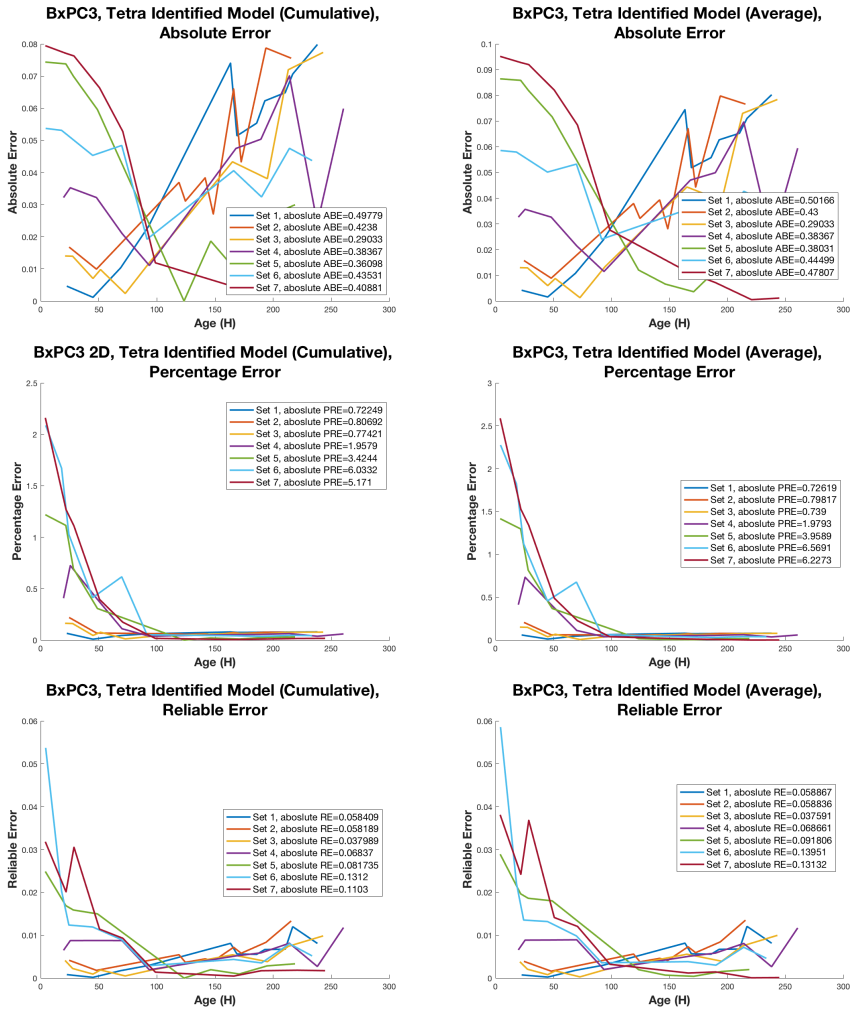

Figure 3.12: *Tetra (6H) identified model of both Cumulative and Average identification showing absolute error with respect to experimental data of all 7 sets of BxPC3*

Table 3.12: Error Index estimated from best 3 models for each set of experiment of BxPC3 growth

Best Model	1 SET	2 SET	3 SET	4 SET	5 SET	6 SET	7 SET	Sum
Logistic model (6H)	15.7915	13.0285	3.4591	7.3326	9.6761	12.4407	28.1945	**89.9230**
Cubic model (6H)	18.3349	17.4046	6.6309	12.3413	6.3782	10.2367	23.2030	94.5296
Tetra (6H)	17.1330	12.1826	4.8158	7.0221	17.8724	23.1328	26.7592	108.9180

only cumulative since the averaging procedure can not guarantee that the constraints are always satisfied, cumulative models turn out more reliable, and we suggest their use over the average versions.

3.8 Identification of best mathematical models for 2D MiaPaCa2 growth data

As mentioned earlier for PANC1 and BxPC3, we also used normalized and resampled MiaPaCa2 growth data of 7 different experiments with triplicates to identify the best model to explain about the growth behavior of this cell lines in two dimensional culture.

Selection of best models

As earlier, for MiaPaCa2 we have identified the best models as mentioned in section 3.5. Table 3.13 shows a ranking table of different models for MiaPaCa2.

From the table 3.13, we selected the best 3 models as Logistic, Cubic and Tetra models fit better for MiaPaCa2 growth. So we selected these 3 models for further studies.

Selection of best fixed time

We selected the best fixed time point for logistic, cubic and tetra models based on the least error index. Figure 3.13 shows the best three models error index with different sampling time. Form the figure 3.13 it can be seen that all the 3 models have 3H sampling time the least error index.

Table 3.13: Ranking table of different models for MiaPaCa2 growth. 1st best is number of times least error has appeared and 2nd best is the number of times 2nd least error has appeared out of 42 cases containing MiaPaCa2 2D growth

MODELS	**1st Best**	**2nd Best**	**Total**
LOGISTIC	6	12	**18**
DELAYED LOGISTIC	5	4	**9**
GOMPERTZ	1	3	**4**
CUBIC	8	7	**15**
DELAYED CUBIC	8	2	**10**
PARABOLA	4	3	**7**
SQUARE ROOT	0	2	**2**
TETRA	11	10	**21**
BERTANLAFFY	0	0	**0**

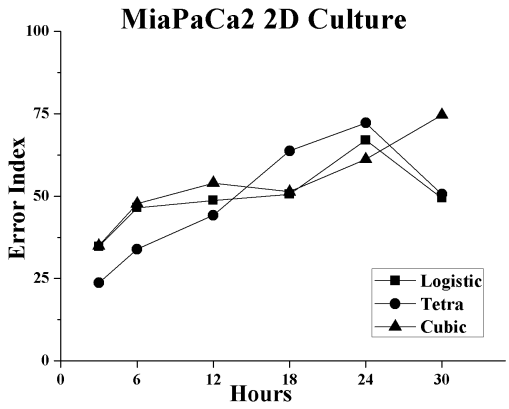

Figure 3.13: *The best 3 models of MiaPaCa2 to predict the cell growth showing different error index at different sampling time*

Table 3.14: Identified Logistic (3H) Model for MiaPaCa2 Growth showing both Average and Cumulative identified coefficients

Logistic Coefficients	SET 1	SET 2	SET 3	SET 4	SET 5	SET 6	SET 7	Average	Cumulative
a1	1.0215	1.1416	1.1501	1.1528	1.1188	1.0937	1.1393	**1.1168**	**1.0530**
b1	0.0138	0.0979	0.1197	0.1285	0.1078	0.0787	0.1195	**0.0951**	**0.0366**

Table 3.15: Identified Cubic (3H) Model for MiaPaCa2 Growth showing both Average and Cumulative identified coefficients

Cubic Coefficients	SET 1	SET 2	SET 3	SET 4	SET 5	SET 6	SET 7	Average	Cumulative
a1	1.0174	1.1085	1.1123	1.1116	1.0883	1.0584	1.0998	**1.0852**	**1.0327**
b1	0.0072	0.0518	0.0714	0.0790	0.0727	0.0412	0.0734	**0.0567**	**0.0156**

Identification of coefficients

We redid the identification for the selected models and identified the coefficients for both Average and Cumulative as mentioned in section 3.6.1 . Table 3.14 shows coefficients for the identified logistic model, table 3.15 shows coefficients for the identified cubic model and table 3.16 coefficients of identified tetra model for both 'Average' and 'Cumulative' cases at the 3H sampling time.

Behavior of Growth rate

We studied the growing behavior of MiaPaCa2 using growth rate graph shown in figure 3.14, It is worth stressing that as the cell number reaches 1 the growth stops. It is clear from the figure 3.14 that all the cumulative identification growth rates are higher in the initial period then gradually decreases this indicates that system supports the cell growth higher initially and then it decreases. Whereas in case of average identification, logistic and

Table 3.16: Identified Tetra (3H) Model for MiaPaCa2 Growth showing both Average and Cumulative identified coefficients

Tetra Coefficients	SET 1	SET 2	SET 3	SET 4	SET 5	SET 6	SET 7	Average	Cumulative
a1	1.0000	1.0000	1.0000	1.0495	1.0808	1.0608	1.0662	**1.0368**	**1.0744**
b1	-0.0317	-0.3005	-0.8507	-0.4440	-0.2265	-0.4552	-0.6827	**-0.4273**	**-0.0671**
b2	0.1057	0.8224	1.9011	1.0094	0.4781	0.9278	1.3627	**0.9439**	**0.1496**
b3	-0.0878	-0.5609	-1.0510	-0.5309	-0.1785	-0.4122	-0.6099	**-0.4901**	**-0.0226**

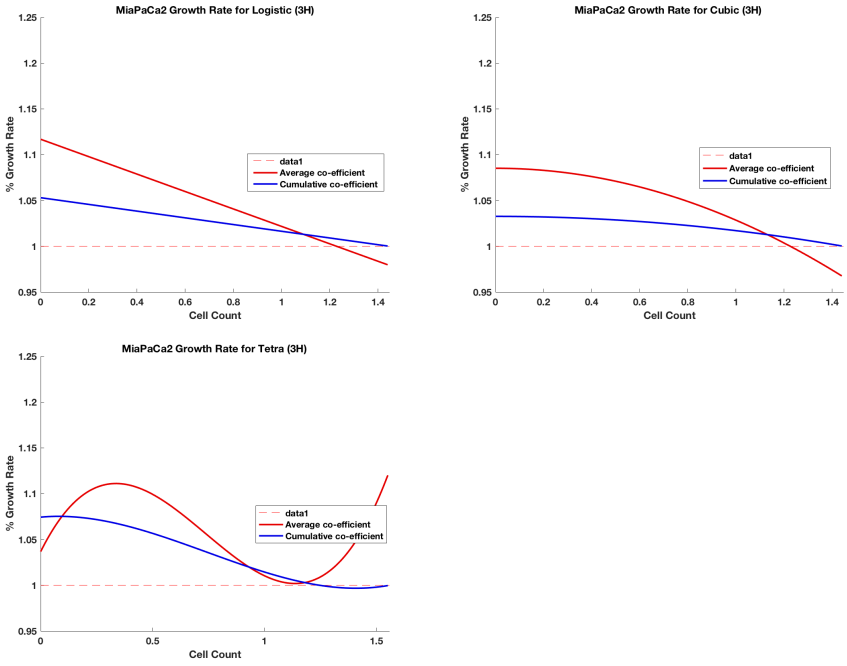

Figure 3.14: *Logistic, Cubic and Tetra model showing growth rate behavior for MiaPaCa2 cells culture in 2D at 3H sampling time, showing the difference in growth rate between cumulative and average tetra identification*

cubic model shows that initially growth is higher and then decreases with different slopes. In tetra model especially in average identified coefficients, the growth rate was slow and then increases and then slows down.

Following are the growth rates for the identified models at 3H fixed sampling time

Logistic Model

Average: $G(Y(k-)) = 1.1168 - 0.0951Y(k-1)$

Cumulative: $G(Y(k-1)) = 1.053 - 0.0366Y(k-1)$

Cubic Model

Average: $G(Y(k-1)) = 1.0852 - 0.0566Y(k-1)^2$

Cumulative: $G(Y(k-1)) = 1.0326 - 0.0155Y(k-1)^2$

Tetra Model
Average: $G(Y(k-1)) = 1.0367 + 0.4273Y(k-1)^3 - 0.9438Y(k-1)^2 + 4901Y(k-1)$
Cumulative: $G(Y(k-1)) = 1.0744 + 0.0671Y(k-1)^3 - 0.1496Y(k-1)^2 + 0.0226Y(k-1)$

Equations the identified models of MiaPaCa2

All the 3 identified models structure with the respectively identified coefficients of both 'Average' and 'Cumulative' are presented below.

Identified Logistic Model equations at 3H sampling time with the identified coefficients of average and cumulative identifications are as follows
Average
$Y(k) = 1.1168Y(k-1) - 0.0951Y(k-1)^2$
Cumulative
$Y(k) = 1.053Y(k-1) - 0.0366Y(k-1)^2$

Identified Cubic Model equations at 3H sampling time with identified 'Average' and 'Cumulative' coefficients are as follows
Average
$Y(k) = -0.0566Y(k-1)^3 + 1.0852Y(k-1)$
Cumulative
$Y(k) = -0.0155Y(k-1)^3 + 1.0326Y(k-1)$

Identified Tetra Model equation at 3H sampling time with identified 'Average' and 'Cumulative' coefficients are as follows
Average
$Y(k) = 0.4273Y(k-1)^4 - 0.9438Y(k-1)^3 + 4901Y(k-1)^2 + 1.0367Y(k-1)$
Cumulative
$Y(k) = 0.0671Y(k-1)^4 - 0.1496Y(k-1)^3 + 0.0226Y(k-1)^2 + 1.0744Y(k-1)$

Table 3.17: Error Index estimated from best 3 models for each set of experiment of MiaPaCa2 growth

Best Model	1 SET	2 SET	3 SET	4 SET	5 SET	6 SET	7 SET	Sum
Logistic model (3H)	14.6503	15.3426	10.5631	15.5998	4.9847	9.8621	20.8780	**91.8805**
Cubic model (3H)	14.8368	15.4911	12.3341	17.8637	9.4226	10.0499	13.3247	93.3229
Tetra (3H)	15.4787	13.8955	9.4155	13.3708	7.2518	16.3430	30.0000	105.7553

Error of identified models of MiaPaCa2

All the three identified models logistic, cubic, and tetra models absolute errors with respect to each set of experiment was calculated. All the three errors were estimated. Figure 3.15 shows the identified logistic model error. Figure 3.16 shows all three errors of cubic model identification and figure 3.17 shows the errors of identified tetra model.

3.8.1 Selection of best-identified model out of 3 identified models for MiaPaCa2

Like earlier from three best models, we identified the best model to predict the growth of MiaPaCa2 cells. Since the averaging procedure can not guarantee that the constraints are always satisfied, cumulative models turn out more reliable, and we used cumulative version over the average versions. We estimated the error index for the best 3 identified models, logistic (3H), cubic (3H) and tetra (3H) models for all the 7 set of experiments. The table 3.17 shows the error index for each experiment with respect to identified model and according to the table logistic model shows the better fitting for the MiaPaCa2 growth. This model can be considered for understanding the growth of the cells.

3.9 Tetra Model is the best model for all the cell lines of reliable data

Earlier best model identification for all the cell lines are based on the sets, which are not 'equivalent' in terms of modeling error. There may be some difference among these sets, which are not evident by a simple look at the data. So we decided to 'falsify' the not good sets by repeating the analysis considering only first 5 sets of 7 in term of modeling error. The repetition

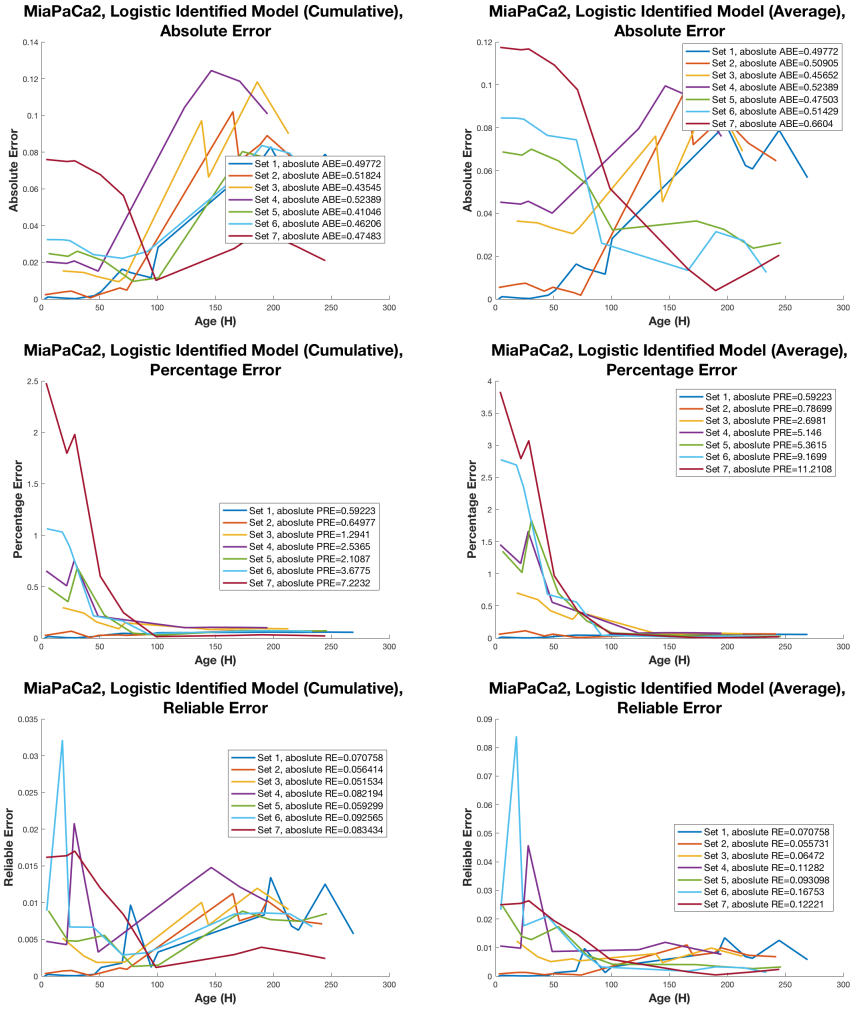

Figure 3.15: *Logistic (3H) identified model of both Cumulative and Average identification showing absolute error with respect to experimental data of all 7 sets of MiaPaCa2*

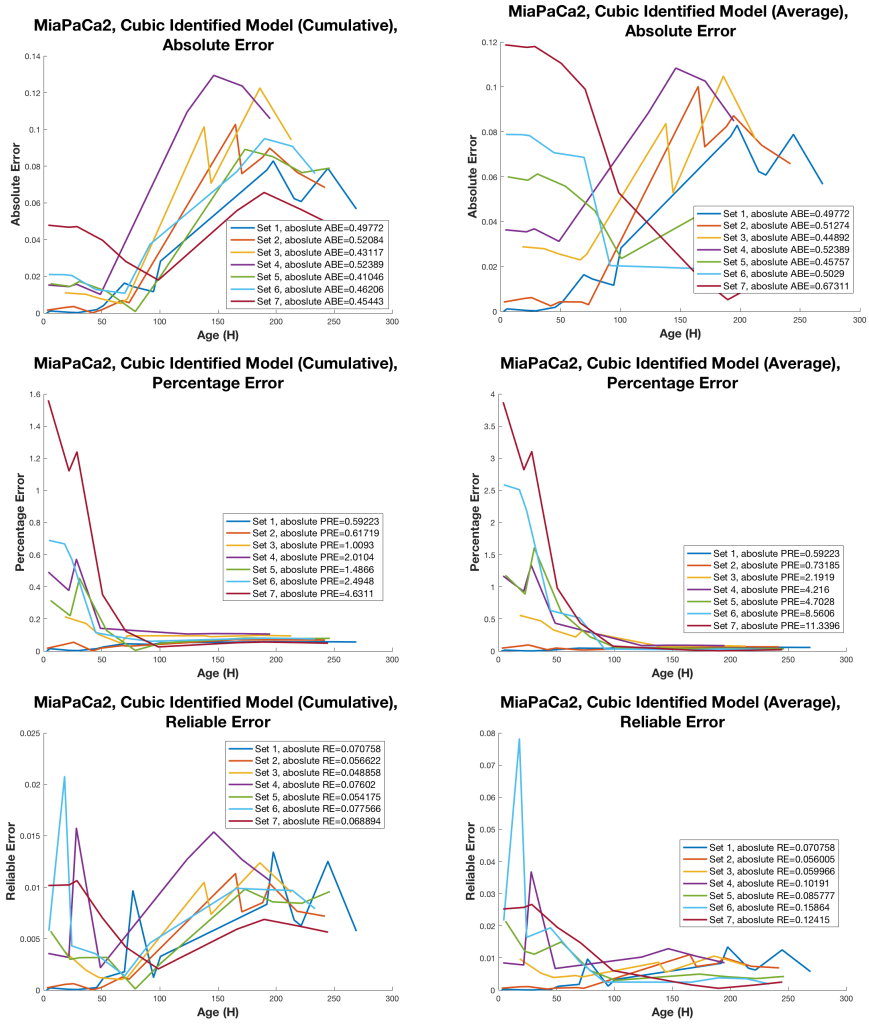

Figure 3.16: *Cubic (3H) identified model of both Cumulative and Average identification showing absolute error with respect to experimental data of all 7 sets of MiaPaCa2*

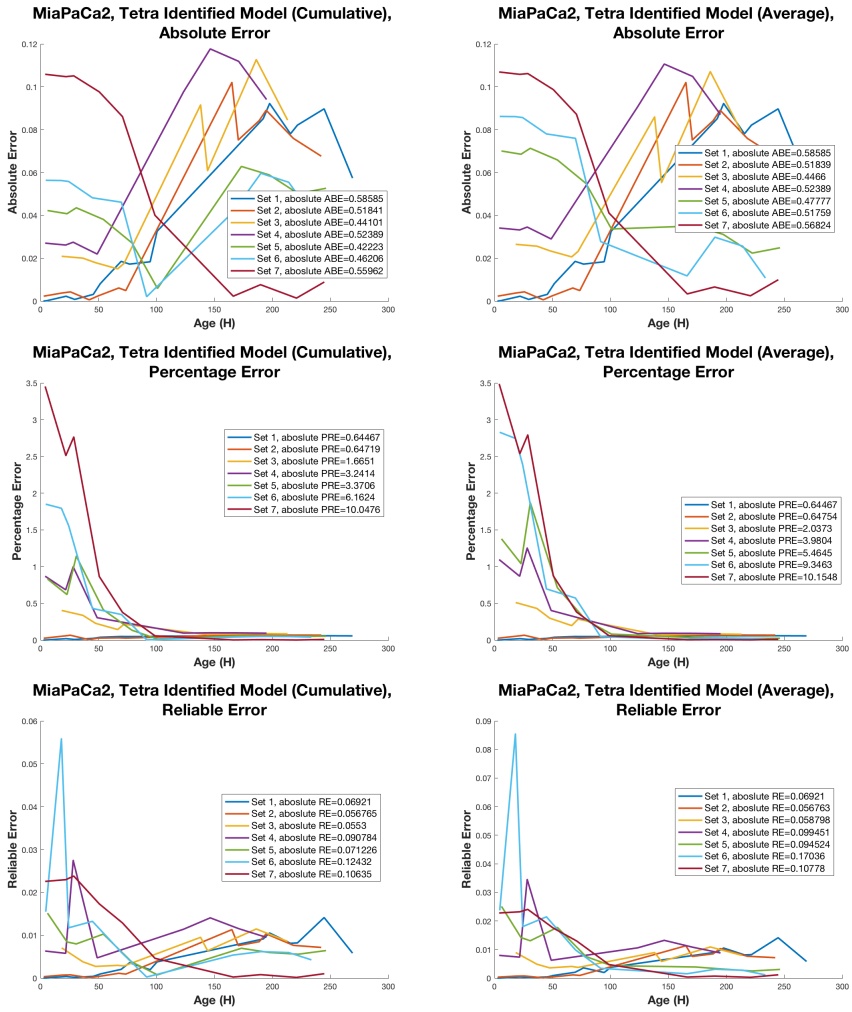

Figure 3.17: *Tetra (3H) identified model of both Cumulative and Average identification showing absolute error with respect to experimental data of all 7 sets of MiaPaCa2*

Table 3.18: New Error Index for 5 good sets of PANC1

PANC1 Best 3 models	**SET 1**	**SET 3**	**Set 5**	**SET 6**	**SET 7**	**Sum**
Delyaedcubic model (18H)	4.803	11.291	17.161	11.379	30.000	**74.635**
Cubic model (3H)	7.502	10.686	24.657	17.160	27.068	**87.074**
Tetra (3H)	10.515	10.359	21.791	10.164	14.586	**67.415**

of analysis with bigger reduction of sets resulted in not sufficient consistent results. The error index of repeating the analysis with 5 sets was completely different than earlier results. The new error index was shown in Table 3.18 for PANC1 table 3.19 for BxPC3 and table 3.20 for MiaPaCa2 with 5 sets. Repetition of analysis with 5 good sets error index showed the following differences in comparison with earlier error index, which used to estimate the best model among three better models,

1. First, we see a major change in the error index in all the three cell lines with respect to each set.

2. All the three cell lines showed tetra model as the 1st best model with least sum of error index

3. This tetra identification lead that all the cell line have general shape of the growth rate

4. Among these cell lines, BxPC3 has different sampling time i.e 6H whereas other two cell lines have 3H sampling time, which indicates that BxPC3 growth behavior is 'slower' compared to other two cell lines.

Overall we could say that when the data were less reliable, the best model was logistic and cubic which were 'simpler' compared to tetra model. This simple model like logistic was able to catch the more evident behavior. When the data were more reliable, the model was able to grab the details which might be not evident. The growth rate of tetra i.e. cubic shape was much better than logistic, which had constant decreasing shape.

Table 3.19: New Error Index for 5 good sets of BxPC3

BxPC3 Best 3 models	**SET 1**	**SET 2**	**SET 3**	**Set 6**	**SET 7**	**Sum**
Logistic model (6H)	21.182	18.349	5.678	17.827	14.364	77.401
Cubic model (6H)	21.539	20.755	4.528	18.301	16.229	81.352
Tetra (6H)	21.000	15.616	6.119	15.748	14.581	73.065

Table 3.20: New Error Index for 5 good sets of MiaPaCa2

MiaPaCa2 Best 3 Models	SET 4	SET 3	Set 5	SET 6	SET 7	SUM
Logistic (3H)	21.182	13.600	12.280	13.267	12.000	72.329
Cubic model (3H)	27.159	5.665	7.739	12.117	17.462	70.142
Tetra (3H)	21.891	8.180	9.039	10.447	12.000	61.557

3.10 Discussion

We have used discrete non-linear autoregressive logistic family for building the growth model for all the cell lines cultured in 2D condition. We studied the growing capabilities of three different PDAC cell lines PANC1, BxPC3, and MiaPaCa2. The growth data of these cell lines were acquired for 10 days and all the experiments were performed seven times in triplicates. We had 42 cases for each cell line by normalizing and resampling the data in order to build a mathematical model. We compared 9 different structures of model equation 3.1 based on the 'growth rate' paradigm for each case and selected the three best structures depending on the least error for all the cell lines. The error is described through a special index which represents the ability of a model in describing the real data. We selected the best sampling time for these 3 models based on the least error index followed by re-identification using the averaging and cumulative methods. These latter methods behave in a similar way, but Averaging identification is not forced to satisfy the identification constraints. So we focused only on cumulative identification.

For PANC1 tetra and cubic models with 3H sampling time and delayed cubic model with 18H were the three most suitable models out of nine for

fitting the growth. Out of these three models, we re-identified the best model based on the least error and Cubic model with 3H sampling was best (Table 3.18). According to cubic, the growth rate was simpler, as it was higher in the beginning and then gradually decreases as the cell grew with time (Figure 3.4).

For BxPC3 cells logistic, cubic and tetra models with 6H sampling time were the three most suitable models for fitting the growth. Again we selected the best among these three identified models using error index. Among these three models, a logistic model with 6H was best based on the least error (Table 3.19). According to logistic model, BxPC3 has a higher growth rate in the beginning and then sharply decreases (Figure 3.9). This perhaps indicates that cells were very sensitive to the presence of the other neighbor cells.

For MiaPaCa2 cells logistic, cubic and tetra models with 3H sampling time were the three best models for fitting the growth. Among these three models, a logistic model with 3H sampling time was best for describing the growth of the cells (Table 3.20) based on the error index. Logistic growth rate showed that MiaPaCa2 has higher growing capabilities in the beginning and then decreases gradually as the cells grew (Figure 3.14).

During the identification certain set of experiments emerged as hard to model. For each cell line, two sets of experiments were falsified. We narrowed our identification to only good sets, which were modeled with less model error. We reidentified the best model, which turned out to be tetra model for all the three cell lines, indicating some similarity in all of them. We compared all the three cell lines with a sampling time of 3H for sake of similarity even though BxPC3 best sampling time was 6H against the 3H of PANC1 and MiaPaCa2. All the cell lines showed tetra model as the best. Thus, the three cell lines turned out to share the same growth rate structure. Figure 3.18 shows the comparison of tetra growth rate with 3H. Even though all the cell lines have the same structure of growth rate, they differ in the other features such as the position of the peak, maximum attained, slope during the decreasing phase of the growth rate. This may be due to cells require some time for attaching and adapting to a new environment and also in tetra growth rate decreasing phase of growth rate can show differences in slope due to lack of nutrients and cell numerosity. PANC1 showed lower cell count at the beginning as they were isolated. This may be related to the need of the cell to create a special environment around itself or to adapt

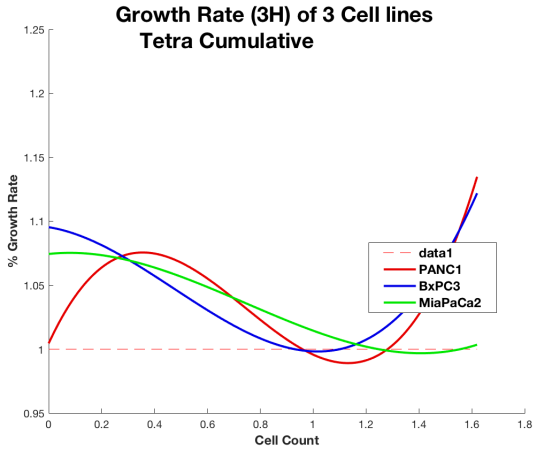

Figure 3.18: *Growth rate for Tetra (3H) identified model for all three PDAC cell lines*

to the new environment. Whereas BxPC3 and MiaPaCa2 showed higher growing abilities at the beginning. All the three cell lines showed different decreasing growth rates. We anticipate the growth rate of BxPC3 higher at the beginning but the best sampling time is 6H.

Figure 3.19 shows the new best models comparison with a single set of actual data for all the cell lines. We could see the similarity between them.

A posteriori reliability analysis of the identified parameters has been taken into account for these set of experiments. It has been performed for all the three cell lines by randomly varying the identified parameters within intervals of amplitude from 1 to 5 percentage. The resulting randomly varied models have been simulated and their mean absolute error with respect to the original identified model has been computed. The average errors of the varied models with respect to the original identified ones are shown in figure 3.20. As expected, higher variations generate bigger deviations from the original identified models. However, within the considered percentage scopes, the error values are a small fraction of the signals range, and moreover no sudden increases of the errors have been observed. Therefore, the identified models have shown a reliable behaviour with respect to small changes in the parameters.

Overall we can conclude that reliable data are very crucial in the identi-

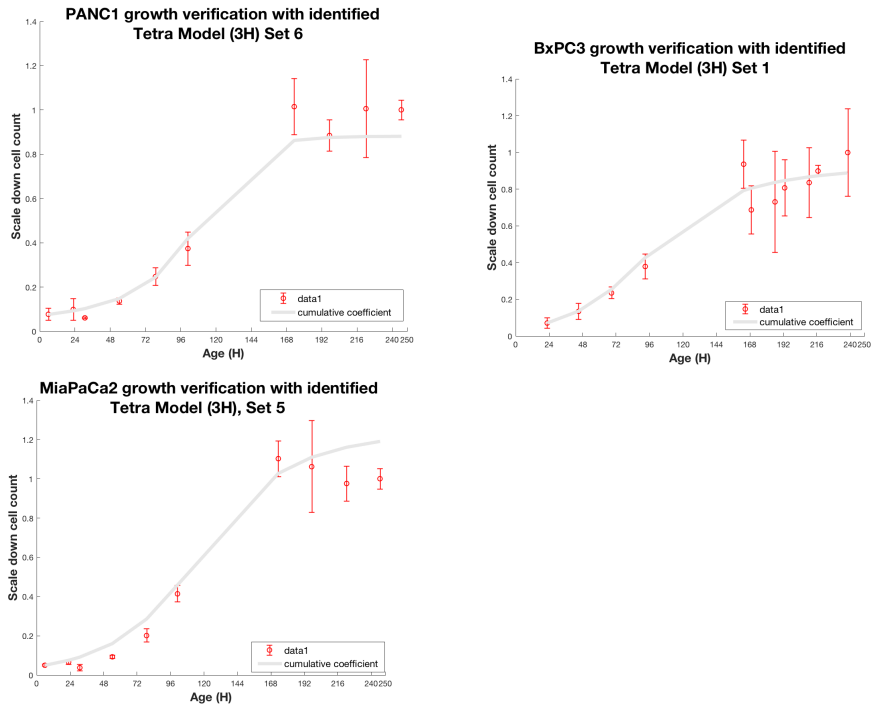

Figure 3.19: *Comparison of identified tetra model (3H) with the experimental data of all three cell lines*

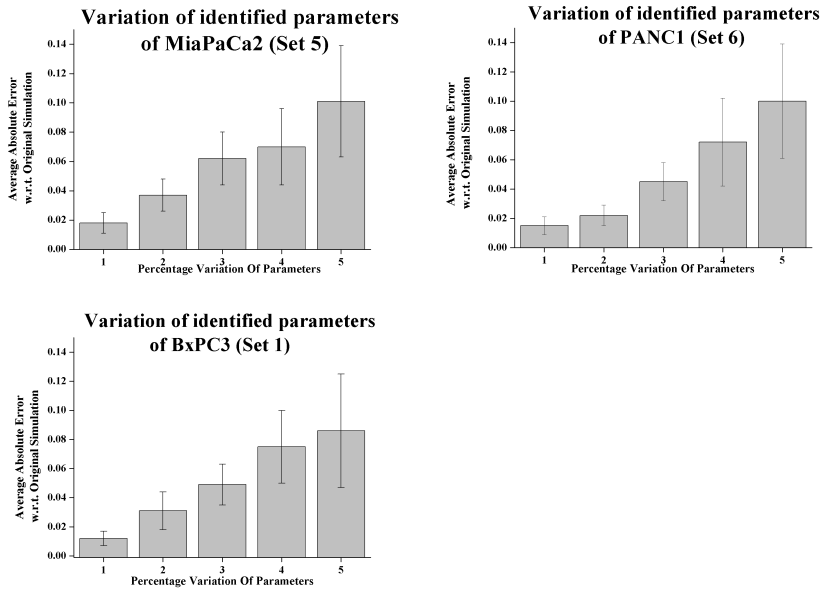

Figure 3.20: *Variation of identified parameters to understand the sensitivity of the model*

fication process. This can also be achieved by re-designing the experiments in order to collect more data, so that the differences among the experiments may be clearly explained. All the cell lines showed qualitatively similar growth rate. This suggests the possibility of their reproduction is based on common mechanisms. Cell lines seem to be differently affected by their own numerosity. This factor should be carefully checked to understand the reason. From this analysis more sophisticated models could be designed.

Chapter 4

Conclusion

In spite of continuous advancements in medical treatment pancreatic ductal adenocarcinoma (PDAC) related high mortality remains unchanged. There are few or no effective therapies for the advanced PDAC [19]. Conventional and effective experimental methods are required to examine the biological behavior of PDAC and develop the therapeutic strategies for PDAC. We studied the behavior of PDAC cell lines in terms of growth profiles, cell morphology, drug responses in 2D, 3D and *in vivo* systems.

Traditionally cancer cells are cultured in two-dimensional (2D) culture that has many advantages. 2D culture is more convenient, easy to handle and perform experiments to explain the mechanisms of disease and helps in drug development. In this work, we have studied the differences in cell growth profile, cell morphology, and drug resistance capacity in three different cell lines (PANC1, BxPC3, and MiaPaCa2) of PDAC. In terms of growth profile, all the PDAC cell lines proliferated to the same extent with similar growth rates. In terms of cell morphology BxPC3 cells have flattened morphology, MiaPaCa2 have round and mesenchymal while PANC1 with intermediate morphology between mesenchymal and epithelial. The actin filaments organizations, as a pro-migratory functional marker, were long and elongated and localized in the cytoplasm.

In three-dimensional (3D) culture, cells were grown on agarose scaffold to form aggregates/spheroids that enhances cell-cell interactions and partially mimic the *in vivo* environment. Additionally, 3D spheroids comprised of different stages of cells that includes cells are highly proliferative, quiescent, apoptotic, hypoxic and necrotic. The outer layer of a spheroid, which is

highly exposed to the medium is mainly composed of proliferating cells and inner core cells receive less oxygen, growth factors and nutrients from the medium tend to be in a quiescent or hypoxic state [27]. As we studied the proliferation of these PDAC cell lines PANC1, MiaPaCa2 and BxPC3 in 3D culture, we observed a significant difference in their growth rate and morphology. BxPC3 spheroids were highly compact and almost null growth rate, whereas MiaPaCa2 and PANC1 showed loosely arranged cells of larger spheroids with comparable growth rates. Three dimensional (3D) spheroids showed altered cytoskeleton structure compared to 2D culture having short actin filaments localized near the cell membrane.

Later we examined the possibility of using more complex 3D cell culture systems in microfluidic platform suitable for studying characteristics of PDAC cells. This microfluidic system also called as HepaChip® was coated with collagen-1, a highly secreted extracellular matrix (ECM) in around pancreatic cancer that plays a crucial role, among many, in drug resistance and cancer progression. HepaChip® also uses continuous perfusion of cell culture system where cells are assembled on the collagen and cells are superfused with growth medium. Such a platform could be further employed to improve drug testing and screening of PDAC. The 3D structure of the HepaChip® enabled the formation of cell aggregates especially in areas of reduced flow between the pillars. These aggregates were still in direct contact with the medium flow and hence delivered a continuously high concentration of nutrients. Media perfused through the chip was assumed to be saturated by oxygen upon entering the chip as the tubing employed was permeable to oxygen. We cultured PDAC cells onto a novel microfluidic chamber, the HepaChip®, maintaining cell vitality, morphological appearance and growth characteristics that more closely resemble 3D cultures. Furthermore, the actin organization, taken as a functional marker of a proper pro-migratory, neoplastic phenotype, showed a typical cancer-type assembly.

After characterizing the cell growth, morphology in the above three cell culture systems we evaluated the cytotoxic effect of cisplatin, a common chemotherapeutic agent used in against PDAC, in all the three systems. Pancreatic cancer cells are expected to be sensitive to cisplatin [76] [17]. We tested cisplatin on PANC1 cells in 2D and 3D spheroids. The determined IC_{50} values in 2D and 3D system are $3.25 \pm 0.2\,\mu M$ and $14.6 \pm 1.6\,\mu M$ respectively. Panc1 cells in collagen-coated microfluidic chip were treated with high dose of cisplatin of 100 µM, which is much higher dose than used 2D and

3D agarose spheroids. After 72hours of treatment, 70% of the Panc1 cells were still viable. We further tested cisplatin in PANC1 cells subcutaneously injected into mice. The cisplatin dose used to obtain complete growth inhibition (10 mg/kg) *in vivo* is much higher, corresponding to an estimated plasma concentration of 240 µM [102]. Although experiments performed in microfluidic chip did not include dose-response the data suggest that drug responses by cells in collagen coated chip clearly showed higher resistance to drugs.

Overall Microfluidic chips are better than 2D and 3D spheroid cultures and mimic the *in vivo* culture, so it can be used as an alternative system of *in vivo* culture, which are expensive and time-consuming.

Mathematical models help in understanding the complex biological systems such as cells, tissues and even human body. These mathematical models have been extensively used in cancer research. These quantitative models address many fields such as tumor initiation, progression and metastases as well as tumor heterogeneity, treatment response and resistance. It helps in understanding the mechanism of the disease and provides the quantitative predictions that can be validated. Mathematical models can complement the experimental and clinical studies and redefine our understanding of mechanisms driving tumorigenesis. In this regard we studied the PDAC cell lines growth in terms of mathematical modeling for better understanding the growing nature and capabilities of PDAC cell lines PANC1, BxPC3, and MiaPaCa2 cultured in 2D culture

Effectively modeling, describing and understanding the system is difficult. An optimal growth model should allow one to describe the changes in the system. We used discrete nonlinear autoregressive logistic family of the form

$$Y(k) = \underbrace{G(Y(k-1))}_{\text{growth rate}} Y(k-1)$$

to model the PDAC cell lines growth. Using nonlinear model we attempted to define the system with respect to change in the cell growth rate of three different PDAC cell lines of 42 cases for each cell line.

We tested 9 different structures with 6 different sampling (fixed) time to identify the best model for each cell line. We selected the best 3 structures for each cell line based on the least error of simulated and experimental data. We chose cumulative identification as the best over average identification as

they were not falling under the constraints all the time. BxPC3 showed logistic, cubic and tetra models with 6H fixed time are better for estimating the growth rate. According to all these models, BxPC3 have a higher growth rate in the beginning as the system is rich in nutrients supports the maximum growth. As the time lapses growth rate decreases sharply according to logistic model, which means cells are very sensitive to the surrounding system. Out of which logistic was best for understanding the growth of BxPC3 cells. For MiaPaCa2, logistic, cubic and tetra models with 3H fixed time are ideal for modeling the growth. All the cumulative identification showed higher growth rate in the beginning and the growth rate decreases as the system was changing with time and cell count. Even for MiaPaCa2, a logistic model was better. PANC1 showed cubic (3H), delayed cubic model (18H) and tetra models (3H) were better for modeling the growth rate, out of which cubic model was the best based on the error index.

Finally, we narrowed our identification to most reliable data and redid the identification. For all the cell lines tetra model turned out to be the best model to predict the growth. Despite all the cell lines showed Tetra model as their best representation, a number of important differences are in order. First, BxPC3 (having 6H sampling time) need a longer time step to be precisely described. This suggests its dynamics be slower than the others having sampling time 3H. MiaPaCa2 has the peak of the growth rate just at the beginning, i.e. when the cell count is still very small, whereas PANC1 has its maximum peak later. This may suggest for MiaPaCa2 to reach its maximum reproducing capability when the cells are isolated, while for PANC1 particularly sensitive of the surrounding, meaning the cells need a certain time to settle down in the new environment.

Overall we can conclude that reliable data are very crucial in the identification process. All the cell lines showed qualitatively similar growth rate. This suggests the possibility that their growth is based on common mechanisms. Cell lines seem to be differently affected by their own numerosity. From this analysis more sophisticated models could be designed.

Appendix A

Appendix

This appendix is related to Chapter 3 Here we provide the raw data of all the cell counts, which we used for the identification of best models for PDAC cell growth.

A.1 Cell count data of PANC1

SET 1 T01 = [2.5, 5.5, 22, 29.5, 45.5, 51.5, 69.5, 76.75, 94.5, 100.5, 192, 197.5, 215.5, 221.5, 244.5]; X01 = [17777.77, 12222.22, 25555.55, 30000, 22222.22, 24444.44, 27777.77, 54444.44, 78888.88, 67777.77, 238000, 178000, 292000, 210000, 202000]; X02 = [25555.55, 20000, 26666.66, 31111.11, 25555.55, 45555.55, 48888.88, 44444.44, 81111.11, 80000, 214000, 224000, 332000, 182500, 254000]; X03 = [23333.33, 26666.66, 30000, 21111.11, 36666.66, 20000, 51111.11, 38888.88, 56666.66, 78888.88, 254000, 218000, 256000, 186000, 228000];

SET 2 T02= [2.75, 18.75, 25.75, 42, 49.5, 67.5, 73.5, 165, 170.5, 188.5, 194.5, 218, 236.5, 242]; X05= [25555.55, 21111.11, 14444.44, 25555.55, 20000, 22222.22, 32222.22, 160000, 158000, 176000, 220000, 174000, 252000, 198000]; X06= [18888.88, 24444.44, 20000, 20000, 13333.33, 21111.11, 27777.77, 140000, 154000, 218000, 164000, 222000, 280000, 202000]; X04= [16666.66, 17777.77, 21111.11, 20000, 18888.88, 27777.77, 35555.55, 236000, (158000+154000)/2, 178000, 156000, 260000, 320000, 132000];

SET 3 T03= [18.25, 36.5, 47.5, 66.5, 72, 138, 144, 186, 213]; X07= [17777.77, 21111.11, 12222.22, 26666.66, 20000, 208000, 168000, 198000, 292000]; X08=

[31111.11, 25555.55, 18888.88, 38888.88, 35555.55, 216000, 198000, 200000, 260000]; X09= [23333.33, 22222.22, 34444.44, 37777.77, 26666.66, 156000, 174000, 292000, 210000];

SET 4 T4= [4, 21.66, 28.16, 48.83, 123.22, 146.22, 170.83, 194.83, 218.83]; X10= [7777.77, 16666.66, 26666.66, 52222.22, 134000, 120000, 118000, 154000, 114000]; X11= [26666.66, 21111.11, 6666.66, 28888.88, 78000, 80000, 128000, 130000, 94000]; X12= [14444.44, 13333.33, 18888.88, 26666.66, 132000, 138000, 176000, 164000, 102000];

SET 5 T5= [1.41, 17.83, 23.83, 48.33, 72.83, 97.33, 169.33, 193.33, 216.83, 241.33]; X14= [23333.33, 25555.55, 30000, 38888.88, 61111.11, 143333.33, 278000, 284000, 276000, 244000]; X15= [26666.66, 28888.88, 45555.55, 30000, 52222.22, 115555.55, 322000, 290000, 276000, 262000]; X13= [(23333.33+26666.66)/2, 26666.66, 23333.33, 43333.33, 92222.22, 100000, 260000, 260000, 294000, 284000];

SET 6 T6= [6, 22.83, 30.83, 54.16, 78.83, 100.83, 173.16, 197.16, 222.16, 246.16]; X16= [24444.44, 14444.44, 17777.77, 47777.77, 72222.22, 116000, 352000, 298000, 366000, 296000]; X17= [15555.55, 44444.44, 18888.88, 38888.88, 91111.11, 93333.33, 324000, 276000, 340000, 320000]; X18= [32222.22, 33333.33, 20000, 41111.11, 67777.77, 140000, 274000, 254000, 236000, 320000];

SET 7 T7= [4, 21.83, 28.66, 50.66, 70.66, 98.66, 166.16, 189.66, 220.66, 244.66]; X19= [15555.55, 25555.55, 12222.22, 42222.22, 101111.11, 188000, 262000, 318000, 278000, 266000]; X20= [23333.33, 36666.66, 23333.33, 46666.66, 77777.77, 228000, 262000, 298000, 346000, 272000]; X21= [17777.77, 30000, 20000, 48888.88, 64444.44, 136000, 190000, 300000, 274000, 248000];

A.2 Cell count data of BxPC3

SET 1 T1=[22.5, 45, 68.83, 92.83, 163.33, 168.83, 185.83, 192.83, 210.33, 216.83, 238.08]; X01=[23333.33, 36666.66, 115555.55, 132000, 460000, 330000, 182000, 322000, 264000, 386000, 462000]; X02=[44444.44, 65555.55, 88888.88, 190000, 396000, 324000, 348000, 296000, 412000, 398000, 510000]; X03=[23333.33, 71111.11, 98888.88, 164000, 348000, 230000, 410000, 420000, 398000, 372000, 314000];

SET 2 T2=[24.5, 48, 119, 124.5, 141.5, 148.5, 166, 172.5, 193.75, 215.5]; X04=[22222.22, 64444.44, 216000, 246000, 216000, 202000, 390000, 264000, 394000, 374000]; X05=[32222.22, 55555.55, 248000, 204000, 278000, 176000, 348000, 272000, 450000, 370000]; X06=[32222.22, 44444.44, (216000+248000)/2, 180000, 218000, 206000, 288000, 232000, 326000, 390000];

SET 3 T3=[21, 27.5, 45, 51.5, 72.75, 94.5, 165, 195, 213, 243]; X07=[40000, 61111.11, 106666.66, 52222.22, 87777.77, 175555.55, 330000, 430000, 342000, 450000]; X08=[36666.66, 31111.11, 52222.22, 74444.44, 98888.88, 185555.55, 280000, 188000, 520000, 514000]; X09=[47777.77, 33333.33, 66666.66, 58888.88, 106666.66, 145555.55, 344000, 260000, 506000,(450000+514000)/2];

SET 4 T4=[19.66, 25.5, 48, 70, 93.5, 168, 189.5, 214, 238, 260.5]; X10=[38888.88, 15555.55, 42222.22, 88888.88, 147777.77, 366000, 454000, 490000, 254000, (498000+476000)/2]; X11=[48888.88, 30000, 31111.11, 95555.55, 151111.11, 496000, 478000, 584000, 320000, 498000]; X12=[27777.77, 25555.55, 42222.22, 94444.44, 125555.55, 418000, 390000, 536000, 364000, 476000];

SET 5 T5=[4, 21.66, 28.16, 48.83, 123.33, 146.33, 170.83, 194.83, 218.83]; X13=[35555.55, 45555.55, 67777.77, 108888.88, 416000, 420000, 404000, 576000, 494000]; X14=[40000, 26666.66, 47777.77, 120000, 398000, 498000, 526000, 464000, 592000]; X15=[28888.88, 41111.11, 56666.66, 103333.33, 436000, 620000, 450000, 614000, 626000];

SET 6 T6=[4.3, 18, 24.25, 44.75, 69.75, 91.5, 166, 190, 214, 233.5]; X16=[11111.11, 20000, 16666.66, 52222.22, 27777.77, 196000, 536000, 496000, 522000, 526000]; X17=[13333.33, 14444.44, 24444.44, 61111.11, 52222.22, 190000, 394000, 440000, 492000, 442000]; X18=[13333.33, 12222.22, 32222.22, 47777.77, 35555.55, 158000, 492000, 366000, 510000, 500000];

SET 7 T7=[4, 21.83, 28.66, 50.66, 70.66, 98.66, 166.16, 189.66, 220.66, 244.66]; X19=[21111.11, 23333.33, 34444.44, 87777.77, 131111.11, 280000, 480000, 434000, 498000, 508000]; X20=[14444.44, 35555.55, 27777.77, 62222.22, 135555.55, 348000, 414000, 414000, 432000, 350000]; X21=[15555.55, 25555.55, 33333.33, 83333.33, 155555.55, 362000, 324000, 426000, 436000, 532000];

A.3 Cell count data of MiaPaCa2

SET 1 T1=[2.5, 5.5, 22, 29.5, 45.5, 51.5, 69.5, 76.75, 94.5, 100.5, 192, 197.5, 215.5, 221.5, 244.5, 269]; X01=[10000, 13333.33, 26666.66,21111.11, 34444.44, 66666.66, 94444.44, 81111.11,98888.88, 147777.77,330000, 348000, 350000,398000,360000,212000]; X02=[26666.66, 17777.77, 23333.33, 25555.55, 38888.88, 43333.33, 108888.88, 85555.55, 55555.55, 154444.44, 372000, 372500, 274000, 256000, 362000, 298000]; X03=[21111.11, 24444.44, 33333.33, 20000, 20000, 40000, 64444.44, 86666.66, 111111.11, 124444.44, 320000, 382000, 318000, 334000, 352000, 198000];

SET 2 T2=[2.75, 18.75, 25.75, 42, 49.5, 67.5, 73.5, 165, 170.5, 188.5, 194.5, 218, 242]; X04=[21111.11,15555.55, 23333.33, 20000, 17777.77, 52222.22, 47777.77, 418000, 252000, 274000, 342000, 234000, 320000]; X05=[35555.55, 24444.44, 13333.33, 36666.66, 26666.66, 57777.77, 55555.55, 384000, 292000, 344000, 378000, 382000, 244000]; X06=[21111.11, 21111.11, 18888.88, 40000, 32222.22, 61111.11, 54444.44, 434000, 394000, 420000, 372000, 330000, 290000];

SET 3 T3=[18.25, 36.5, 47.5, 66.5, 72, 138, 144, 186, 213]; X07=[20000, 27777.77, 21111.11, 44444.44, 37777.77, 410000, 326000, 428000, 420000]; X08=[22222.22, 16666.66, 40000, 42222.22, 22222.22, 348000, 240000, 582000, 454000]; X09=[17777.77, 24444.44, 30000, 34444.44, 34444.44, 474000, 346000, 442000, 284000];

SET 4 T4=[4, 21.66, 28.16, 48.83, 123.33, 146.33, 170.83, 194.83]; X10=[11111.11, 21111.11, 11111.11, 32222.22, 414000, 470000, 416000, 386000]; X11=[10000, 12222.22, 11111.11, 33333.33, 460000, 498000, 452000, 532000]; X12=[17777.77, 14444.44, 12222.22, 24444.44, 412000, 518000, 560000, 332000];

SET 5 T5=[6, 22.83, 30.83, 54.16, 78.83, 100.83, 173.16, 197.16, 222.16, 246.16]; X13=[14444.44, 20000, 6666.66, 26666.66, 74444.44, 147777.77, 330000, 386000, 280000, 340000]; X14=[16666.66, 17777.77, 16666.66, 31111.11, 53333.33, 128888.88, 386000, 382000, 326000, 310000]; X15=[17777.77, 25555.55, 13333.33, 31111.11, 66666.66, 122222.22, 344000, 254000, 332000, 312000];

SET 6 T6=[4.5, 18, 24.25, 44.75, 69.75, 91.5, 166, 190, 214, 233.5]; X16=[14444.44, 13333.33, 14444.44, 44444.44, 35555.55, 230000, 398000, 520000, 424000, 380000]; X17=[14444.44, 13333.33, 20000, 50000, 64444.44, 266000, 424000,

412000, 520000, 484000]; X18=[8888.88, 12222.22, 10000, 44444.44, 64444.44, 266000, 430000, 544000, 480000, 376000];

SET 7 T7=[4, 21.83, 28.66, 50.66, 70.66, 98.66, 166.16, 189.66, 220.66, 244.66]; X19=[6666.66, 13333.33, 7777.77, 31111.11, 74444.44, 184000, 280000, 304000, 344000, 304000]; X20=[13333.33, 15555.55, 13333.33, 40000, 72222.22, 216000, 338000, 368000, 338000, 280000]; X21=[7777.77, 8888.88, 13333.33, 31111.11, 60000, 224000, 348000, 384000, 292000, 322000];

Appendix B

Publications

This research activity has led to publication in international journal.

International Journals

1. Meike Beer*, **Nirmala Kuppalu***, Matteo Stefanini, Holger Becker, Ingo Schulz, Sagar Manoli, Julia Schuette, Christian Schmees, Armando Casazza, Martin Stelzle* and Annarosa Arcangeli*. "A novel microfluidic 3D platform for culturing pancreatic ductal adenocarcinoma cells: comparison with *in vitro* cultures and *in vivo* xenografts", *Scientific Reports*, 25 April, 2017. [DOI:10.1038/s41598-017-01256-8]

Bibliography

[1] B. Alexandra, R. Li, M. B. Chen, S. C. Wong, and R. D. Kamm, "Microfluidics: A new tool for modeling cancer-immune interactions." *Trends Cancer*, vol. 2, no. 1, pp. 6–19, 2016.

[2] P. M. Altrock, L. L. Liu, and F. Michor, "The mathematics of cancer: integrating quantitative models," *Nature Reviews Cancer*, vol. 15, no. 12, pp. 730–745, 2015.

[3] M. Alvin and I. C. A, "Pancreatic cancer biology and genetics from an evolutionary perspective," *Nat Rev Cancer*, vol. 16, no. 9, pp. 553–565, 2016.

[4] D. An, K. Kim, and J. Kim, "Microfluidic system based high throughput drug screening system for Curcumin/TRAIL combinational chemotherapy in human prostate cancer PC3 cells," *Biomol Ther*, vol. 22, no. 4, pp. 355–362, 2014.

[5] S. Arao, A. Masumoto, and M. Otsuki, "Beta1 integrins play an essential role in adhesion and invasion of pancreatic carcinoma cells." *Pancreas*, vol. 20, no. 2, pp. 129–37, 2000.

[6] V. V. Artym and K. Matsumoto, "Imaging cells in three-dimensional collagen matrix," *Current protocols in cell biology*, pp. 10–18, 2010.

[7] A. Astashkina and D. W. Grainger, "Critical analysis of 3-D organoid in vitro cell culture models for high-throughput drug candidate toxicity assessments." *Adv. Drug Deliv. Rev.*, vol. 69-70, pp. 1–18, 2014.

[8] S. Benzekry, C. Lamont, A. Beheshti, A. Tracz, J. M. Ebos, L. Hlatky, and P. Hahnfeldt, "Classical mathematical models for description and prediction of experimental tumor growth," *PLoS computational biology*, vol. 10, no. 8, p. e1003800, 2014.

[9] M. Boiron, B. Guillemain, C. Bernard, J. Peries, and Chuat, "Presence in murine sarcoma virus stocks of a 3d component which alone initiates cellular conversion." *Nature*, vol. 219, no. 5155, pp. 748–9, 1968.

[10] S. Breslin and O. Lorraine, "Three-dimensional cell culture: the missing link in drug discovery." *Drug Discov. Today*, vol. 18, no. 5-6, pp. 240–9, 2013.

[11] H. Burris, M. Moore, J. Andersen, M. Green, M. Rothenberg, M. Modiano, M. Cripps, R. Portenoy, A. Storniolo, P. Tarassoff, R. Nelson, F. Dorr, C. Stephens, and V. D. Hoff, "Improvements in survival and clinical benefit with gemcitabine as first-line therapy for patients with advanced pancreas cancer: a randomized trial." *J Clin Oncol*, vol. 15, no. 6, pp. 2403–2413, 1997.

[12] H. M. Byrne, "Dissecting cancer through mathematics: from the cell to the animal model," *Nat Rev Cancer*, vol. 10, no. 3, p. nrc2808, 2010.

[13] J. Chen, J. Li, and Y. Sun, "Microfluidic approaches for cancer cell detection, characterization, and separation," *Lab on a Chip*, vol. 12, no. 10, pp. 1753–1767, 2012.

[14] W. Chen, C. Wong, E. Vosburgh, A. J. Levine, D. J. Foran, and E. Y. Xu, "High-throughput image analysis of tumor spheroids: a user-friendly software application to measure the size of spheroids automatically and accurately." *J Vis Exp*, no. 89, p. 51639, 2014.

[15] D. Chiu, N. Jeon, S. Huang, R. Kane, C. Wargo, I. Choi, D. Ingber, and G. Whitesides, "Patterned deposition of cells and proteins onto surfaces by using three-dimensional microfluidic systems." *Proc. Natl. Acad. Sci. U.S.A.*, vol. 97, no. 6, pp. 2408–13, 2000.

[16] S. J. Coleman, J. Watt, P. Arumugam, L. Solaini, E. Carapuca, M. Ghallab, R. P. Grose, and H. M. Kocher, "Pancreatic cancer organotypics: High throughput, preclinical models for pharmacological agent evaluation." *World J. Gastroenterol.*, vol. 20, no. 26, pp. 8471–81, 2014.

[17] A. D. D'Andrea and M. Grompe, "The fanconi anaemia/brca pathway," *Nature Reviews Cancer*, vol. 3, no. 1, pp. 23–34, 2003.

[18] E. L. Deer, G. Jessica, J. D. Coursen, J. E. Shea, J. Ngatia, C. L. Scaife, M. A. Firpo, and S. J. Mulvihill, "Phenotype and genotype of pancreatic cancer cell lines." *Pancreas*, vol. 39, no. 4, pp. 425–35, 2010.

[19] ——, "Phenotype and genotype of pancreatic cancer cell lines." *Pancreas*, vol. 39, no. 4, pp. 425–35, 2010.

[20] T. Denayer, T. Stöhr, and M. Roy, "Animal models in translational medicine: Validation and prediction," *New Horizons Transl Medicine*, vol. 2, no. 1, pp. 5–11, 2014.

[21] L. E. Dickinson, C. Lütgebaucks, D. M. Lewis, and S. Gerecht, "Patterning microscale extracellular matrices to study endothelial and cancer cell interactions in vitro." *Lab Chip*, vol. 12, no. 21, pp. 4244–8, 2012.

[22] M. Distler, D. Aust, J. Weitz, C. Pilarsky, and R. Grützmann, "Precursor lesions for sporadic pancreatic cancer: PanIN, IPMN, and MCN," *Biomed Res Int*, vol. 2014, pp. 1–11, 2014.

[23] C. R. Drifka, K. W. Eliceiri, S. M. Weber, and W. Kao, "A bioengineered heterotypic stroma-cancer microenvironment model to study pancreatic ductal adenocarcinoma." *Lab Chip*, vol. 13, no. 19, pp. 3965–75, 2013.

[24] ——, "A bioengineered heterotypic stroma-cancer microenvironment model to study pancreatic ductal adenocarcinoma." *Lab Chip*, vol. 13, no. 19, pp. 3965–75, 2013.

[25] ——, "A bioengineered heterotypic stroma-cancer microenvironment model to study pancreatic ductal adenocarcinoma." *Lab Chip*, vol. 13, no. 19, pp. 3965–75, 2013.

[26] R. Edmondson, J. J. Broglie, A. F. Adcock, and L. Yang, "Three-dimensional cell culture systems and their applications in drug discovery and cell-based biosensors." *Assay Drug Dev Technol*, vol. 12, no. 4, pp. 207–18, 2014.

[27] ——, "Three-dimensional cell culture systems and their applications in drug discovery and cell-based biosensors," *Assay and drug development technologies*, vol. 12, no. 4, pp. 207–218, 2014.

[28] N. T. Elliott and F. Yuan, "A review of three-dimensional in vitro tissue models for drug discovery and transport studies." *J Pharm Sci*, vol. 100, no. 1, pp. 59–74, 2011.

[29] C. Erlichman and D. Vidgen, "Cytotoxicity of adriamycin in MGH-U1 cells grown as monolayer cultures, spheroids, and xenografts in immune-deprived mice." *Cancer Res*, vol. 44, no. 11, pp. 5369–75, 1984.

[30] E. W. Esch, A. Bahinski, and D. Huh, "Organs-on-chips at the frontiers of drug discovery." *Nat Rev Drug Discov*, vol. 14, no. 4, pp. 248–60, 2015.

[31] G. Feldmann, S. Rauenzahn, and A. Maitra, "In vitro models of pancreatic cancer for translational oncology research." *Expert Opin Drug Discov*, vol. 4, no. 4, pp. 429–443, 2009.

[32] E. Fokas, E. O'Neill, A. Gordon-Weeks, S. Mukherjee, W. G. McKenna, and R. J. Muschel, "Pancreatic ductal adenocarcinoma: From genetics to biology to radiobiology to oncoimmunology and all the way back to the clinic," *Biochimica et Biophysica Acta (BBA)-Reviews on Cancer*, vol. 1855, no. 1, pp. 61–82, 2015.

[33] J. Friedrich, C. Seidel, R. Ebner, and K. L. A, "Spheroid-based drug screen: considerations and practical approach," *Nat Protoc*, vol. 4, no. 3, pp. 309–324, 2009.

[34] M. Fujiwara, K. Izuishi, T. Sano, M. A. Hossain, S. Kimura, T. Masaki, and Y. Suzuki, "Modulating effect of the PI3-kinase inhibitor LY294002 on cisplatin in human pancreatic cancer cells." *J. Exp. Clin. Cancer Res.*, vol. 27, no. 1, p. 76, 2008.

[35] H. Funahashi, H. Takeyama, H. Sawai, A. Furuta, M. Sato, Y. Okada, T. Hayakawa, M. Tanaka, and T. Manabe, "Alteration of integrin expression by glial cell line-derived neurotrophic factor (gdnf) in human pancreatic cancer cells," *Pancreas*, vol. 27, no. 2, pp. 190–196, 2003.

[36] P. Gerlee, "The model muddle: in search of tumor growth laws," *Cancer research*, vol. 73, no. 8, pp. 2407–2411, 2013.

[37] M. Gnanamony and C. Gondi, "Chemoresistance in pancreatic cancer: Emerging concepts (Review)," *Oncol Lett*, vol. 13, no. 4, pp. 2507–2513, 2017.

[38] R. Gradiz, H. C. Silva, L. Carvalho, M. F. Botelho, and A. Mota-Pinto, "Mia paca-2 and panc-1–pancreas ductal adenocarcinoma cell lines with neuroendocrine differentiation and somatostatin receptors," *Scientific reports*, vol. 6, p. 21648, 2016.

[39] E. Greco, D. Basso, P. Fogar, S. Mazza, F. Navaglia, C. Zambon, A. Falda, S. Pedrazzoli, E. Ancona, and M. Plebani, "Pancreatic cancer cells invasiveness is mainly affected by interleukin-1beta not by transforming growth factor-beta1," *International Journal of Biological Markers*, vol. 20, no. 4, p. 235, 2005.

[40] N. Gupta, J. R. Liu, B. Patel, D. E. Solomon, B. Vaidya, and V. Gupta, "Microfluidics-based 3d cell culture models: Utility in novel drug discovery and delivery research," *Bioengineering & Translational Medicine*, vol. 1, no. 1, pp. 63–81, 2016.

[41] B. Hagmeyer, F. Zechnall, and M. Stelzle, "Towards plug and play filling of microfluidic devices by utilizing networks of capillary stop valves." *Biomicrofluidics*, vol. 8, no. 5, p. 056501, 2014.

[42] W. L. Haisler, D. M. Timm, J. A. Gage, H. Tseng, T. Killian, and G. R. Souza, "Three-dimensional cell culturing by magnetic levitation," *Nat Protoc*, vol. 8, no. 10, pp. 1940–1949, 2013.

[43] J. Haqq, L. M. Howells, G. Garcea, M. S. Metcalfe, W. P. Steward, and A. R. Dennison, "Pancreatic stellate cells and pancreas cancer: Current perspectives and future strategies," *Eur J Cancer*, vol. 50, no. 15, pp. 2570–2582, 2014.

[44] V. Heinemann, D. Quietzsch, F. Gieseler, M. Gonnermann, H. Schönekäs, A. Rost, H. Neuhaus, C. Haag, M. Clemens, B. Heinrich, V. Ursula,

M. Fuchs, D. Fleckenstein, W. Gesierich, D. Uthgenannt, H. Einsele, A. Holstege, A. Hinke, A. Schalhorn, and R. Wilkowski, "Randomized phase III trial of gemcitabine plus cisplatin compared with gemcitabine alone in advanced pancreatic cancer." *J. Clin. Oncol.*, vol. 24, no. 24, pp. 3946–52, 2006.

[45] D. Herrmann, J. R. Conway, C. Vennin, A. Magenau, W. E. Hughes, J. P. Morton, and P. Timpson, "Three-dimensional cancer models mimic cell-matrix interactions in the tumour microenvironment." *Carcinogenesis*, vol. 35, no. 8, pp. 1671–9, 2014.

[46] F. Hirschhaeuser, H. Menne, C. Dittfeld, J. West, M. Wolfgang, and K. L. A, "Multicellular tumor spheroids: an underestimated tool is catching up again." *J. Biotechnol.*, vol. 148, no. 1, pp. 3–15, 2010.

[47] C. T. Ho, R. Z. Lin, W. Y. Chang, H. Y. Chang, and C. H. Liu, "Rapid heterogeneous liver-cell on-chip patterning via the enhanced field-induced dielectrophoresis trap." *Lab Chip*, vol. 6, no. 6, pp. 724–34, 2006.

[48] F. Holzner, B. Hagmeyer, J. Schütte, M. Kubon, B. Angres, and M. Stelzle, "Numerical modelling and measurement of cell trajectories in 3-D under the influence of dielectrophoretic and hydrodynamic forces." *Electrophoresis*, vol. 32, no. 17, pp. 2366–76, 2011.

[49] V. Hongisto, S. Jernström, V. Fey, J.-P. Mpindi, K. K. Sahlberg, O. Kallioniemi, and M. Perälä, "High-throughput 3d screening reveals differences in drug sensitivities between culture models of jimt1 breast cancer cells," *PloS one*, vol. 8, no. 10, p. e77232, 2013.

[50] J. L. Horning, S. K. Sahoo, S. Vijayaraghavalu, S. Dimitrijevic, J. K. Vasir, T. K. Jain, A. K. Panda, and V. Labhasetwar, "3-D tumor model for in vitro evaluation of anticancer drugs," *Mol Pharm*, vol. 5, no. 5, pp. 849–62, 2008.

[51] R. H. Hruban, N. V. Adsay, J. Albores-Saavedra, C. Compton, E. S. Garrett, S. N. Goodman, S. E. Kern, D. S. Klimstra, G. Klöppel, D. S. Longnecker *et al.*, "Pancreatic intraepithelial neoplasia: a new nomenclature and classification system for pancreatic duct lesions," *The American journal of surgical pathology*, vol. 25, no. 5, pp. 579–586, 2001.

[52] D. Huh, G. A. Hamilton, and D. E. Ingber, "From 3D cell culture to organs-on-chips." *Trends Cell Biol.*, vol. 21, no. 12, pp. 745–54, 2011.

[53] D. Huh, Y.-s. S. Torisawa, G. A. Hamilton, H. J. Kim, and D. E. Ingber, "Microengineered physiological biomimicry: organs-on-chips." *Lab Chip*, vol. 12, no. 12, pp. 2156–64, 2012.

[54] C. I. Hwang, S. F. Boj, H. Clevers, and D. A. Tuveson, "Preclinical models of pancreatic ductal adenocarcinoma." *J. Pathol.*, vol. 238, no. 2, pp. 197–204, 2016.

[55] I. G. Hwang, J. S. Jang, S. Y. Oh, S. Lee, H. C. Kwon, G. W. Lee, S. Go, M. H. Kang, Y. J. Cha, and J. H. Kang, "A phase II trial of erlotinib in combination with gemcitabine and cisplatin in advanced pancreatic cancer." *Invest New Drugs*, vol. 30, no. 6, pp. 2371–6, 2012.

[56] I. G. Hwang, J.-S. Jang, S. Y. Oh, S. Lee, H. C. Kwon, G. W. Lee, S. Go, M. H. Kang, Y. J. Cha, and J. H. Kang, "A phase ii trial of erlotinib in combination with gemcitabine and cisplatin in advanced pancreatic cancer," *Investigational new drugs*, vol. 30, no. 6, pp. 2371–2376, 2012.

[57] N. Kashaninejad, M. R. Nikmaneshi, H. Moghadas, A. Kiyoumarsi Oskouei, M. Rismanian, M. Barisam, M. S. Saidi, and B. Firoozabadi, "Organ-tumor-on-a-chip for chemosensitivity assay: A critical review," *Micromachines*, vol. 7, no. 8, p. 130, 2016.

[58] L. Kelland, "The resurgence of platinum-based cancer chemotherapy," *Nat Rev Cancer*, vol. 7, no. 8, pp. 573–584, 2007.

[59] P. A. Kenny, G. Y. Lee, C. A. Myers, R. M. Neve, J. R. Semeiks, P. T. Spellman, K. Lorenz, E. H. Lee, M. H. Barcellos-Hoff, O. W. Petersen *et al.*, "The morphologies of breast cancer cell lines in three-dimensional assays correlate with their profiles of gene expression," *Molecular oncology*, vol. 1, no. 1, pp. 84–96, 2007.

[60] E. Knight and S. Przyborski, "Advances in 3d cell culture technologies enabling tissue-like structures to be created in vitro," *Journal of anatomy*, vol. 227, no. 6, pp. 746–756, 2015.

[61] A. C. Koong, V. K. Mehta, Q. T. Le, G. A. Fisher, D. J. Terris, J. Brown, A. J. Bastidas, and M. Vierra, "Pancreatic tumors show high levels of hypoxia," *Int J Radiat Oncol Biology Phys*, vol. 48, no. 4, pp. 919–922, 2000.

[62] A. K. Laird, "Dynamics of tumour growth: comparison of growth rates and extrapolation of growth curve to one cell," *British Journal of Cancer*, vol. 19, no. 2, p. 278, 1965.

[63] E. Lastraioli, G. Perrone, A. Sette, A. Fiore, O. Crociani, S. Manoli, D. M, M. Masselli, J. Iorio, M. Callea, D. Borzomati, G. Nappo, F. Bartolozzi, D. Santini, L. Bencini, M. Farsi, L. Boni, D. F. Costanzo, A. Schwab, O. A. Muda, R. Coppola, and A. Arcangeli, "hERG1 channels drive tumour malignancy and may serve as prognostic factor in pancreatic ductal adenocarcinoma," *Brit J Cancer*, vol. 112, no. 6, pp. 1076–1087, 2015.

[64] G. Y. Lee, P. A. Kenny, E. H. Lee, and M. J. Bissell, "Three-dimensional culture models of normal and malignant breast epithelial cells," *Nat Methods*, vol. 4, no. 4, pp. 359–365, 2007.

[65] M. Lee, A. R. Kumar, S. M. Sukumaran, M. G. Hogg, D. S. Clark, and J. S. Dordick, "Three-dimensional cellular microarray for high-throughput toxicology assays," *Proc National Acad Sci*, vol. 105, no. 1, pp. 59–63, 2008.

[66] X. Li, A. V. Valadez, P. Zuo, and Z. Nie, "Microfluidic 3D cell culture: potential application for tissue-based bioassays," *Bioanalysis*, vol. 4, no. 12, pp. 1509–1525, 2012.

[67] M. Lieber, J. Mazzetta, W. Nelson-Rees, M. Kaplan, and G. Todaro, "Establishment of a continuous tumor-cell line (panc-1) from a human carcinoma of the exocrine pancreas," *International journal of cancer*, vol. 15, no. 5, pp. 741–747, 1975.

[68] R.-Z. Lin and H.-Y. Chang, "Recent advances in three-dimensional multicellular spheroid culture for biomedical research," *Biotechnology journal*, vol. 3, no. 9-10, pp. 1172–1184, 2008.

[69] D. Loessner, K. S. Stok, M. P. Lutolf, D. W. Hutmacher, J. A. Clements, and S. C. Rizzi, "Bioengineered 3D platform to explore cell–ECM interactions and drug resistance of epithelial ovarian cancer cells," *Biomaterials*, vol. 31, no. 32, pp. 8494–8506, 2010.

[70] C. J. Lovitt, T. B. Shelper, and V. M. Avery, "Advanced cell culture techniques for cancer drug discovery." *Biology (Basel)*, vol. 3, no. 2, pp. 345–67, 2014.

[71] J. Lowengrub, H. Frieboes, F. Jin, Y. Chuang, X. Li, P. Macklin, S. Wise, and V. Cristini, "Nonlinear modelling of cancer: bridging the gap between cells and tumours." *Nonlinearity*, vol. 23, no. 1, pp. R1–R9, 2010.

[72] J. Luo, P. Guo, K. Matsuda, N. Truong, A. Lee, C. Chun, S.-Y. Cheng, and M. Korc, "Pancreatic cancer cell-derived vascular endothelial growth factor is biologically active in vitro and enhances tumorigenicity in vivo," *International journal of cancer*, vol. 92, no. 3, pp. 361–369, 2001.

[73] B. A. M, R. L. Carpenedo, and M. T. C, "Engineering the embryoid body microenvironment to direct embryonic stem cell differentiation," *Biotechnol Progr*, vol. 25, no. 1, pp. 43–51, 2009.

[74] H. Marta, E. Hijona, A. Cosme, and L. Bujanda, "Mouse models of pancreatic cancer." *World J. Gastroenterol.*, vol. 18, no. 12, pp. 1286–94, 2012.

[75] J. M. Messana, N. S. Hwang, J. Coburn, J. H. Elisseeff, and Z. Zhang, "Size of the embryoid body influences chondrogenesis of mouse embryonic stem cells," *J Tissue Eng Regen M*, vol. 2, no. 8, pp. 499–506, 2008.

[76] R. Mezencev, L. Matyunina, G. Wagner, and J. McDonald, "Acquired resistance of pancreatic cancer cells to cisplatin is multifactorial with cell context-dependent involvement of resistance genes," *Cancer gene therapy*, vol. 23, no. 12, pp. 446–453, 2016.

[77] S. Michelson, A. Glicksman, and J. Leith, "Growth in solid heterogeneous human colon adenocarcinomas: comparison of simple logistical models," *Cell Proliferation*, vol. 20, no. 3, pp. 343–355, 1987.

[78] C. G. Moertel, "Chemotherapy of gastrointestinal cancer," *New Engl J Medicine*, vol. 299, no. 19, pp. 1049–1052, 1978.

[79] F. Navaglia, P. Fogar, E. Greco, D. Basso, A. Stefani, S. Mazza, C. Zambon, W. Habeler, G. Altavilla, A. Amadori, A. Cecchetto, and M. Plebani, "CD44v10: an antimetastatic membrane glycoprotein for pancreatic cancer." *Int J Biological Markers*, vol. 18, no. 2, pp. 130–8, 2003.

[80] Y. Nio, H. Ohmori, Y. Minari, N. Hirahara, S. Sasaki, M. Takamura, and K. Tamura, "A quinolinone derivative, vesnarinone (opc-8212), significantly inhibits the in vitro and in vivo growth of human pancreatic cancer cell lines." *Anti-cancer drugs*, vol. 8, no. 7, pp. 686–695, 1997.

[81] P. Olson and D. Hanahan, "Breaching the cancer fortress," *Science*, vol. 324, no. 5933, pp. 1400–1401, 2009.

[82] G. Ouyang, Z. Liu, S. Huang, Q. Li, L. Xiong, X. Miao, and Y. Wen, "Gemcitabine plus cisplatin versus gemcitabine alone in the treatment of pancreatic cancer: a meta-analysis," *World J Surg Oncol*, vol. 14, no. 1, p. 59, 2016.

[83] F. Pampaloni, E. G. Reynaud, and E. H. Stelzer, "The third dimension bridges the gap between cell culture and live tissue." *Nat. Rev. Mol. Cell Biol.*, vol. 8, no. 10, pp. 839–45, 2007.

[84] M. Pickl and C. Ries, "Comparison of 3d and 2d tumor models reveals enhanced her2 activation in 3d associated with an increased response to trastuzumab," *Oncogene*, vol. 28, no. 3, pp. 461–468, 2009.

[85] S. Pillozzi, M. Masselli, E. De Lorenzo, B. Accordi, E. Cilia, O. Crociani, A. Amedei, M. Veltroni, D. Massimo, G. Basso, A. Becchetti, D. Campana, and A. Arcangeli, "Chemotherapy resistance in acute lymphoblastic leukemia requires hERG1 channels and is overcome by hERG1 blockers." *Blood*, vol. 117, no. 3, pp. 902–14, 2011.

[86] K. Polireddy and Q. Chen, "Cancer of the pancreas: Molecular pathways and current advancement in treatment," *J Cancer*, vol. 7, no. 11, pp. 1497–1514, 2016.

[87] D. Pollack, "Modeling tumor growth and quantifying the duration of time between metastasis, detection, and mortality in breast cancer patients," 2011.

[88] M. Ravi, V. Paramesh, S. Kaviya, E. Anuradha, and F. Solomon, "3D cell culture systems: Advantages and applications," *J Cell Physiol*, vol. 230, no. 1, pp. 16–26, 2015.

[89] M. Santini, G. Rainaldi, and P. Indovina, "Apoptosis, cell adhesion and the extracellular matrix in the three-dimensional growth of multicellular tumor spheroids." *Crit. Rev. Oncol. Hematol.*, vol. 36, no. 2-3, pp. 75–87, 2000.

[90] J. Schütte, C. Freudigmann, K. Benz, J. Böttger, R. Gebhardt, and M. Stelzle, "A method for patterned in situ biofunctionalization in injection-molded microfluidic devices." *Lab Chip*, vol. 10, no. 19, pp. 2551–8, 2010.

[91] J. Schütte, B. Hagmeyer, F. Holzner, M. Kubon, S. Werner, C. Freudigmann, K. Benz, J. Böttger, R. Gebhardt, H. Becker, and M. Stelzle, ""Artificial micro organs"–a microfluidic device for dielectrophoretic assembly of liver sinusoids." *Biomed Microdevices*, vol. 13, no. 3, pp. 493–501, 2011.

[92] B. R. Seo, P. Delnero, and C. Fischbach, "In vitro models of tumor vessels and matrix: engineering approaches to investigate transport limitations and drug delivery in cancer." *Adv. Drug Deliv. Rev.*, vol. 69-70, pp. 205–16, 2014.

[93] ——, "In vitro models of tumor vessels and matrix: engineering approaches to investigate transport limitations and drug delivery in cancer." *Adv. Drug Deliv. Rev.*, vol. 69-70, pp. 205–16, 2014.

[94] G.-B. Stan, "Modelling in biology," 2017.

[95] S. H. Strogatz, *Nonlinear dynamics and chaos: with applications to physics, biology, chemistry, and engineering.* Westview press, 2014.

[96] M. Takada, Y. Nakamura, T. Koizumi, H. Toyama, T. Kamigaki, Y. Suzuki, Y. Takeyama, and Y. Kuroda, "Suppression of human pancreatic carcinoma cell growth and invasion by epigallocatechin-3-gallate," *Pancreas*, vol. 25, no. 1, pp. 45–48, 2002.

[97] M. H. Tan, N. Nowak, R. Loor, H. Ochi, A. A. Sandberg, C. Lopez, J. W. Pickren, R. Berjian, H. O. Douglass, and M. T. Chu, "Characterization of a new primary human pancreatic tumor line," *Cancer Invest*, vol. 4, no. 1, pp. 15–23, 2009.

[98] D. Tang, D. Wang, Z. Yuan, X. Xue, Y. Zhang, Y. An *et al.*, "Persistent activation of pancreatic stellate cells creates a microenvironment favorable for the malignant behavior of pancreatic ductal adenocarcinoma," *Int J Cancer*, vol. 132, no. 5, pp. 993–1003, 2013.

[99] A. Teague, K. Lim, and W. Andrea, "Advanced pancreatic adenocarcinoma: a review of current treatment strategies and developing therapies," *Ther Adv Medical Oncol*, vol. 7, no. 2, pp. 68–84, 2015.

[100] Y. C. Toh, T. C. Lim, D. Tai, G. Xiao, D. van Noort, and H. Yu, "A microfluidic 3D hepatocyte chip for drug toxicity testing." *Lab Chip*, vol. 9, no. 14, pp. 2026–35, 2009.

[101] O. Trédan, C. M. Galmarini, K. Patel, and I. F. Tannock, "Drug resistance and the solid tumor microenvironment." *J. Natl. Cancer Inst.*, vol. 99, no. 19, pp. 1441–54, 2007.

[102] M. van Hennik, W. van der Vijgh, I. Klein, F. Elferink, J. Vermorken, B. Winograd, and H. Pinedo, "Comparative pharmacokinetics of cisplatin and three analogues in mice and humans." *Cancer Res.*, vol. 47, no. 23, pp. 6297–301, 1987.

[103] M. Verhulsel, M. Vignes, S. Descroix, L. Malaquin, D. M. Vignjevic, and J. L. Viovy, "A review of microfabrication and hydrogel engineering for micro-organs on chips." *Biomaterials*, vol. 35, no. 6, pp. 1816–32, 2014.

[104] P. A. Vidi, T. Maleki, M. Ochoa, L. Wang, S. M. Clark, J. F. Leary, and S. A. Lelièvre, "Disease-on-a-chip: mimicry of tumor growth in mammary ducts." *Lab Chip*, vol. 14, no. 1, pp. 172–7, 2014.

[105] A. C. Wan, "Recapitulating cell–cell interactions for organoid construction–are biomaterials dispensable?" *Trends in biotechnology*, vol. 34, no. 9, pp. 711–721, 2016.

[106] B. Weigelt, A. T. Lo, C. C. Park, J. W. Gray, and M. J. Bissell, "Her2 signaling pathway activation and response of breast cancer cells to her2-targeting agents is dependent strongly on the 3d microenvironment," *Breast cancer research and treatment*, vol. 122, no. 1, pp. 35–43, 2010.

[107] C. Wenzel, B. Riefke, S. Gründemann, A. Krebs, S. Christian, F. Prinz, M. Osterland, S. Golfier, S. Räse, N. Ansari *et al.*, "3d high-content screening for the identification of compounds that target cells in dormant tumor spheroid regions," *Experimental cell research*, vol. 323, no. 1, pp. 131–143, 2014.

[108] C. J. Whatcott, R. G. Posner, D. D. Von Hoff, and H. Han, "Desmoplasia and chemoresistance in pancreatic cancer," 2012.

[109] H. Xu, W. Liu, X. Z. Zhang, L. Hou, Y. J. Lu, P. P. Chen, C. Zhang, D. Feng, L. Kong, and X. L. Wang, "[Development of three-dimensional breast cancer cell culture drug resistance model]." *Sheng Li Xue Bao*, vol. 68, no. 2, pp. 179–84, 2016.

[110] B. B. Yahia, L. Malphettes, and E. Heinzle, "Macroscopic modeling of mammalian cell growth and metabolism," *Applied microbiology and biotechnology*, vol. 99, no. 17, pp. 7009–7024, 2015.

[111] H. Yamaguchi and J. Condeelis, "Regulation of the actin cytoskeleton in cancer cell migration and invasion," *Biochimica Et Biophysica Acta Bba - Mol Cell Res*, vol. 1773, no. 5, pp. 642–652, 2007.

[112] C. Yates, C. R. Shepard, G. Papworth, A. Dash, D. Beer Stolz, S. Tannenbaum, L. Griffith, and A. Wells, "Novel three-dimensional organotypic liver bioreactor to directly visualize early events in metastatic progression." *Adv. Cancer Res.*, vol. 97, pp. 225–46, 2007.

[113] A. A. Yunis, G. K. Arimura, and D. J. Russin, "Human pancreatic carcinoma (mia paca-2) in continuous culture: sensitivity to asparaginase," *International journal of cancer*, vol. 19, no. 1, pp. 128–135, 1977.

[114] Y. Zhang, D.-w. W. Qian, Y. Pan, Y.-j. J. Zhai, X.-p. P. Zhou, G.-s. S. Zhong, Z.-h. H. Zhu, and J.-a. A. Duan, "[comparisons of pharmacokinetic profile of eleven bioactive components in haizao yuhu decoction modified with haizao and gancao anti-drug pair in normal rats]." *Zhongguo Zhong Yao Za Zhi*, vol. 40, no. 23, pp. 4672–9, 2015.

[115] Y. Zhou, H. Chen, H. Li, and Y. Wu, "3d culture increases pluripotent gene expression in mesenchymal stem cells through relaxation of cytoskeleton tension," *Journal of cellular and molecular medicine*, vol. 21, no. 6, pp. 1073–1084, 2017.

[116] J. Zurlo, D. Rudacille, and A. M. Goldberg, *Animals and alternatives in testing: History, science, and ethics*. Mary Ann Liebert New York, 1994.